OSLOMET

Master's Thesis

Biomedicine

May 2021

Migration of prostate cancer cells along neurite outgrowths: optimalization of experimental conditions and characterization of nerve-cancer co-cultures

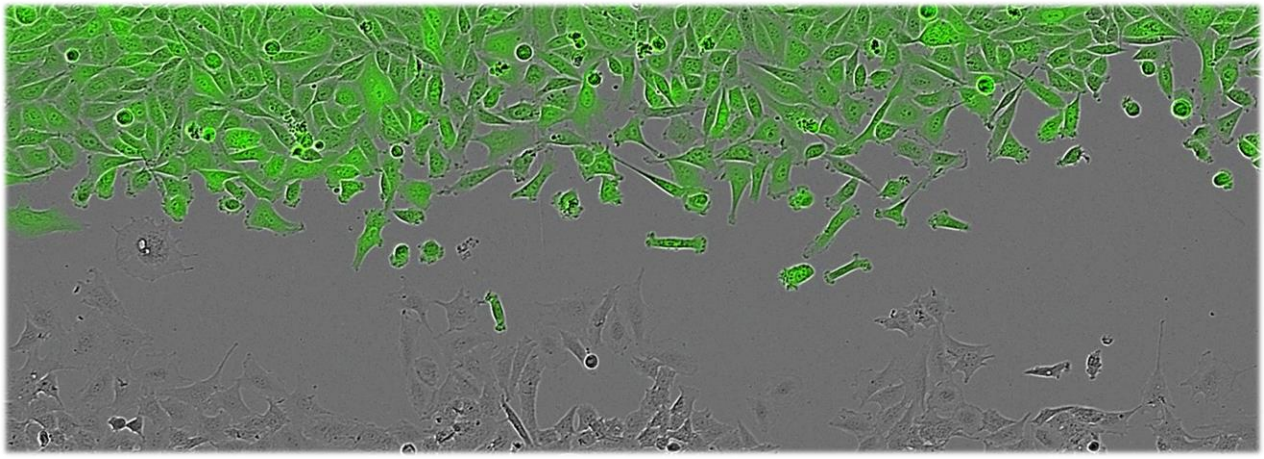

Sergen Kilinc
MABIO5900

60 ECTS

Fakultet for helsevitenskap
OSLO METROPOLITAN UNIVERSITY
STORBYUNIVERSITETET

Migration of prostate cancer cells along neurite outgrowths: optimalization of experimental conditions and characterization of nerve-cancer co-cultures

---

A master thesis in biomedicine submitted by

(60 ETC)

Sergen Kilinc

Supervisors

Håkon Ramberg and **Kristin Austlid Taskèn**

Department of Tumor Biology, Institute for Cancer Research, Radiumhostpitalet
Oslo University Hospital (OUH)

Faculty of Health Sciences, Department of Natural Sciences Health Sciences,
OsloMet – Oslo Metropolitan University

May 2021

OSLOMET

Oslo universitetssykehus
Radiumhospitalet

Acknowledgements

This work of this master thesis was carried out in the Department of Tumor Biology, Institute of Cancer Research in Radiumhostpitalet, Oslo University Hospital from August 2020 to May 2021.

First and foremost, I want to express my gratitude to my supervisor Håkon Ramberg and thank him for always supporting me and helping me with all aspects throughout the whole thesis. Thank you for the knowledge and experience you gave me in the laboratory as well as in the making of the thesis. I would also like to give my special thanks to my co-supervisor Kristin Austlid Taskén for guiding me and sharing her knowledge with me in order to get a better understanding of the study. I want to thank both of them for always being available whenever I had question about the experiments or thesis. Without their help nothing in this thesis would have been possible, as they guided me to the right direction and never giving up on me. So I want to express my gratitude to them once again, and I really appreciate the energy and time they have put in the making and forming of this thesis.

Further, I would like to thank Stein Waagene from the Department of Tumor Biology for isolating- and supplying us with DRG multiple times and Kjetil Wessel Andressen from the Department of Pharmacology at the University of Oslo, for performing receptor radioligand binding assay for our membrane protein samples.

Lastly, I what to thank my family and friends, for supporting me and motivating me throughout the whole thesis. Their support was very needed after long days at the laboratory and long nights of writing this thesis.

Oslo, May 2021

Sergen Kilinc

Abstract

As approximately 5000 males are diagnosed with prostate cancer every year in Norway, prostate cancer persists as a medical issue today. It is shown that tumor innervation is important for development and progression of the tumor, as sympathetic impulses induces adrenergic activity in the tumor microenvironment. Increased adrenergic activity plays an important part of supplying the tumor with blood and nutrients by inducing angiogenesis and neurogenesis. The β2-adrenergic receptor (ADRB2) is the most prevalent adrenergic receptor in luminal cells of the prostate, contributing to progression and development of prostate cancer. ADRB2 has been shown to induce neuroendocrine differentiation (NED), trans differentiating prostate cancer cell to neuroendocrine-like (NE-like) cells, which is known to promote tumor progression and recurrence by autocrine stimulation and apoptosis resistance by attaining NE-like characteristics. Our research group have shown that patients using β-blockers, ADRB antagonists, have reduced prostate cancer related mortality.

The overall aim of this study is to demonstrate the migration of the prostate cancer cells (PC-3-Luc2-GFP and C4-2B) towards neural PC-12 ADH cells pre-stimulated to induce neurite outgrowth and Schwann cells (RSC96), to characterize their migration rate. By stimulating the cell lines with the rho-associated kinase-inhibitor (ROCK-inhibitor) and the ADRB2 agonist isoproterenol (ISO), we wanted to determine the optimal concentration and time of each stimulation to induce the longest and highest number of neurite.

By stimulating the cells with ROCK-inhibitor and ISO, we demonstrated that 50 μM ROCK-inhibitor induced the highest total neurite length per cell. This was mainly due to the increased number of neurites per cell although the average neurite length was also substantially increased in PC-3-Luc2-GFP cells. A migration assay was performed, demonstrating that the PC-3-Luc2-GFP cell line had the highest migration rate, in which the stimulation with ROCK-inhibitor did not decrease the migration in our study. We demonstrated that stimulation with ROCK-inhibitor, decreased the migration of PC-12 ADH cells and RSC96 cells. In contrast to C4-2B cells, stimulation with 50 μM ROCK were shown to decrease the proliferation in PC12 ADH and RSC96 cells as well as in PC-3-Luc2-GFP cells. ISO had no effect on cell growth in either cell lines. Taken together, the results of this study indicates that use of ROCK inhibitor can reduce the growth and progression of prostate by suppressing prostate cancer proliferation and cell migration toward nerves.

Sammendrag

Ettersom cirka 5000 menn diagnostiseres med prostatakreft hvert år i Norge, vedvarer prostatakreft som et medisinsk problem i dag. Det er vist at tumor innervasjon er viktig for utvikling og progresjon av svulsten, da sympatiske impulser induserer adrenerg aktivitet i svulstens mikromiljø. Økt adrenerg aktivitet spiller en viktig rolle ved å forsyne svulsten med blod og næringsstoffer ved å indusere angiogenese og neurogenese. β2-adrenerg reseptor (ADRB2) er den mest utbredte adrenerge reseptoren i prostata, og bidrar til progresjon og utvikling av prostatakreft. ADRB2 har vist seg å indusere nevroendokrin differensiering (NED), transdifferensiering av prostatakreftceller til nevroendokrine-lignende (NE-lignende) celler, som er kjent for å fremme svulstprogresjon og tilbakefall ved autokrin stimulering og apoptose resistens ved å tilegne NE-lignende egenskaper. Forskningsgruppen vår har vist at bruk av spesifikke ADRB2-antagonister, β-blokkere, redusere dødelighet av prostatakreft.

Det overordnede målet for denne studien er å demonstrere migrasjonen av prostatakreftceller (PC-3-Luc2-GFP og C4-2B) mot nevrale PC-12 ADH celler forhånds-stimulert for å indusere vekst av neuritter og Schwann-celler (RSC96), for å karakterisere deres migrasjons frekvensen. Ved å stimulere cellelinjene med rho-assosierte kinase inhibitoren (ROCK-inhibitor) og ADRB2-agonisten isoproterenol (ISO), ønsket vi å bestemme den optimale konsentrasjonen og tiden for hver av stimuleringene for å indusere det høyeste antallet- og de lengste utløperne.

Ved å stimulere cellene med ROCK-inhibitor og ISO, demonstrerte vi at 50 μM ROCK-inhibitor induserte den høyeste totale neuritt lengden per celle. Dette skyldtes hovedsakelig det økte antallet neuritter per celle, selv om den gjennomsnittlige neurittlengden også ble betydelig økt i PC-3-Luc2-GFP-celler. Det ble utført en migrasjonsanalyse, som demonstrerte at PC-3-Luc2-GFP-cellelinjen hadde den høyeste migrerings frekvensen, der stimulering med ROCK-hemmer viste seg å ikke redusere migrasjonens frekvens i vårt studie. Vi demonstrerte at stimulering med ROCK-hemmer, reduserte migrasjonen av PC-12 ADH-celler og RSC96-celler. I motsetning til C4-2B-celler ble stimulering med 50 μM ROCK vist å redusere spredning i PC12 ADH- og RSC96-celler så vel som i PC-3-Luc2-GFP-celler. ISO hadde ingen effekt på cellevekst i noen av cellelinjene. Til sammen indikerer resultatene av denne studien at bruk av ROCK-hemmer kan redusere vekst og progresjon av prostata ved å undertrykke spredning av prostatakreft og cellevandring mot nerver.

Abbreviations

ADRB2 – β2-adrenergic receptor

ISO – Isoproterenol

DRG – Dorsal Root Ganglia

PNI – Perineural invasion

SNS – Sympathetic nervous system

CNS – Central nervous system

NE – Neuroendocrine

shRNA – Short-hairpin Ribonucleic acid

HS – Horse serum

FBS – Fetal bovine serum

IF – Immunofluorescence

HCI – Hydrogen chloride

EtOH – Ethanol

Ach – Acetylcholine

PFA – Paraformaldehyde

NGF – Nerve growth factor

GPCR – G-protein coupled receptor

BPH – Benign prostatic hyperplasia

MLC – Myosin light-chain

GFP – Green fluorescent protein

PH – Phase contrast

PKA – Protein kinase A

GDNF – Glial cell line-derived neurotrophic factor

ROCK – RhoA-associated kinase

AR – Androgen Receptor

PC – Prostate cancer

KO – Knock-out

PNS – Parasympathetic nervous system

ANS – Autonomic nervous system

NED – Neuroendocrine differentiation

PBS – Phosphate buffered saline

FCS – Fetal calf serum

DMEM – Dulbecco's Modified Eagle Medium

BCA – Bicinchoninic acid

MetOH – Methanol

WR – Working reagent

STE – Sodium Chloride-Tris-EDTA

BSA – Bovine serum albumin

DCX – Doublecortin

Epi – Epinephrine

TME – Tumor microenvironment

VEGF – Vascular endothelial growth factor

DAPI – 4′,6-diamidino-2-phenylindole

TRITC – Tetramethylrhodamine

cAMP – Cyclic adenosine monophosphate

NOD – Non-obese diabetic

Rap1 – Ras-related protein 1

CAF – Cancer-associated fibroblast

NPY – Neuropeptide Y

CO_2 – Carbone dioxide

Ca^{2+} – Calcium ions

ECM – Extracellular matric

RhoA – Ras homolog family member A

IL-6 – Interleukin 6

H_2O – Water

FITC – Fluoresceinisotiocyanat

TRIS-HCL – Trisaminometan hydrochloride

Table of contents

1. Introduction

Prostate cancer (PC) is one of the most prevalent neoplasm among men today, and generally (8). In 2019, total of 4877 men were diagnosed with PC in Norway, in which 37% of the incidents were discovered in the early stages. Most of those diagnosed are over 60 years old and the median age is approx. 70 (9).

Cancer neurobiology have become an emerging field and it is of big interest to see how the nerves can contribute to tumor growth and distant metastasis (10). The neuro signaling and the crosstalk between the nerves and PC cells have become important for treatment, as the mechanism leading to tumor growth and metastasis can be used as therapeutic targets for PC. Blocking communication between nerves and cancer cells may be a new way to stop cancer development and metastasis in the future.

Previous studies have demonstrated that the mechanisms causing PC is not only restricted to cells in the prostate epithelium but is also strongly associated with the communication of nerves and cancer cells in the prostate stroma, suggesting that nerves are active players in PC metastasis (10).

Perineural invasion (PNI) has been defined as the invasion of cancer cells in and on nerves (11, 12) and is the most prominent association between PC and the nervous system, and is known to be one of the most important mechanisms for PC metastasis (13). PNI are more commonly observed in adenocarcinomas, which has a low rate of distant metastasis but is more locally aggressive (14) and is considered being accountable for extracapsular metastasis (15). PNI is associated with poor tumor prognosis and is often linked with a low survival rate in most cancer types (16). Studies suggest that PNI in prostate cancer have been associated with poor tumor prognosis, having a high score on the Gleason grading system (11, 17). In PNI, the prostate cancer cells invade and surround the nerves (15) where the PC cells can metastasis to other tissues by the nerves (18) and enables the cancer cells to spread and migrate on the nerves extending from the tumor towards the central nervous system (CNS). It is found that the PC cells can metastasis by using the nervous system as a track, and in master's project, we wanted to investigate underlying mechanisms for metastasis in PC.

1.1 The human prostate gland

The prostate gland is a part of the male reproductive system (19), located under the bladder neck and posteriorly to the rectum.

The main function of the prostate gland is to provide the seminal fluid (semen) with secretory proteins secreted from the prostate lumen. The secretory prostatic proteins have various roles in the semen, like protecting the sperm cells or increasing the fluidity of the semen (19). The prostatic proteins leave through the prostatic ducts, and mixes with the pre-semen released from the seminal colliculus and forms the semen before ejaculations (3).

1.1.1 Anatomy of the human prostate gland

The prostate gland consists of a base and an apex. The base is the upper part of the gland and is located under the bladder neck. The apex is the lower part of the prostate, right over the external urethral sphincter. The prostate surrounds the urethra extending from the bladder to the external urethral pincer, in addition to surrounding the ejaculatory duct branching from the urethra.

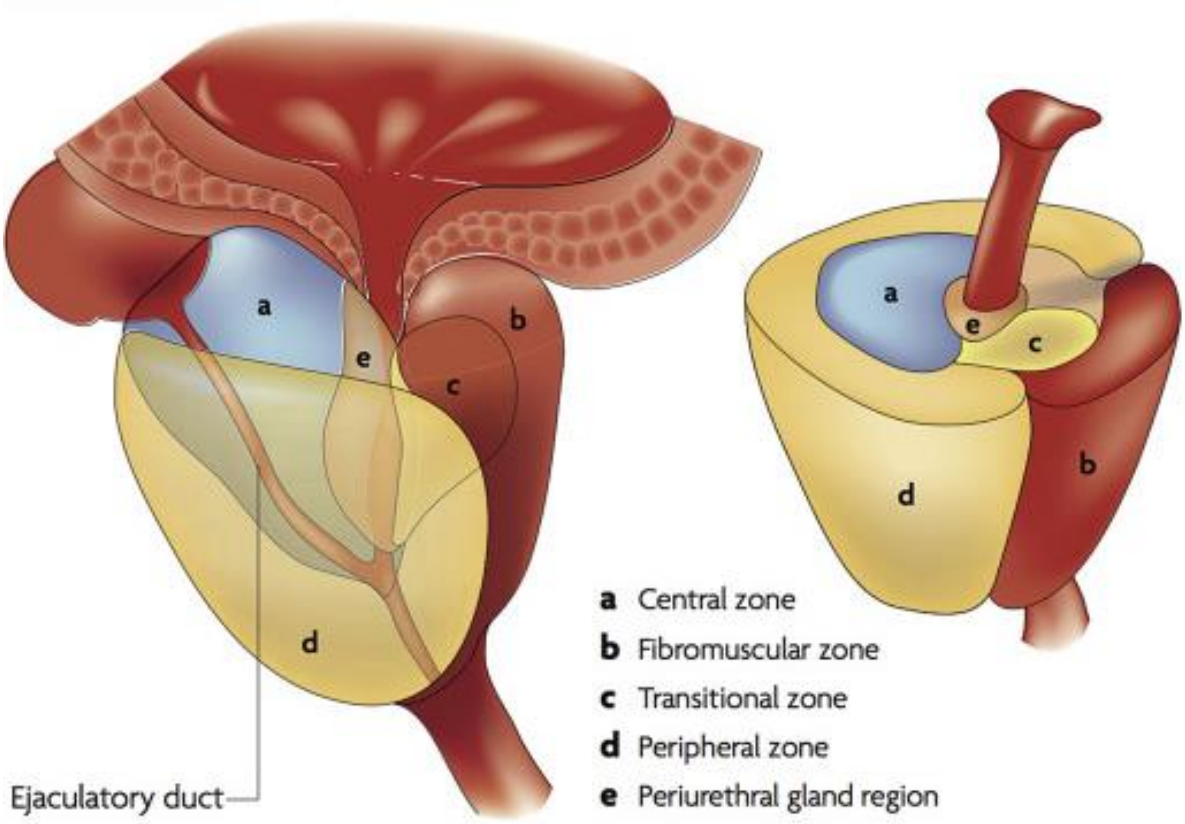

Figure 1 | The anatomy of theprostate gland Schematic illustration of the anatomical strcuture of human prostate gland, with each zone within the gland and adjacent structure. The figure illustrates the compostion of the gland, and the enclosement of the urethra duct in the transizional zone, brancing to ejaculatory ducts through the central zone. Adapted from Reeves et al. (6) with permission from ScienceDirect and RightsLink.

The prostate is divided into 3 different zones, consisting of a central-, peripheral- and transition zone (Figure 1). The transitional zone is the portion of the prostate which enclose the urethra and is located between the anterior region and the peripheral zone. The transition zone is the smallest zone in the gland and represents only 5% of the gland and is the inner zone of the gland (20, 21). The peripheral zone is located in the prostate posterior, accommodating 70% of the whole gland, and is considered the largest zone in the prostate gland (22). The peripheral zone enclose the central zone which envelopes the ejaculatory duct, leading to the seminal vesicle which secretes fluids necessary for the seminal fluid (21).

Prostate enlargement often occurs in the transition zone and is generally caused by a prevalent benign prostatic hyperplasia, and is often seen in elderly men (21). Depending on the size of the enlargement, the hyperplasia can pressurize the bladder which may lead to urination complications. While benign enlargements occur in the transition zone, malignant tumors often grow in the peripheral zone (20).

1.1.2 Tumor growth in the prostate gland

PC mostly arises as adenocarcinomas and is defined as an neoplasm (neoplasia). The peripheral zone is most prone to malignant PC and up to 70-75% of all tumors arise in this zone, whilst the transition zone is more prone to benign prostatic hyperplasia (BPH) (23). Most of the nerves are located in the peripheral zone (24, 25). The cancers which may arise in different zone of the gland can differ structurally and clinically (21). PC is diagnosed based on results from pathological assessment of morphological tissue samples (26).

Even though it is many factors which can lead to PC, there is no factor alone which directly leads to it. Some actors related to occurrence of PC is: aging, heritage, unhealthy lifestyle, and smoking (27). As the tumor is usually diagnosed in men over 50 of age, age may be one of the most influential factors associated with tumor development in the prostate gland.

1.1.3 Tissue and cellular structure of the human prostate gland

The prostate gland is composed of an outer basement membrane, a prostate epithelium, lumen and fibromuscular stroma. The prostate gland consists of basal cells lining the basement membrane and luminal cells enclosing the lumen, whilst the neuroendocrine cells are spread throughout the gland (Figure 2) (22). Generally, these cells can be separated based on expression of different keratin in each cell type and some specific proteins which they secrete and express (28).

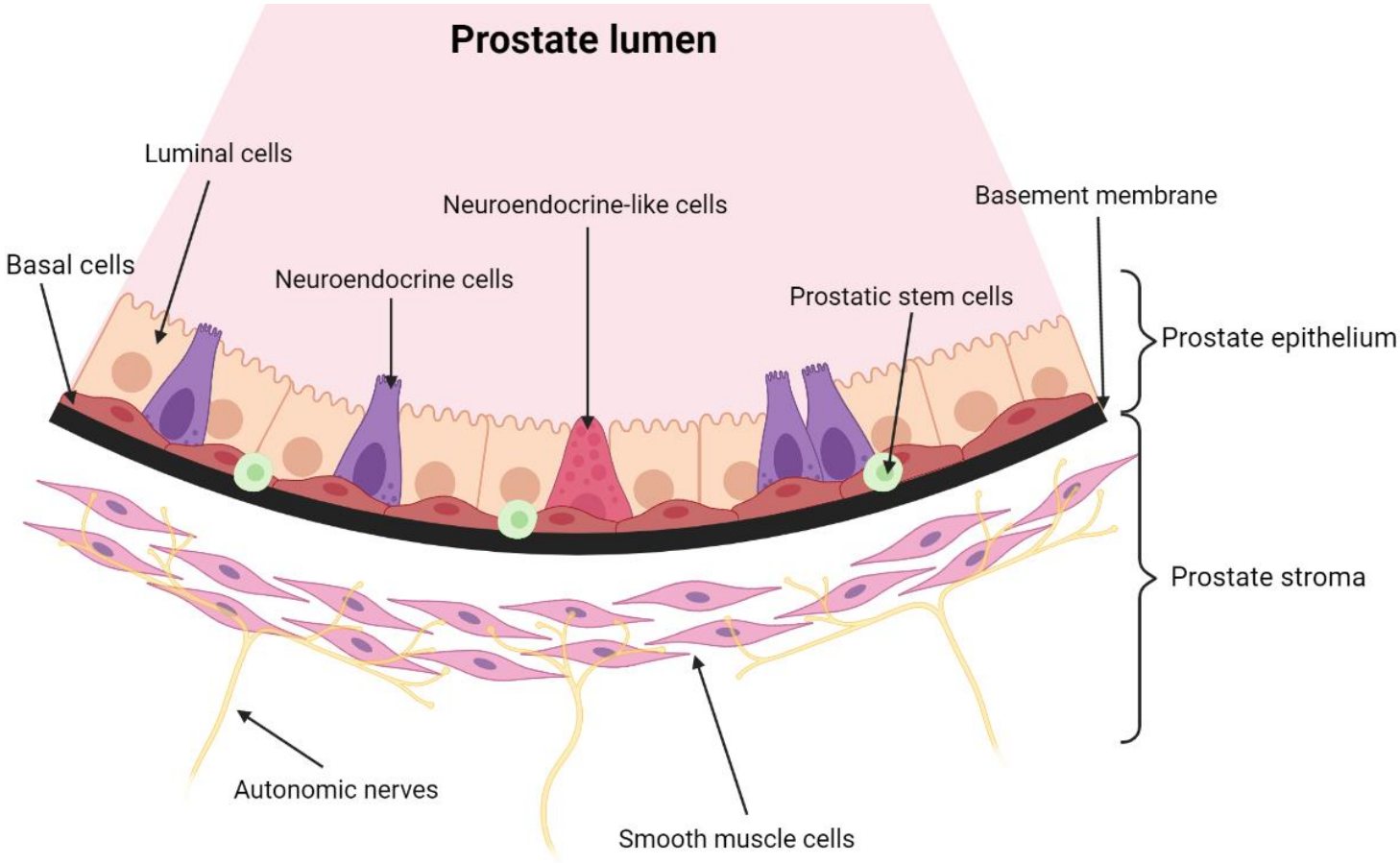

Figure 2 | Cellular structure of the prostate epithelium. A illustration of the placement of each cell line in the epithelium of the prostate gland. Proteins and cytokeratin's expressed by the prostatic cells is illustrated, used as markers for identification of each cell line in the prostate lumen (1-3). Created with BioRender.com

The luminal cells are androgen dependent cells and are androgen receptor (AR) positive cells (29), expressing high levels of the nuclear receptor which also can be detected on the membrane (25). Th luminal cells function to secrete proteins into the lumen where its joined with the pre-seminal fluid (semen) (21). Some of the most important proteins secreted by the

luminal cells are the prostate specific antigen (PSA) also called kallikrein related peptidase 3 (KLK3) (30). PSA is a serine protease known to functioning to liquefies the seminal fluid and enable the sperm cells to swim freely in the fluid (31). Elevated or high levels of PSA is often related to malignant tumor or other prostatic ailments.

Located at the basement membrane, the basal cells are epithelial cells which lack PSA and are AR negative cells or express very low levels of it (2, 3, 29). Unlike the luminal cells expressing important secretory proteins, the function of the basal cells is not clear, but it is believed that these cells are important for supporting the luminal cells and the glandular structure.

The last cells in the prostate epithelium is the neuroendocrine cells. They are intraepithelial cells which secrete prostatic proteins like serine protease. Some theories suggest that these cells ae in control of growth and differentiation in the prostate epithelium and controlling the vesicular transport. The prostatic stroma, which is a fibromuscular layer of the gland located just under the false capsule. The prostate stroma is composed of various cells, like neurons, blood vessels, smoot muscle, endothelial cells and fibroblasts. The smooth muscle fiber laying in the stroma is innervated by nerves extending from the spinal cord (23).

1.1.4 Neural innervation of the prostate gland

Innervation of the prostate is among the most thoroughly studied organ innervations, because of the perceptible nervous inputs from the autonomic nervous system (ANS) (32). The ANS is responsible for controlling and regulating the autonomic and reflexive physiological processes in the body, and innervates the smooth muscles in the body (33, 34). The neural inputs are essential for contraction of the smooth muscles in the gland, which is responsible for proper functioning of the gland (35) and is also important for maturation of the prostate gland (36-39). The prostate gland is well-supplied with nerves from ANS and receives inputs from the pelvic nerve and the hypogastric nerve, and they regulate the gland by inputs from the brainstem through the spinal cord (40), controlling the smooth muscle fibers in the stroma (10, 41). The nerves are innervated both in the prostate epithelium and prostate stroma. Prostate glands deprived of nerves cannot develop or mature and alters the proper functioning of the gland (15).

The nerves innervate the prostate gland as bundles and extends through the outer prostate capsule and passes through the central- and transition zone (25). The nerves extending from

the ANS and further divides into the sympathetic nervous system (SNS) and the parasympathetic nervous system (PSNS), which have efferent and afferent axons innervating the stroma and are proportionately distributed on the outside of the gland (15). The sympathetic fibers are derived from the hypogastric nerve, whilst the parasympathetic inputs arrive from the pelvic nerve (23, 35). The SNS is responsible for controlling the "fight-or-flight" responses (42), primarily increasing the blood pressure and other physiological processes in response to stressors (33).

Unlike the distribution of the parasympathetic nerves, the quantity and density of the branches from SNS are higher in the dorsal-lateral apex (25, 40). The preganglionic parasympathetic goes through the pelvic nerve and joins the pelvic plexus, whereas the preganglionic sympathetic fibers extends from the lumbar spinal cord and goes through the hypogastric nerve and joins the pelvic plexus (10, 29, 35).

The brain and the nerves communicate with the target tissue by using messengers known as neurotransmitters. The release of the neurotransmitters are dependent on the SNS and PSNS innervating the prostate gland. These messengers are synthetized in nerve cells (neuron) and transported in axon of the presynaptic cell synaptic vesicles (5). After a nerve impulse, the vesicles fuses with the membrane of the axon terminal (pre-synaptic cell) and released into the synaptic cleft where it can start a signal cascade by binding receptors on the dendrites (post-synaptic cell) (43).

1.1.5 Cholinergic and Adrenergic nerves in the prostate gland

The nerve fibers from ANS innervating the prostate are divided in two group based on the neurotransmitters they secrete; the cholinergic nerve fibers which secrete acetylcholine (ACh) and the adrenergic nerve fibers which secrete norepinephrine. The cholinergic fibers innervate the epithelium, whilst the noradrenergic nerve fibers innervate the stroma (24, 44). Both cholinergic and adrenergic receptors are transmembrane proteins which are G-protein coupled receptors (GPCRs). Activation of both receptors leads to activation of the G-proteins, which induce second messengers that activates downstream proteins which in turn elicit a response that can be excitatory or inhibitory (45). As a result, a neurotransmitter can cause different responses when activating tissue-specific receptors (46).

The adrenergic nerve fibers secrete norepinephrine and include majority of the postganglionic sympathetic fibers. Short adrenergic nerve fibers are innervated in prostate stroma, where they induce contractions in the smooth muscle fibers (35).

The majority of the α-adrenergic receptors have a propensity of being excitatory, and activation of these receptors may result increased secretion of substances as a result of a contraction of smoot muscles. Further, the adrenergic nerves are known to induce the secretion of the prostatic secretory protein from the luminal cells which expresses the β-adrenergic receptors (24, 47).

1.2 Tumor innervation

Tumor innervation can arise as a result of axonogenesis or neurogenesis. As a result of cancer invasion, axons extend into the tumor from the nerves. The axons may be pre-existing axons or they can be grown by axonogenesis (10, 15, 48, 49). These axons are promoted by chemokines and other neurotrophic factors released in the microenvironment of the tumor, promoting a neural network. It is believed that most of the neurotropic factors are a part of the neurotrophin family, related to the nerve growth factor (NGF) (43, 50). The PC cells can stimulate axonogenesis through the neurotrophic factors. This were demonstrated in a co-culture study, were neurites from dorsal root ganglia (DRG) were grown towards the PC cells in the co-culture (51).

The precursor neurite growth factor (proNGF) have been suggested to promote innervation of cancer in PC and other types of cancer (50). By immunohistochemical analysis, it has been observed that malignant epithelial cells had a high cytoplasmic concentration of proNGF compared normal stromal cells in the prostate. High cytoplasmic concentration of proNGF have also been associated with cancers having a high Gleason score (≥7). Further experiments have also shown that neurite outgrowth toward PC cells can be blocked by using antibodies against the proNGF, suggesting that proNGF promote PC cell induced axonogenesis (15, 43, 50).

In neurogenesis, the number of nerves penetrating the tumor may increase by formation of new nerve fibers through neurogenesis (10, 15, 52). In vitro studies suggested that some of the neurons in the PC extends from the CNS. It is also suggested that these neurons are progenitors from the subventricular region of brain, transported through the blood stream. The

progenitors can penetrate the tumor, where they can increase and develop as autonomic nerve fibers (48, 50, 53). This is a tumor distinct process, which acquires neurons from the tumor microenvironment (TME) that promote tumor growth and metastasis (54). The progenitors migrating to the prostate gland are developed progenitors expressing the neural migration protein doublecortin (DCX) (55-57), making the progenitors doublecortin positive (DCX+). DCX+ is used as a marker for the progenitors, which can be used to track these neurons in the TME as they develop and serve as autonomic fibers and generate adrenergic nerve fibers. The establishment of new autonomic nerves also leads to activation of the cholinergic receptors as well as the β-adrenergic receptors, which leads to the progression of the PC (48, 58).

Inhibition of the neuro signaling in the TME may contribute to suppressing the tumor growth and metastasis, specifically blocking the cholinergic and adrenergic receptors in the gland and TME (13). However, Mauffrey et al. (59) suggested that genetic depletion of DCX+ can suppress the development of tumor, when employed in the early stages. The density of DCX+ in the neural progenitors, is suggested to be associated with the aggressivity of the PC, where higher density gives a more aggressive PC. These findings shows a cross link between the nervous system and PC, which can be potential targets for PC treatment (59).

1.2.1 Perineural invasion and neural innervation of the tumor

In recent years, it has been that the neurons in the TME plays an important role in growth and metastasis of PC. The best evidence is perineural invasion (PNI) of the cancer cells from the tumor to the neurons, creating a crosstalk between the PC and CNS. As well as the neural tissue, the TME contains neurotrophic factors, neurotransmitter and axon guidance molecules which is crucial for tumor innervation. These proteins and molecules are secreted from the active cells within the tumor: neuroendocrine cells, cancer cells and elements in the prostate stroma (10, 60). The signaling in the TME, consisting of cancer cells and nerve cells, results in crosstalk between these cells leading to growth and progression of PC, through perineural invasion (PNI) (51, 61). One of the well-known elements in the TME are the activated fibroblasts, referred to as cancer associated fibroblasts (CAF). CAFs are known to regulate PNI, cell growth, and to regulate the release of chemokines, cytokines and growth factors. These soluble molecules and proteins are important for the communication and interactions between the PC cells and TME, increasing growth and proliferation of PC.

In recent years, it has been revealed that nerve filaments are an important participant in TME in some neoplasm, especially PC. This participation has been suggested to help migration of the PC and promote the growth of the tumor through various mechanism (10).

1.2.2 Chemokines inducing perineural invasion (PNI)

Some theories imply that chemokines released from the nerves may engage the migration of the cancer cells towards the chemokines (11, 62-64). Chemokines are soluble signaling proteins, which is secreted by cells and may regulate cell migration (65). These chemoattractant have also been suggested to play a crucial role in PNI and tumor progression (66-68) and may also contribute to distant organ metastasis through the nervous system (11, 69, 70). It is believed that norepinephrine released from the sympathetic nerves in the dorsal root ganglia (DRG) can attract the tumor cells to neural tissue, promoting migration and metastasis and thus inducing PNI (71).

Recent studies have also suggested that Schwann cells in the peripheral nerves is associated with the invasion of the PC cells. It is known that these cells are crucial actors in nerve regeneration and mediate repair of the axons (72). An earlier study by Deborde et al. (73) demonstrated that the Schwann cells recruited pancreas cancer cells on nerves, an initiated migration along the nerves. This experiment suggested that physical contact is a crucial factor for the migration (61, 74). Earlier studies have also proclaimed that these Schwann cells release soluble substances which is important in signaling with the cancer cells, leading to migration of the cancer cells toward the nerves. However, this has only been demonstrated in a pancreatic cancer model (61).

A number of studies have investigated the targeting of chemokine ligand 2 (CCL2) for suppressing PNI in PC (68), given its function in PNI in other cancers. It was revealed that CCL2 is associated with development of cancer and cancer progression in other cancers as well (65, 69). It is suggested that CCL2 is one of the soluble proteins secreted by the Schwann cells, which can lead to cancer invasion. CCL2 is known to be a chemoattractant in neural injuries, facilitating the attraction of macrophages to the damaged nerve or neural tissue (75). Interestingly, expression of the CCL2 receptor, CCR2, has been detected in cancer cells membrane (11). Earlier studies demonstrated that binding of CCL2 to its receptor CCR2, caused pancreatic adenocarcinoma (67, 68). It was stated that activated CCR2 can induce the invasion of cancer an promote the growth of cancer. It was also reported that metastasis

induced by CCR2, led to colonization of the cancer cell in the metastasized tissues and organs (76). However, there is a small number of studies on chemoattraction induced PNI in PC.

1.2.3 β-2 adrenergic receptor (ADRB2)

The adrenergic receptors are divided into two classes: α- and β-adrenergic receptors and further to subgroups of: α-1 and -2, β-1,-2 and -3 (77).

When released, norepinephrine binds and activates the β2-adrenergic receptor (ADRB2) which in turn activates the GPCR. Active GPCR causes increase in cellular concentration of cyclic adenosine monophosphate (cAMP), which in turn activates the cAMP dependent protein kinase A (PKA) (78). Active PKA may then activate downstream proteins, and then elicit the excitatory or inhibitory response, one being increased concentrations of Ca2+ (24, 79).

The β2-subtype is the most prevalent out of the β-class in the prostate and are generally expressed by the luminal cells in the prostate gland (24). ADRB2 is also the most active adrenergic receptor in the human prostate cancer cell line like PC-3, LNCaP and C4-2B (77).

ADRB2 is primarily activated by binding of adrenalin and norepinephrine, having a higher affinity towards adrenalin (78). Moreover, activation of the ADRB2 receptor can lead to outgrowth of neurites. Active PKA can suppress the activity of ras homolog family member A (RhoA) by two mechanisms; directly inhibiting the ras-related protein 1 (Rap1) or activate the serine/threonine-protein kinase 4 (PAK4) which may lead to the suppression of RhoA (80). When inactivated, the RhoA cannot activate the Rho-associated kinase (ROCK), leading to outgrowth of neurites (24).

1.2.4 ADRB2 activity in PC

ADRB2 is expressed in both benign and malignant tumors (81, 82), but studies have revealed that the receptor is overexpressed in malignant tumor cells (81, 83). A study by Yu et al. (83) showed that the level of ADRB2 expression was altered in the metastatic process of PC. Both in vitro and in vivo PC studies have demonstrated that ADRB2 activity in mice is increased upon exposure to stress, and leads to promotion of angiogenesis (84-86) and metastasis (83, 87), illustrating the adrenergic activity can induce PC progression (24).

The ADRB2 receptor is believed to be an important target for PC treatment. Studies on transgenic PC mouse models have demonstrated that deletion of the ADRB2 gene or inhibition by ADRB2 antagonists, caused inhibition of adrenergic activity, which resulted in tumor repression (88, 89). These findings suggest that adrenergic signaling can induce tumor growth and progression, and that specific inhibitors of ADRB2 can inhibit the pro-tumorigenic effects (32).

Recent studies in PC mouse models, have shown that adrenergic signaling is important for tumor progression and may promote angiogenesis under tumor growth (10, 90). Deletion and suppression of the ADRB2 gene have shown to inhibit angiogenesis to the tumor (4). These observations suggest that angiogenesis is strongly connected to ADRB2 signaling in PC (88).

Additionally, Magnon et al. (48) revealed that the density of adrenergic nerves was correlated with the aggressiveness of the tumor. The study found that the density of both sympathetic and parasympathetic nerves adjacent to the tumor were linked with poor prognosis of PC (48).

It is shown that norepinephrine may promote metastasis on PC-3 xenograft mouse. In a study by Lang et al.(87) they demonstrated that stimulation with norepinephrine in PC-3 cells led to high migratory activity (24, 87). These findings suggest that metastasis promoted by norepinephrine, may be a result of the high migratory activity in the PC-3 cells. This activity was inhibited by treating the cells with ADRB2 specific β-blocker ICI-118,551.

Isoproterenol (ISO) is a non-selective short acting β2-adrenergic agonist (91, 92). In a study by Huang et al. (61) PC-3 cells were stimulated with 10 μM of ISO in order to see if ISO influences the migration and invasion of the PC cells through adrenergic nerve activation. The results stated that ISO did not increase the migration of the PC cells, proposing that ISO stimulation does not affect the migration of the PC cells directly (93). However, it remains unknown whether ISO can cause migration of PC cells indirectly.

While the mechanism in which ADRB2 directly contributes to tumor progression is not clear, many theories about the mechanism has occurred. It has been proposed that stress induced catecholamine secretion by the nerves activate ADRB2 on luminal cells and that ADRB2 on the stromal cells are activated by sympathetic stimulation. Preclinical studies have demonstrated that adrenergic signaling induced by stress enhance the tumor progression in PC and other cancers (32, 94, 95). Chronic stress has been detected in many cancer incidences (96) and have been suggested to increase the levels of circulating and intracellular levels of noradrenaline (4, 97). Upon activation, the stromal and luminal cells start the expression of

anti-apoptotic and proangiogenic factors. This leads to favorable environment for PC cells and leads to differentiation of the PC cancer cells to neuroendocrine-like cells (24).

1.2.5 Neuroendocrine differentiation (NED)

Neuroendocrine (NE) cells are a part of the epithelium of normal prostate and is known to produce most of the VEGF in the prostate gland (98). It is known that NE cells are present in the prostate adenocarcinoma as both cluster or individually (99). Studies have observed elevated numbers of neuroendocrine-like (NE-like) cells in PC (100, 101) and adjacent to PNI (102). NE cells are neuroendocrine cells found in normal prostate tissue and are distinguished form the NE-like cells which are trans-differentiated cancer cells (103, 104).

Earlier data strongly suggests PC cells is the origin of the NE-like cells, and that this is accomplished by the process of neuroendocrine differentiation (NED) (103, 105, 106) induced by β-adrenergic stimulation and hormone deprivation therapy (79, 103, 104). NED is associated with poor prognosis, progression of PC and it have also been linked to androgen independence (107, 108).

Several studies have proposed that NED is induced by the increased stress levels, which in turn is induced by adrenergic activity and hormone deprivation therapy. It is suggested that increased intracellular levels of cAMP mediated by the PKA/CREB signaling pathway (104, 109, 110) and by IL-6 mediated by the STAT3 and PI3K signaling pathways (109, 111-113) (Figure 3). The activation of both cAMP- and PI3K/AKT signaling pathways are usually linked to growth and progression of PC, and it is suggested that some of the PC cells can get transdifferentiated amid the growth of a PC (7). In consequence, NE-like cells are preexisting in the PC before diagnosis, thus creating a resistance against treatments and therapies targeting the PC (7, 101, 105, 114). Besides pre-existing NE-like cells in PC, NED can be induced by therapy or by several therapeutic agent (7). Recent studies have shown that agents against castration resistant prostate cancer (CRPC), like enzalutamide, can induce NED and revealed that NED increases mortality in CRPC (106, 115). Further, in a study by Lin et al. (116) it was reported that NED was induced subsequent to castration in a patient derived xenograft (7, 116), suggesting that castration may result in NED.

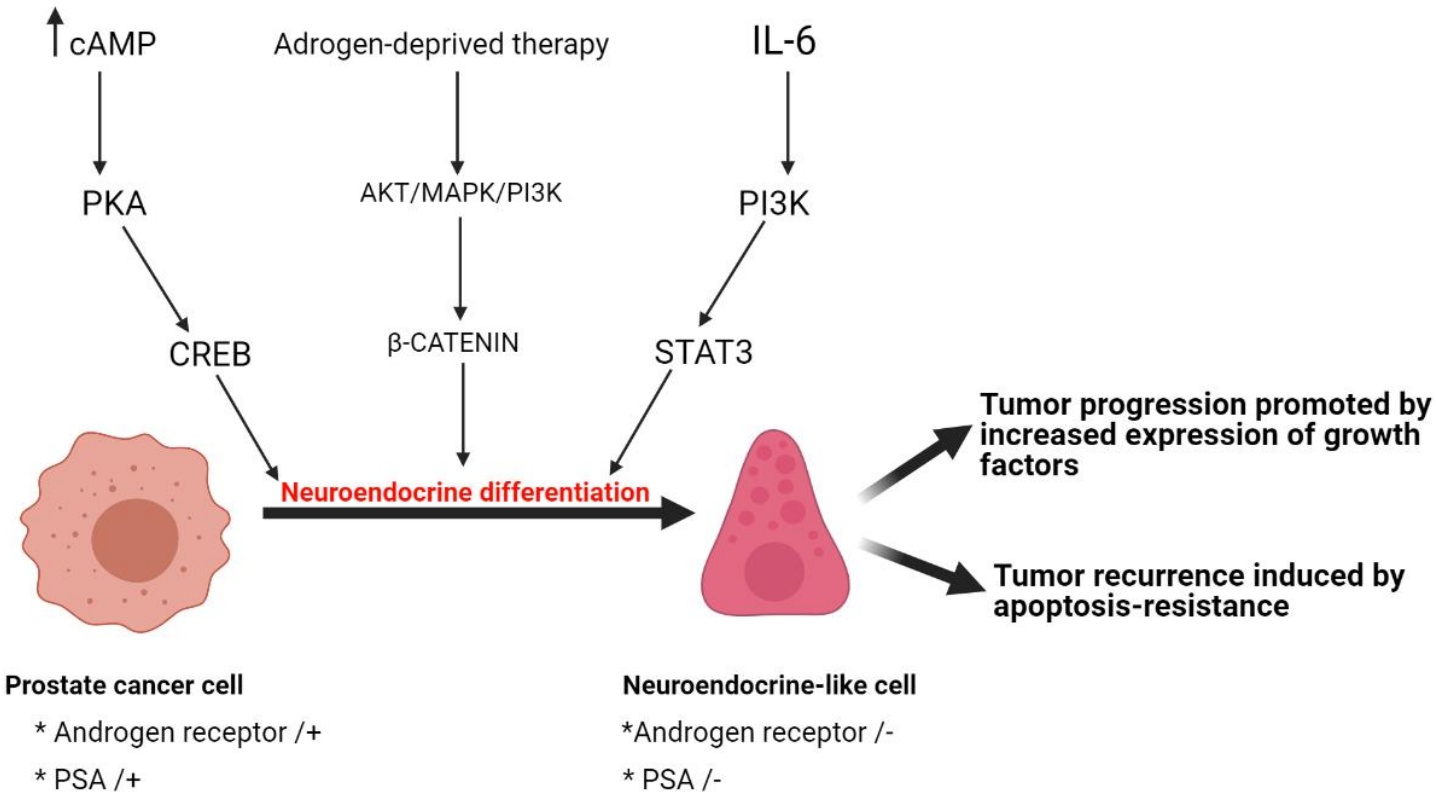

Figure 3 | Purposed mechanism of neuroendocrine differentiation of prostate cancer cells. Schematic illustration of NED in prostate cancer cells, induced by several mechanisms which in turn is induced by high concentrations of stress. It is proposed that stress induces higher intracellular levels of both cAMP and IL-6, leading to NED by different signaling pathways. Additionally, androgen-deprived therapy has been shown to stress the prostate cancer cells, promoting NED (7). Created with BioRender.com

Both in-vivo and in-vitro PC studies in mice have shown that increased ADRB activity induced by stress promotes NED (79, 103, 104, 117), in addition to inducing angiogenesis (84-86), metastasis (83, 87) and causing resistance against apoptosis (95, 118). A couple of studies by Cox et al. (79, 104) stated that both isoproterenol (ISO) and epinephrine can increase intracellular concentration of cAMP, increasing the activity of PKA and the number of NE-like cells (79, 104). Further, it has been shown that cAMP induce NED in both PC-3 and LNCaP cells (117, 119, 120).

Some studies have also established that NE cells within the tumor can secrete neuropeptides (24, 121, 122), enhancing growth of PC cells and also increase the energy intake through the blood vessels. The NE-like cells is not capable of proliferation and do not express PSA and AR like PC cells (Figure 3), but in contrast they express anti-apoptotic genes like BCL-2 (123) and survivin (124), contributing to resistance against treatments and therapies (7) and are the factors distinguishing NE-like cells from NE cells(103). These factors all together ensure therapeutic resistance and contributes to growth and progression of NED PC (7).

1.2.6 Angiogenic switch induced by adrenergic stimulation

A study by Decker et al. (125) revealed that latent prostate cancer laying in the bone, were reactivated through adrenergic signaling in the sympathetic nerves inside the bone marrow. This was shown using a in vivo mouse model, where NE secreted by the SNS could reactivate the PC cells in latent bone metastasis through ADRB2 activation (125). These results revealed that adrenergic signaling, which is involved in growth of PC (48), also have an important role by exhibiting the same response in PC that metastasis through the bone. Importantly, the study stated the importance of nerves in PC, in which they play an active role in both tumor growth and metastasis (43).

This mechanism were then further analyzed by Zahalka et al. (4), who demonstrated that sympathetic stimulation can lead to activating a angiogenic switch in knockout mice with low expression of the adrenergic receptors ADRB2 and ADBR3 (ADRBko). Further, by employing a tumor cell implantation in the ADRBko mice, it was observed that the growth of the tumor were arrested as well as an shrinkage of vascular density. These findings suggested that active adrenergic signaling is important for angiogenesis in the TME (43).

Combined, these studies defined the angiogenic-switch which controls the metabolism of the endothelial cells and asserts the critical role of the ADRB2 for tumor growth and progression (Figure 4). The experiments exhibit the importance of the adrenergic innervation of the endothelium, and how the adrenergic signaling control the metabolism of the endothelial cells by stimulating the angiogenic switch which in turn leads to a high-grade prostatic intraepithelial neoplasia that can develop into an aggressive malignant tumor. Noteworthy, the study by Magnon at al. (48) claimed that both the ADRB2 and ADRB3 is required for the PC progression, whilst the study by Zahalka et al.(4) found that only ADRB2 were decisive for the PC progression. These observations make the ADRB2 a clearly target for suppressing the growth and progression of PC (43).

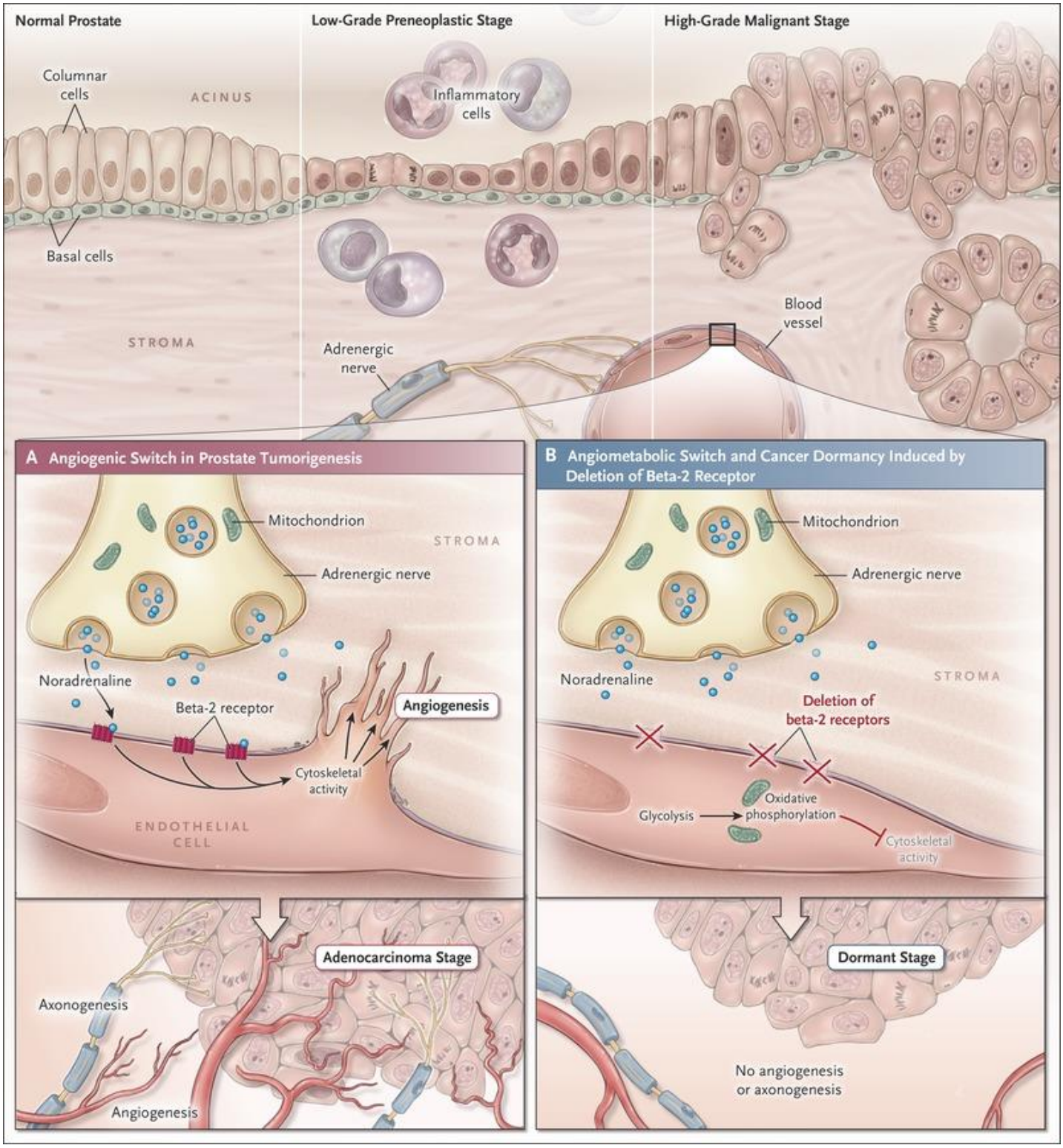

Figure 4 | Angio-metabolic switch in the prostate gland. Schematic illustration of the importance of ADRB2 activity in the progression and development of PC. **(A)**The figure illustrates the mechanism of angiogenic switch, were released noradrenaline activates the luminal ADRB2 receptors, inducing angiogenesis and axonogenesis by enhancing cytoskeletal activity. This activation enables progression and growth of the tumor, resulting in a adenocarcinoma. **(B)** The figure illustrates the angio-metabolic switch, where the deletion or inhibition of ADRB2 leads to oxidative phosphorylation, inhibiting cytoskeletal activity. This mechanism inhibits angiogenesis as well as axonogenesis, leaving the tumor in the dormant stage (4, 5). This figure was adapted from Chen et al.(5) by permission from NEJM and RightsLink

1.2.7 Rho-associated kinase (ROCK)

The Rho-associated kinase (ROCK) is an important kinase in mammals, which is involved in many mechanisms including migration of cells through the cytoskeleton and a crucial downstream effector of the Rho-GTPase (88, 89, 126). There are two isoforms of ROCK, referred to as ROCK1 and ROCK2 (127). The isoforms are not so different from each other having a 92% homology between their catalytic domains (128), but they are expressed differently in tissues and have different targets (129, 130). ROCK 2 is known to be expressed in nervous system and neural tissues, whilst ROCK 1 is expressed in mostly skeletal-muscle and non-neuronal tissues (69). An overexpression of ROCK1 (ROCK) is seen in many cancer types, PC included, and have shown to increase metastasis and migration of tumor cells (131, 132).

The high levels of ROCK are associated with poor prognosis and tumor progression in PC (133-136), and it is also proposed that ROCK contributes to growth of tumor cells even though the details of this mechanisms are not known (128, 137). Recent studies have shown that ROCK signaling can promote tumor growth, through regulating the ECM and alter the flexibility of the tissues (130, 138).

Earlier studies have shown that ROCK is involved in c-Myc stabilization through S62 phosphorylation in breast cancer, but how ROCK contributes to this mechanism is not clear. ROCK is activated by binding to RhoA-GTP, and the active ROCK can then activate downstream proteins by phosphorylation like for example myosin light-chain (MLC), resulting in changes of the cytoskeleton architecture (126). Activation by ROCK usually results in the regulation of the cytoskeleton. A study by Zhang et al. (128) demonstrated that involvement of the ROCK regulation in PC growth. It was shown that active ROCK induced phosphorylation of the proto-oncogene c-Myc, which lad to an increased transcription of c-Myc. It was revealed that, increased transcription of the RhoA-gene resulted in a positive feedback regulation by c-Myc on ROCK. The findings showed that, by directly or indirectly inhibiting the ROCK activity can suppress the progression of a prostatic tumor, providing a new target for PC treatment (128).

1.2.8 Inhibition of ROCK activity

ADRB2 signaling studies have shown that, by inhibiting the downstream protein of the RhoA signaling pathway ROCK can be inhibited, resulting in the outgrowth of neurites (139). It is theorized that neurite outgrowth arises after recovery of damaged neurons and nerve related disorder, linked glial scars and death of neurons (140, 141). It were reported that these injuries and disorders may arise from upregulation or overexpression of ROCK (140, 141). Inhibiting the ROCK activity with ROCK inhibitor Y27632 induced the recovery of both neural fibers and functions (142-144). Further observation in cell models, demonstrated that use of Y27632 also induced neurite outgrowth in the cells (140), linking the response of Y27632 with neural regeneration. In a study by Fujita et al. in a cell model, the effect of Y27632 and nerve growth factor (NGF) were observed to give the same response (145-147).

In the same way as Y27632, NGF were able to suppress the expression of ROCK. Further, the neurite outgrowth by NGF stimulation were virtually everted by activation of ROCK, suggesting that ROCK inhibition through NGF promoted neurite outgrowth (145-147). The outgrowth of the neurites was observed within 3 days upon stimulation with Y27632 and NGF, but it were speculated if the neurites were keep growing after 3 days and more. This were tested on PC-12 cells (pheochromocytoma cell line), which were inhibited with Y27632 and NGF for 6 days. The PC-12 cell line is optimal for studying and altering the neural functions. The inhibition with Y27632 for 6 days resulted in decrease in norepinephrine secretion, whilst the cells stimulated with NGF did not respond the same way (148, 149). These results suggested that inhibition of ROCK with Y27632 may cause a resistance against neurite outgrowth after 3 days, because stimulation for more than 3 days resulted in the collapse of neurite outgrowth (139, 141).

Earlier study by Yin et al. (139) proved that the adherent PC-12 ADH, a subline of PC-12, had a higher sensitivity against all ROCK inhibitors in outgrowth of neurites compared to the original PC-12 cell line (150, 151). Additionally, they discovered the resistance against neurite outgrowth were linked to the enhances signaling of the cyclooxygenase-2 (COX-2) pathway, even though the inhibition of the pathway did not fully enhance the resistance. The findings purposed that several other genes and signaling pathways may play a part in this process (139, 141).

The study by Yin et al. (139) demonstrated the effects of NGF and Y27632 in both PC-12 cells and in PC-12 ADH cells. Both cell lines were stimulated with 300 ng/mL of NGF and 33

mM of Y27632. The results showed that cells stimulated with NGF had neurite outgrowth after 48 hours, whilst Y27632 did not induce neurite outgrowth in the PC-12 cells, coherent with previous studies (151). In contrast, Y27632 were able to induce neurite outgrowth in the PC-12 ADH cells, causing a resistance to neurite outgrowth after 72 hours or more. Both the NGF and Y27632 induced neurite outgrowth in the PC-12 ADH cells, but the NGF did not cause resistance as seen in Y27632. These results were coherent by the study carried out by Duan et al (150). The effect of both inhibitors was similar in the PC-12 ADH cells, and there was no significant difference was observed until 72 hours. Further, it was observed that the resistance against Y27632 in the PC-12 ADH cells occurred after stimulation 72 hours or more, causing a significant difference in the effect of the inhibitors as the Y27632 effect decreased significantly (139). The resistance were proved by visually assessment and by time-response curve, and were also coherent with earlier study by Duan et al (150).

1.2.9 β-blockers

Epidemiological studies in different cancer types, have reported that the β-adrenergic antagonist (β-blockers), have shown beneficial and promising effects on mortality in some studies whereas other studies have not seen a association (152, 153). Oure research group, the tumor biological department at Radiumhospitalet, was the first group to demonstrate that β-blocker use were shown to reduce PC related mortality, and this were also seen in other cancer types. As a result, β-blockers are used in clinical studies today, and can soon be used to treat PC and inhibit metastasis.

In a study by Cardwell et al., a case-control study was employed on β-blockers and the PC mortality was assessed. The findings of the study suggested the use of β-blockers was associated with decreased risk of PC (152). In another study by Assayag et al. (153) they observed no association with the use of β-blockers and reduction in cancer mortality. Furthermore, a meta-analysis on 16,825 patients showed that β-blockers use was associated with decreased risk of cancer mortality (154). Further, in two clinical cohort studies with aggressive PC patients were carried out in Norway, reported that β-blocker use was related to decreased mortality caused by PC (155, 156). In opposition to this study, another case-control study in UK did not see an association with decreased PC-related mortality and β-blocker use (152).

Without regard to the findings, it has been stated that β-blockers have been linked to suppress the progression of some cancer types (157) and inhibiting distant metastasis. It is also proposed that the use of β-blocker lowers the risk of tumor recurrence (158) and can provide a longer relapse free prognosis (24, 159).

All together these data suggest that β-blocker is a promising candidate for inhibiting metastasis in PC, but more studies are needed in order to demonstrate the role of ADRB2 in progression and metastasis of PC.

2. Aims of study

The overall aim of this study is to demonstrate how the activity of β-adrenergic receptors and Rho-associated kinases regulate the migration of prostate cancer cells towards the differentiated neural cells and how this effect is modulated by Schwann cells, previously shown to support nerve-cancer cell interactions.

Prostate cancer cells are known to metastasize through nerves and sympathetic activation has been shown to promote metastasis in several cancer types including prostate cancer. Previous work from our lab has shown that use of β-blocker is associated with reduced risk of prostate cancer specific mortality supporting a role of β-adrenergic activity in regulation of the metastatic process. To study migration of prostate cancer cells along nerves, we optimized the experimental conditions for neurite outgrowth. Time- and concentration-dependent effects on several parameters describing neurite outgrowth was determined by treating the cells with a Rho-associated protein kinase-inhibitor, Y27632, and isoproterenol, an β-adrenergic receptor agonist. The migration rate of prostate cancer cell lines (C4-2B and PC-3-Luc2-GFP), differentiated neural cells (PC-12 ADH) and Schwann cells (RSC96) were determined in co-culture experiments. As controls, we determined proliferative capabilities of each cell line in the presence and absence of ROCK inhibitor or isoproterenol. Knock-down cell lines of β2-adrenergic receptor was made confirm the putative role of β-adrenergic activity on neurite outgrowth and migration rate.

Finally, an ex-vivo model system with dorsal root ganglia and C4-2B cells was established to study the migration of the prostate cancer cell lines towards the neural cell.

3. Materials and methods

3.1 Cell Lines, Medium and Stimulations, Thawing and culturing of cells

3.1.1 Cell Lines

The nerve cell used for this study were the adherent pheochromocytoma cell line isolated from the adrenal glands of rats, the PC-12 ADH (ATCC, #CRL-1721.1). The neural rat cell line is widely used in neuroscience research, and the adherent phenotype (PC-12 ADH) is distinguished from the original cell line PC-12 by being a more adherent and enables well-attachment without coating. The PC12-ADH cell line is tumorigenic and expresses catecholamines like norepinephrine and dopamine (160).To improve attachment even more, the PC-12 ADH cells were cultivated modified Corning Cellbind® T-75^2 (Corning #3290) flasks with ventilation caps. (160)

The other neural related cells used in this study was the Schwann cell line RSC96 (ATCC, #CRL-2765). These are glial cells (non-neuronal) that originates from the spinal cord of rat (Rattus norvegicus) and has a myelinating phenotype which provides a myelin coating surrounding the nerves, specifically in the peripheral nervous system. This cell line is widely used in research of regeneration of nerves and to treat axonic damages and neural disorders (161). The RSC96 cells were cultured in Corning® T-75^2 (Corning #430641U) flask with ventilation caps (162, 163).

Two different human prostate cancer cells were employed in this study, both being hormone refractory. The transgene prostate cancer cell line PC-3-Luc2-GFP (Caliperls, #CRL-1435), is isolated from metastatic site in the bone and originates from a human prostatic adenocarcinoma. The PC-3-Luc2-GFP cell line expresses green fluorescent protein (GFP) when expose to UV and expresses luciferase. The cell line is widely used for in vivo experiments and can be used for identification of GFP positive cells and in tumor models by using the fluorescent activated cell sorter (FACS). The PC-3-Luc2-GFP cells were cultured in Corning® T-75^2 flask with ventilation caps.

The main prostate cancer cell line used in this study were the human prostate cancer cell line C4-2B obtained from Professor Leland W.K Chung lab (164, 165).

The C4-2B cell line is derived from the LNCaP cell line from the human prostate cancer, from a metastatic site in the bone.

Originally C4-2B cell line was generated by the injection of LNCaP cells into a male mouse (164) with human fibroblasts. The mouse were castrated post injection, and the injection of the cells caused growth of a tumor, in which the cells were isolated from resulting in the C4-2 sub cell line (165). Further, to generate the bone metastatic subline C4-2B, isolated C4-2 cells injected into pre-castrated mouse orthotopically. Upon developing large tumors in the prostate, the cells were isolated from the tumor, resulting in the hormone refractory C4-2B cell line(164, 165).

The C4-2B cells were incubated in Corning® T-75^2 flask with ventilation caps as well.

3.1.2 Thawing and culturing cells (mono-cultures)

Ampoules from each cell line were gently thawed in water bath, and then added to 15 mL tubes with 10 mL of respective growth medium. The tubes were then centrifugated at 1000 RPM for 5 minutes. Further, the supernatant were discarded and cell pellets were resuspended in 5 mL of growth medium. 10 mL of growth medium were then added to the flasks, and the cell suspension were transferred to the flask. The flasks were then placed in the incubator at 37 °C with 5% Carbon Dioxide (CO_2) and humified air.

When reaching 70-80% confluency, each cell-line were split. The cells were first washed with 2 mL of 1x Trypsin (Trypsin, EDTA 1x, Sigma) further, 3 mL of Trypsin were added. Trypsin is a proteolytic enzyme which breaks down adherent proteins, releasing the cells from the bottom of the flask**.** Cells were then trypsinized at room temperature for about 5 minutes, or to most of the cell had detach from the flask. The cells in the flasks were checked with the aid of a microscope (4x) to confirm that all the cells had come off completely, if not if they were shaken and possibly put back into the incubator for about 2 minutes. The cell suspension were then exposed to 8 mL of growth medium with 10% Fetal Calf Serum (FCS) which cease the trypsinization effect**.** The cell-suspension were then transferred to a 15 mL centrifuge tubes, and then placed in the centrifuge at 1000 RPM for 5 minutes. The centrifugation collects the cells in the suspension into a pellet at the bottom of the tube. The supernatant were discarded, and the pellet were resuspended in 10 mL of growth medium. Following, 100 µL of the cell-suspension were transferred to a Eppendorf tube, and pipetted by Via1-Cassette

™ (Chemometec, #941-0012) and inserted into the NucleoCounter® NC-200™, which provides the number of live, dead and aggregated cells in the cell-suspension. The Vial-Cassette secure high precision and carries built-in fluorescent dyes (Acridine Orange and DAPI) which automatically dyes the cells in the Vial-Cassette. The dyed cells can then be analyzed, counted and categorized on NucleView™, which provides the precise numbers of the living-, dead- and aggregated cells (166). Following, the cells were split; The PC-12 ADH and RSC96 cells were split to new T75 flasks with 500 000 cells per flask, C4-2B cells were split to a new T75-flasks with 1 000 000 cells per flask.

All cell lines were given fresh medium every 2-3 days.

3.1.3 Preparation of growth medium and stimulations

Mediums

The PC-12 ADH cells were incubated Ham's F-12K (Kaighn's) Medium (Gibco™ #21127022) with 15% HS (Horse Serum, Gibco #26050088) and 2,5% FCS (Fetal Calf Serum, Sigma #F7524).

The RSC96 cells were incubated with Dulbecco's Modified Eagle's Medium (DMEM) (ATCC, #30-2002) with 10% FCS.

The PC3-Luc3-GFP were incubated with RPMI-1640 (Sigma, #R8758-500ML) with 10% FCS.

The C4-2B cells were incubate with 4 DMEM with 25% F-12k ham, 5% FCS and 5 mL T-medium.

T-medium (100 mL): 50 mg Insulin (Sigma #I0516) where diluted in 5 mL of PBS with 0,1% Bovine serum albumin (BSA) and transferred to a glass flask. Further, 136 ng of T3 (Sigma #T2877) were dissolved in 1 mL of 1 M NaOH (Sigma, #367176) and then added 24 mL of DMEM. The solution consisting of 40 µg/mL T3 were diluted 1:100 in PBS with 0,1% BSA. Subsequently, 340 µL of this solution were transferred to the flask. Further, 250 mg of Adenine (Sigma #A3159) was dissolved in 1 mL of 10 M HCL and mixed with 24 mL of PBS with 0,1% BSA to a final volume of 25 mL. Furthermore, 2.5 mg of Biotin (Sigma #47868) and 50 mg of Apo-Transferrin (Sigma #T4382) were weighed and dissolved in PBS with 0,1% BSA.

The final volume were then adjusted to 100 mL with PBS with 0,1% BSA. After mixing all solutions, the final solution were filtered with 0,2 µM Cellulose acetate membrane filter (VWR, #514-0064) and divided into 20 tubes individual tubes with 5 mL in each.

Stimulations

A medium with of RPMI 1640 Medium, no glutamine (Gibco™, #21870076) with 1% Glutamax and 1% HS (Horse Serum) were prepared and used for every stimulation throughout the study. A low level of HS (1%) were employed to partially starve the cells in order to synchronize each cell to the same phase of the cell cycle and to prepared the cells upon the treatment and make them more vulnerable in order to ease the uptake of the inhibitors.

Concentration	Stock (µL)	dH_2O (µL)
1 µM	2	98
10 µM	20	80
25 µM	50	50
50 µM	50	0

Table 1 | Dilution for concentrations of Rho protein kinase inhibitor

All cell lines were treated in order to stimulate the outgrowth of neurites and to portray the how each treatment affects the migration and interaction between the prostate cancer cells and nerve cells.

Concentration	Stock (µL)	MetOH (µL)
10 µM	20	80
5 µM	10	90
1 µM	10 µL of 10 µM Dilution	90
0,1 µM	10 µL of 1 µM Dilution	90

Table 2 | Dilution for concentrations of Isoproterenol

An Isoproterenol hydrochloride (ISO, Sigma-Aldrich #I5627) 10mM stock was prepared in MetOH (Methanol) and the concentrations were diluted accordingly to table 1. The Rho-kinase Inhibitor (ROCK, Sigma-Aldrich #Y27632) stock were diluted in 312 µL of dH_2O (distilled water), and the concentrations were diluted accordingly to table 2.

3.2 Detection of neurite outgrowth

Each cell line were stimulated with concentration curves of ROCK-inhibitor and Isoproterenol, in order to observe the effect of each concentration and determine the optimal concentration, inducing the longest and the highest number of neurites.

The cells were stimulated up to 72 hours and the experiment was repeated at least three times (biological replicates).

A total of 6000 cells per well were seeded for the nerve cells (PC-12 ADH and RSC9), and 8000 prostate cancer cells (C4-2B and PC3-Luc3-GFP) were seeded in each well of a 12 well plate. In order to get a more accurate measurement of the neurites and a lower confluence, fewer cells were seeded.

Controls in well A1 and A2 were incubated with respective growth medium, whereas all the other wells were incubated in treatment medium (Figure 5).

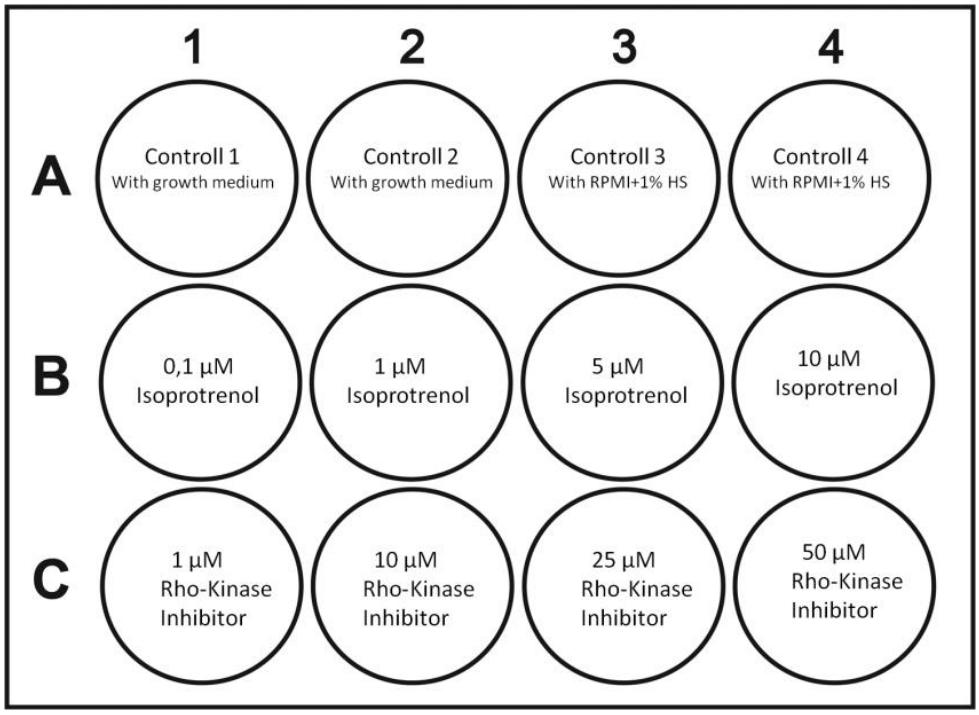

Figure 5 | A schematic illustration of the setup for concentration curves of ROCK-inhibitor and ISO. All cells were cultivated in stimulation medium, except A1 and A2 which was cultivated in respectively growth medium

After 24 hours, the wells were inspected on the microscope in order to see if the cells were attached and healthy. Further, well B1-B4 were treated with a concentration curve of ISO, and well C1-C4 were treated with a concentration curve of ROCK inhibitor. In order to perform the concentration curve on the cell lines, concentrations of each inhibitors were selected based on earlier studies. The concentrations selected for stimulation were chosen based on earlier

studies. The concentrations of ISO were: 0,1 μM, 1 μM, 5 μM and 10 μM, and 1 μM, 10 μM, 25 μM and 50 μM for the Rock-inhibitor.

The diluted concentrations of the ROCK-inhibitor and ISO were stored at -20°C in between use and were always kept on ice under work.

Following treatment, the microplate were inserted in the IncuCyte FLR Imaging system for 5-7 days and all experiments were repeated at least three times.

3.3 Cell counting

In order to get an accurate count and measurement of proliferation and, each cell line were cultivated with stimulation medium with stimulation of ROCK-inhibitor (50 μM) and ISO (10 μM) up to 72 hours in order to assess the effect of the stimulations on proliferation.

Cells were grown in 6-microplate with the same treatments conditions as the IncuCyte experiments.

A total of 50 000 PC-12 ADH and PC3-Luc3-GFP, and 75 000 C4-2B cells were seeded per well. The cells were incubated for 24 hours for attachment after seeding.

Following incubation, the medium were changed to treatment medium. A total of 2 wells were treated with 10 μM ISO, 2 wells were treated with 50 μM and 2 wells were kept as controls. The cells were then grown for 72 hours resembling to neurite outgrowth experiment.

After 72 hours, the cells were controlled by visual inspection assed by optical microscope, to ensure the cells looked normal and health. Further, medium in each well were discarded and the cells were disassociated from the plate with 500 μL of Trypsin. The trypsinization was stopped by adding 2000 μL of RPMI with FCS 10%. The cells in each well were resuspended thoroughly and then 2000 μL of the suspension were transferred to respective Eppendorf tubes. The cells in each suspension were then sucked up with the Via1-Cassette and inserted in the NucleoCounter NC-200 in order to count the cells. Each well were counted individually.

3.4 Co-Culture model studies

3.4.1 Co-culture

A co-culture model study was employed to characterize the migration rate of the prostate cancer cells (C4-2B and PC-3-Luc2-GFP) cells, nerve cells (PC-12 ADH) and Schwann cells (RSC96), with and without stimulation with 50 μM Rho Kinase inhibitor (ROCK inhibitor).

On day 1, the 4-well culture inserts (Ibidi, #80466) with 110 μL volume were placed in 12-well microplate. The number of inserts used were dependent on number of cell lines used for each parallel. Only 1 prostate cancer cell line (C4-2B or PC-3-Luc3-GFP) were used for each insert, whereas the nerve cells were seeded both individually and as co-cultures (Figure 6). A total of 10 000 cells were seeded in each well of the inserts, and the volume were adjusted to 100 μL. Further, 500 μL of treatment medium were added around the inserts to increase the humidity in the microplate. The microplate were incubated for 24 hours.

On day 2, the medium for PC-12 ADH cells in total of 2 inserts were changed to treatment medium with 50 μM ROCK. The PC-12 ADH cells were stimulated for 24 hours, in order to induce long neurites.

A Scan on Demand were employed on day3 with The Essen BioScience IncuCyte® FLR, in order to observe the placement of the inserts. Following the scan, medium in every well were discarded and the inserts were removed. The wells containing stimulated PC-12 ADH cells were changed to treatment medium with 50 μM ROCK inhibitor, whereas the remaining wells were stimulated with vehicle (ethanol) as a control. The plate were then placed in the IncuCyte® FLR for 4-7 days, and 49 images of each well were taken every 3 hour. The confluence data were then analyzed in Excel and the neurite number and length were tracked and quantified using the NeuronJ plugin from Fiji ImageJ.

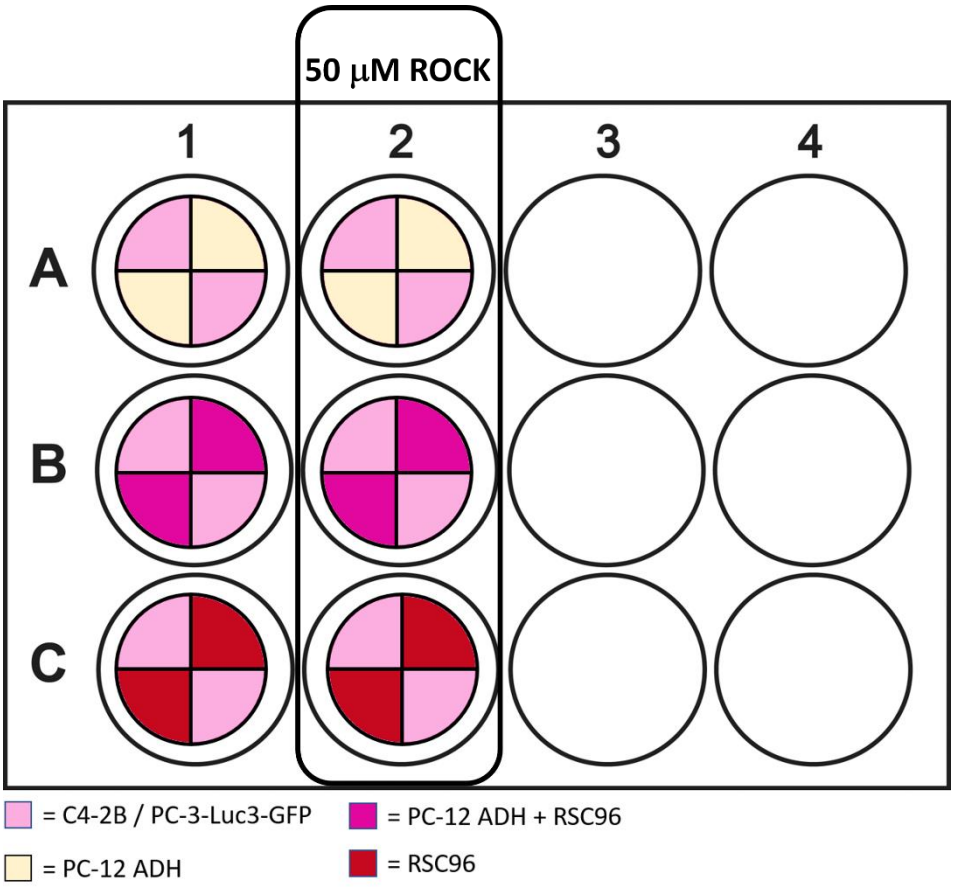

Figure 6 | A schematic illustration of the setup for co-culture migration assay. A schematic illustration of how the cells was harvested for the migration assay

3.4.2 Migration-assay (Co-culture)

In order to characterize the migration rate and pattern of prostate cancer cells and neural cells, a migration assay was employed. The co-cultures were performed with and without the optimal concentration of ROCK-inhibitor (50 µM), to determine whether it increases or decreases the migration rate of the cells.

A total of three images from each well from different time points were chosen, containing both prostate cancer cells and neural cells separated by the insert. The selected images were exported from IncuCyte to Fiji ImageJ, in order the measure the occupied area by each cell line for the three chosen time points. It was ensured the last image had at least 30-20% of unoccupied area in order to increase the accuracy of the results.

The migrated area were measured by tracing the migrated area for each cell line for each of the three time periods, showing the total migrated area at the specific time.

3.5 Dorsal root ganglia

DRG (Dorsal Root Ganglia) were isolated from transgene GFP-expressing NOD scid mouse (non-obese diabetic severe combined immunodeficiency) by Stein Waagene at the Department of Tumor Biology. The mice used for the DRG isolations were between 8-10 weeks old at the day of harvesting. The size of the DRG is often dependent on the age of the mouse and the placement of the DRG in the spine, as are result it is easier to isolate the DRG from the spine of older mice. The isolated DRGs were placed in 10% FCS DMEM growth medium after harvesting at the animal care facility and brought to the unclean cell lab at the department in order to cultivate the isolated DRGs.

A 12-well Corning micro plate were placed on ice, and then 2 µL of Matrigel (growth factor reduced, without phenol red) was pipetted in each well. Furthermore, the microplate were placed in room temperature for 1 minute and then back on ice. This is done to harden the Matrigel before placing the DRG inside the drop.

Each DRG were then scooped from the wells using 2 gauge needles, and then placed in the drop of Matrigel. The microplate were then placed in the incubator for 3 minutes, and then 1 mL of 10% FCS DMEM medium was added to each well. The microplate were then placed in a incubator at 37 °C with 5% Carbon Dioxide (CO_2) and humified air.

3.5.1 DRG and C4-2B co-culture

Neurite outgrowth starts 2-4 days after the harvesting of the DRG, depending on the age of the mouse. The DRGs were observed every day in fluorescence microscope, to observe any neurite activity. 2-5 days after DRG harvesting, 30.000 C4-2B cells were added in each well containing DRG. C4-2B cells were added to assess the interaction between cancer cells (C4-2B) and nerve cells (DRG), and to evaluate if this contact-dependent interaction increases the rate of invasion. The cells were observed and tracked for potential contact with DRG or cells from the DRG.

Images were taken on the fluorescence microscope with fluorescein isothiocyanate (FITC) filter and phase contrast (PH) every day after an interaction between the two cell types were observed. Images taken with FITC-filter and PH were merged to visualize the interaction between GFP expressing DRG derived cells and C4-2B, distinguishing them from each other.

Merging enables visualization of cells in different layers in the well by adjusting the focus. The interaction between the cells were observed for 5-6 days.

The treatment medium for each well were changed every other day. This were done to give the cells nutrients and expose them continuously to the inhibitors. The medium change were done carefully to prevent harm on the Matrigel and relocation of DRG and C4-2B cells.

3.6 Image Analysis

3.6.1 Neurite tracking

Images were selected based on number of neurites and cells. It was ensured that every image had approximately the same number of cells and the same density of cells throughout the whole image. All 16 photos from each well were exported IncuCyte FLR software, and a total of 5 Images were selected for analysis. For quantification and measurement of neurites, the image processing program; Fiji ImageJ (Image J-Win64 v1.153.c) were used. In order to track the neurites, the ImageScience package and NeuronJ plugin were employed.

5 images from each time period and treatment were chosen, and converted to 8-bit Tiff file, which is a requirement in the NeuronJ plugin. Furthermore, the scale was changed from pixels to μm.

Areas with approximately same amount of cells where chosen at 100% zoom (1/4 of the image), and were used to track the neurites. Furthermore, neurites can be quantified by: Add tracings. The neurites were measured by pressing the start point from the cell body and out to the end of the selected sprout. Incorrect quantification were removed by: Delete tracings. Neurites shorter than the cell body were omitted from quantification, and only neurites in the selected area were tracked and quantified. After quantification, the tracings can be displayed by: Measure Tracings> Display group measurements> Run, displaying: number of neurites, total length of neurites, average length of neurites, min and max length of neurites. Total number of cells were counted manually.

The data were plotted and analyzed on Excel.

3.7 ADRB2 gene knockdown

C4-2B cells were transfected with plasmids in order to alter the expression of the gene for the adrenergic intermembrane receptor ADRB2-gene (β2-adrenergic receptor).

Short hairpin RNA (shRNA) are widely used in plasmids for gene knockdown. When the vector is integrated in the host genome, shRNA is expressed and then forms the RISC complex. Active RISC can then bind and cleave the mRNA sequence, suppressing the expression of the gene (167, 168).

The advantage of using shRNA is the generation of stable knockdown cell lines that usually require no more than one round of transfection, but may in turn require more time to successfully construct and select the shRNA-positive cells by using antibiotics (Neomycin G-41) to remove the shRNA-negative cells (167). The selection-gene Neomycin is driven by a SV40 promoter and the shRNA is driven by a U1 small nuclear promoter.

In order to silence the expression of ADRB 2 gene, 2 different plasmids were used: 76 adrb2 shRNA Clone 1 and 79 adrb2 shRNA Clone 1. A third clone were transfected to be used as a control, 81 shRNA Control. Clone 76 and clone 79 consists of different sequences, both targeting and suppressing the ADRB2 gene, whilst the clone 81 is a non-specific sequence which design to not bind any RNA-sequence.

3.7.1 Concentration curve of G-418

To determine the lowest toxic concentration of Neomycin G-418 disulfate salt solution a dose response curve were employed on the C4-2B cell line. By setting up a dose-response curve with G-418, the optimal concentration can be established and used for selection medium and select all transfected cells from untransfected cells.

C4-2B cells were split, and 15 000 cells per well were seeded in 24-well microplates with 1 mL of growth medium. The cells were seeded with a low confluency < 10% and were then incubated for 24 hours.
Following incubation, the cells were treated with the following concentrations of Neomycin G-418: 0, 100, 200, 300, 400, 500, 600, 700, 800 and 1000 µg/mL in separate wells.
The plate were placed in the IncuCyte FLR in order to get an estimate of the confluency from each well every day, medium were changed every 2-3 days.

The experiment were proceeded until the controls reached a confluency of 90%. The most effective concentration were then selected based on total of dead cells compared to the concentration of G-418.

3.7.2 Reverse-transfection

Reverse transfection is a widely used method, which differs from traditional transfection by forming a transfection complex on the plate in absence of cells, whereas in traditional transfection one forms the complex on the plated cells. Reverse transfection requires less DNA and enables a higher expectation of DNA and cell contact, which may secure a higher efficiency compared to normal transfection (169).

A transfection complex consisting of Opti-Mem™ I Reduced Serum Medium, shRNA plasmids and transfection reagent were prepared in the wells of 12-well microplates accordingly to the reverse transfection technique (see appendix). Total of 6 complexes were created for each clone (6 wells for each clone).

First 59,6 µL of Opti-Mem™ I Reduced Serum Medium (Gibco, # 31985062) were pipetted into all wells of 2 different 12-well microplates (6 wells per shRNA plasmid). Further, 0,40 µg/µL of the selected shRNA plasmids were pipetted on the Opti-Mem. The transfection mixture were then gently mixed. Subsequently, 3 µL of X-treme GENE HP DNA Transfection Reagent (Roche, # 6366244001) were added to the well and the mixture were gently shaken av few times. The plate were then incubated for 15 min at room temperature, in order to enable the formation of the transfection complex. After the formation of the transfection complex, the C4-2B cells were then split and 200 000 cells were added to each well along with 2 mL growth medium.

After 48 hours the cells were trypsinized and transferred to Corning 75^2 cell culture flasks with 12 mL of selection medium and incubated for 48 hours. The cells were observed every day under the microscope.

On day two upon harvesting, the medium in the flasks were changed to selection medium in order to select the transfected cells and kill cells which is not transfected. The cells were incubated until approximately 95% of the untransfected control were dead and transfected cells seemed to be growing. At this point the positive selection of the transfectants appeared to be complete and the enrichment of the knockdown cell lines could start. The knockdown

cell lines were split to 6 Corning T-75^2. After approximately 2 weeks of enrichment, the cells were ready to be verified as ADRB2 knockdown cells.

3.8 Detection of ADRB2 receptor and verification of shADRB2 transfectants

3.8.1 Isolation and purification of membrane bound proteins

In order to verify that the different cell lines in the study were ADRB2 positive, a membrane fractionation isolation was done to prepare samples for further analysis to detect the level of ADRB2 expression.

Cells were seeded in 175 flasks and placed in the incubator. When the flask reached the desired confluence (80-90%), they were washed with 10 mL PBS (Dulbeccos Phosphate Buffered Saline, #D8537-500ML) 3 times. Furthermore, 10 mL PBS were added to each flask and the cells were detached with cell scrapers and transferred to 15 mL tubes. The tubes were then centrifuged at 1000 RPM for 5 minutes. The supernatant were then discarded and the pellet were frozen at -80°C until membrane isolation. The pellet from each sample were then resuspended in 1 mL STE homogenization buffer with 27% Sucrose (Sigma, # S7903), 50 mM Tris-HCL-pH 7,5 (Invitrogen, 15567027) and 5 mM of EDTA (see table 5 in appendix). The resuspension were then transferred to Eppendorf tubes. The resuspended samples were then homogenized with a Ultra-sonicator at 60 kHz for 10 seconds. The sonication were repeated 5 times, with 30 seconds of cooling on ice inbetween each sonication. The homogenized samples were then centrifugated for 5 minutes at 1000 RPM at 4°C. Furthermore, the supernatant were decanted to 14 mL Ultra-Clear tubes (Bekman Coulter, #344060). The tubes were then placed in the Beckman Coulter Avanti^{TM} J-35 and centrifuged at 27,000 g for 20 min, 4°C in a Beckman JA-16,250 rotor. Subsequently, the supernatant were discarded, and each pellet were resuspended in 1mL of 50mM Tris-EDTA and the resuspended samples were transferred to a Dounce glass-glass homogenizer (Kontes, #885301-0002) and stroked total of 10 times with pestle B. The stroked samples were then centrifugated a second time in the Beckman Coulter Avanti^{TM} J-35 at 27,000 g for 20 min, 4°C in a Beckman JA-16,250 rotor.

The supernatant were discarded one more time, and the pellet were resuspended with 0,5 mL of 50 mL Tris-HCL + 1mM-EDTA. The resuspended sample were then stroked 10 times in the

Dounce glass-glass homogenizer the pestle B. The samples were then transferred to new Eppendorf tubes and were preserved by snap-freezing, using a dry ice/EtOH bath, and then stored at -80°C.

3.8.2 Protein BCA Assay

The bicinchoninic acid assay (BCA) is a widely used colorimetric assay for detection and quantification of proteins in a sample. The mechanism behind this assay is that proteins in each sample reduce the Copper Nitrate (Cu^{+2}) to Copper Oxide (Cu^{+1}) in the Working Reagent solution with alkaline, causing the color change from green to purple depending on the amount of proteins in the sample. The Pierce BCA Protein Kit Assay (Thermo Scientific, #23227) were utilized in this study.

The prepared membrane samples were thawed on ice. The assay were applied on 4 or 8 samples at a time, and total of 3 parallels were performed for each cell line. Standards were made in order to compare the sample against a known value and eliminate certain inaccuracies which may arise from the variations in the samples.

Albumin protein standards were prepared to be used as a plot, in order to provide the absorbance versus the assorted concentration of known proteins. Further, can the measured amount of the unknown proteins (absorbance) be plotted against the standards and compared with.

The standards were prepared accordingly to table 3 and table 4. The bovine serum albumin (BSA) standards were diluted in TRIS-EDTA accordingly to table 3 and table 4.

A Working reagent (WR) was prepared by using the Pierce™ BCA Protein Assay Kit. The mixture was prepared by using 1 part of BCA reagent B and 50 parts of BCA reagent A. Dependent on the sample size, 10 mL (for 4 samples) of the mixture were prepared (20 mL for 8 samples).

Standard curve (#)	Volume of BSA (µL)	Volume of buffer (µL)	Final Concentration (µg/µL)
10	250	750	2,5
8	800 µL of dilutant 10	200	2
6	800 µL of dilutant 8	266	1,5
4	500 µL of dilutant 6	250	1
2	500 µL of dilutant 4	500	0,5
1	250 µL of dilutant 2	250	0,25

Table 3 | Preparation and dilution of BSA standards 1-10.

Standard curve (#)	Volume of diluent (µL)	Volume of buffer (µL)	Final Concentration (µg/µL)
25	625	375	6,25
20	500 µL of dilutant 25	125 from 25	5
15	400 µL of dilutant 20	100 from 20	3,75
10	200 µL of dilutant 15	100 from 15	2,5
5	150 of dilutant 10	150 from 10	1,25

Table 4 | Preparation and dilution of BSA standards 5-25.

Subsequently, 200µL of the Working Reagent (WR) were added to the selected wells in the 96-well microplates (Corning #CLS3527). Further, 4µL of the standards were pipetted as duplicates to their respective wells. The first row for both standards contained 200 µL of WR and 4µL Tris-EDTA and were used as controls. Two parallels of the samples were added to their respective wells as duplicates. First parallel with 4µL of the samples and 10 µL for the second parallel. The microplate were then gently shaken, and then incubated for 15 minutes at 37 C°.Following, the microplate were gently shaken and then inserted in the The VICTOR3 Multilabel Plate Reader (Perkin Elmer) with absorbance of 562 nm, in order to measure the amount of protein in each well. The data were then exported to Excel for analysis.

3.8.3 Receptor radioligand binding assay

The receptor radioligand binding assay was done by Kjetil Wessel Andressen at the Department of Pharmacology at the University of Oslo. In short, this assay was performed by incubating the prepared membrane samples with a radiolabeled beta-adrenergic agonist, 125? iodocyanopindolol, with or without propranolol, a beta-adrenergic antagonist. This way one can measure total ligand binding (without propranolol) and non-specific binding (with propranolol), and form this get the specific binding and calculate the concentration of the beta-adrenergic receptors in the samples (fmol/mg protein).

3.8.4 Immunofluorescence staining

Two mixtures of antibodies were prepared. The first mixture containing the primary antibody Beta-2 adrenoreceptor (MBL, LS-A2656), diluted 1:200 in IF-buffer (1X PBS supplemented with 0.1% BSA, 0.2% Triton X-100, 0.05% Tween, pH 7.4) with 1% HS. The second mixture consisting of the secondary antibody Alexa Fluor Plus 555 (Invitrogen, #A32794), diluted 1:400 in IF-buffer with 1% HS.

PC-12 ADH- and C4-2B cells were sown out in Ibidi® µ-Slide 8 Well (#80826). Approximately 10 000 cells with 200 µL growth medium were seeded in 8 wells, 4 wells per cell line. The plate where then incubated for 24 hours.

Medium in each well were changed, and 2 wells for each cell line were treated with 50 µM ROCK-inhibitor. The slide where then incubated for 24 hours.

The slide where taken to fume cupboard, because of PFA toxicity. Medium in every well were removed, then washed with 150 µL of PBS Further, the washed cells were then fixated with 150 µL of 4% PFA (paraformaldehyde) for 30 minutes at room temperature in order to preserve the structure of the cells and neurites. The fixated cells where then washed with PBS, and then washed 2x5 minutes with IF buffer (see table 6 in appendix). Furthermore, cells were blocked with IF buffer with 10% HS (Horse Serum) for 30 minutes. Cells were then washed 3x5 minutes with 150 µL of IF-buffer. Following, the cells were incubated with primary antibody mixture overnight at 4 °C. Next, the cells were washed 3x5 minutes with 150 µL of IF-buffer followed by incubation with the secondary antibody mixture for 1 hour at room temperature. Furthermore, the cells were washed 3xwith PBS, and then incubated with

Hoechst blue (Invitrogen, #33258) diluted 1:5000 in PBS. This were done to stain the cell nucleus. The cells were then washed a final round of 3 times with PBS.

The images were then taken with the fluorescence microscope with phase contrast (PH), DAPI filter to detect nucleus and lastly the tetramethyl rhodamine (TRIRC)-filter in order to detect whether the cells were ADRB2 positive.

3.9 Statistics

In order to determine significant difference of the stimulations compare to the controls, a two-tailed student T-test with unequal variance were performed in Excel. Standard deviation was performed on all bar charts in order to shown the variance for each sample/experiment.

3.10 Mycoplasma test

To avoid any infection of bacteria, each cell line were tested for mycoplasma regularly.

A total of 2 mL of medium from each cell flask were extracted to 15 mL tubes, and 100 μL of the extracted medium were transferred to Eppendorf tubes and stored at -20 C°. The samples were then analyzed using Venor GeM Mycoplasma Detection Kit (Minerva Biolabs, #MP0025), which is a PCR based method for mycoplasma detection.

4. Results

4.1 Stimulation with ROCK-inhibitor resulted in outgrowth of neurites in every cell line

In order to study migration of prostate cancer cells along neurites, one can induce the formation of neurites in neuron like cell (PC-12 ADH) and Schwann cells (RSC96), and observe the interaction with prostate cancer cell lines (C4-2B and PC-3-Luc2-GFP.

To induce outgrowth of neurites, the cells were treated with a ROCK-inhibitor (50 μM Y27632) and Isoproterenol (ISO,10 μM) and imaged every 3 hours over a 72 hours period. Representative pictures of the different cell lines at 48 hours are shown in figure 7. By visual assessment, ISO (10 μM) stimulation induced neurite outgrowth only in the prostate cancer cell lines C4-2B and PC-3-Luc2-GFP (Figure 7).

Quantification of the total length of neurites showed that PC12 ADH cells treated with ROCK-inhibitor (50 μM) reached maximum at 24 hours, whereas the neurite length increased till 48 hours in RSC96 and C4-2B cells (Supplementary Figure 1). The effect was slightly lower after 72 hours in all cell lines. These findings were supported by the neurite parameter, demonstrated by the length of neurites divided by total cells (Figure 8), total number of neurites per cell (Figure 9) and the average length of neurites per cell (Figure 9).

As shown in supplementary figure 1, 50 μM ROCK-inhibitor induced ($p<0,01$) neurites in PC-12 ADH cells within 24 hours of stimulation. A slow decrease of the neurite length was noticed after 24 hours of stimulation (Supplementary figure 1) but the number of neurites increased up until 48 hours of stimulation. ISO (10 μM) was observed to induce neurite outgrowth upon 6 hours of stimulation in the C4-2B cells (Supplementary figures 2), and similar results was observed for the PC-3-Luc2-GFP cells.

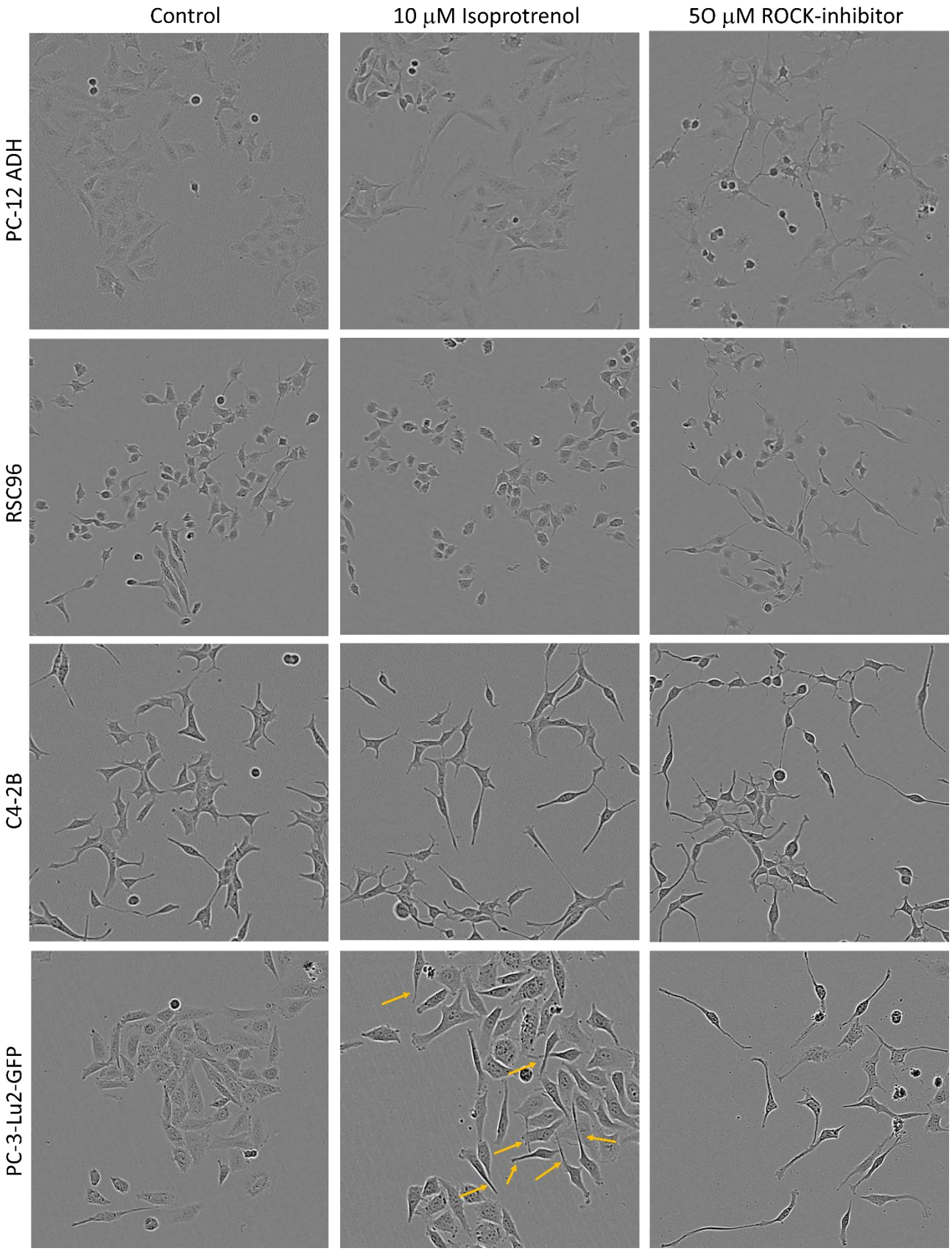

Figure 7 | Morphological changes induce by the stimulation with ROCK and ISO. Representative pictures of control cells and stimulated cells after 48 h of every cell line used in the study. All tested cell line were sensitive to the ROCK-inhibitor (50 μM), whilst the prostate cancer cell lines (C4-2B and PC-3-Luc2-GFP) were the only cell lines sensitive to ISO (10 μM) observed by visual inspection. Images was obtained from IncuCyte (10x). The arrow indicates neurites induced by ISO (10 μM) stimulation.

4.1.2 ROCK-inhibitor significantly increased the total length of neurites in all cell lines

The outgrown neurites induced by the stimulations was tracked and quantified in order to determine concentration that gave the longest neurites in each cell line.

A dose-response effect was observed on cells stimulated with ROCK-inhibitor. As shown by figure 8, the lowest concentration of ROCK-inhibitor which induced longer neurites, was 10μM ROCK, which increased neurite length in the RSC96 cells ($p<0,01$) and in the C4-2B cells ($p<0,05$) as shown in figure 8B and 8C. Furthter, stimulation with 25 μM ROCK ($p<0,05$) influenced the total length of neurites in the neural cell lines, PC-12 ADH and RSC96 (Figure 8A and Figure 8B). In the same way, 50 μM ROCK ($p<0,005$) increased the total length of the neurites in all of the cell lines. These findings suggests that the C4-2B cell line and the RSC96 are more senstive to ROCK-inhibitor, based on the fact that 10 μM ROCK indicued neurites in both of the cell lines. More data is needed for the PC-3-Luc2-GFP cell line, as it was not perform a concentration curve on the cell line.

It is possible to se a pattern in that increasing concentration of ROCK-inhibitor provides longer neurites and the highest concentration (50 μM) has a difference ($p<0,005$) between the control respectively in each cell line, suggesting that increased concetration of ROCK-inhibitor is higliy associated with inducing longer neurites, ergo there is a dose-response effect. The PC-3-Luc2-GFP cell line was employed late in the study, and as a result there was not time to perform a concentration curve of ROCK-inhibitor and 50 μM ROCK-inhibtior timer intervall for this cell line.

Stimulation with ISO (10 μM) increased ($p<0,05$) the total length of the neurites in the PC-3-Luc2-GFP cell line (Figure 10D) compared to the control, and was the only cell line with increased neurite length upon ISO stimulation.

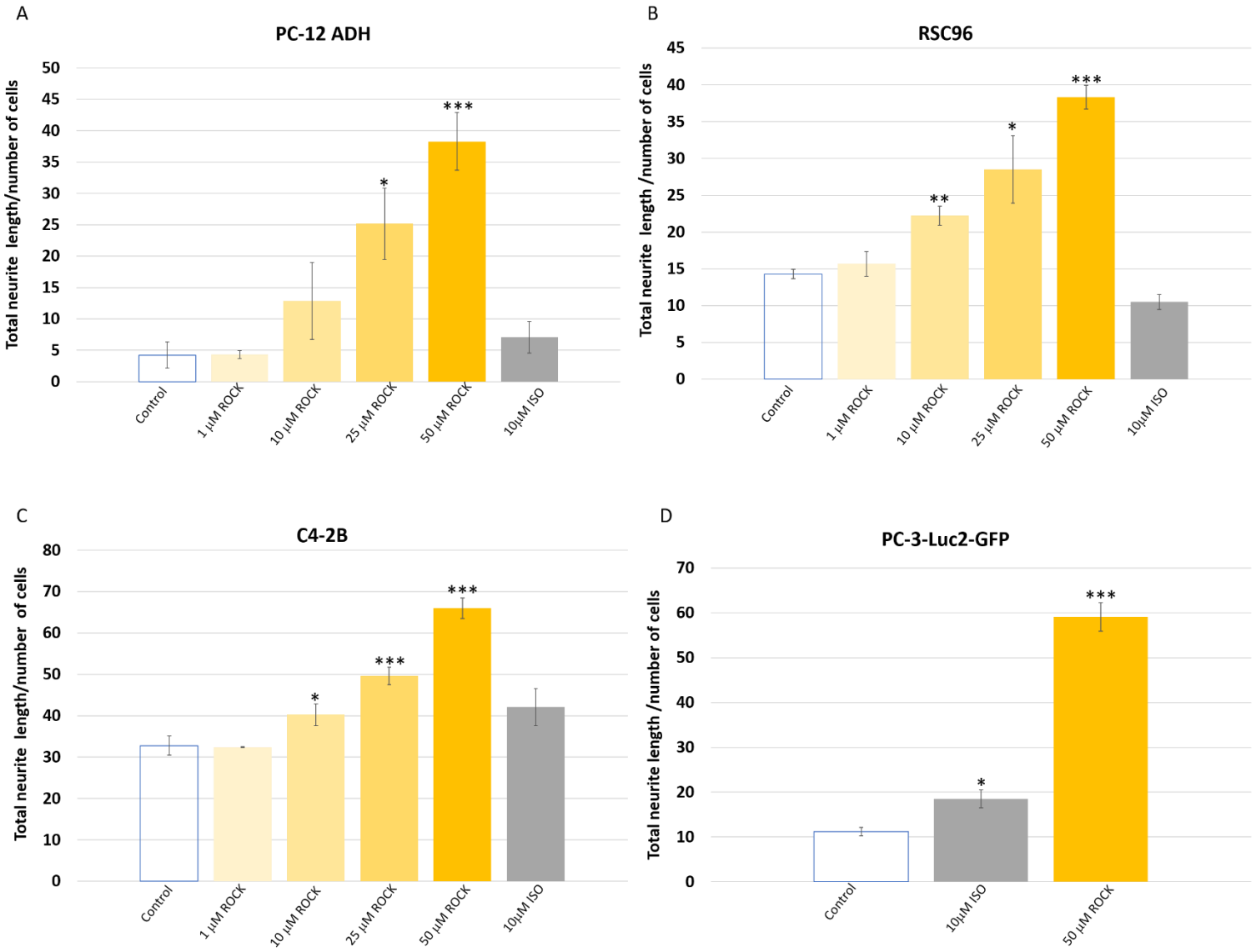

Figure 8 | The total length of neurites divided by the number of cells. Neurites within selected area of each image were tracked and analyzed using ImageJ. The figure illustrates the average for the total length of neurites divided by the total amount of cells for each stimulation. Error bars are presented as standard deviation. *****p<0,05, ******p<0,01, ***p<0,005. (n=3)

4.1.3 ROCK-inhibitor significantly increased the number of neurites in the PC-12 ADH cells and in the PC-3-Luc2-GFP cells

To examine whether stimulations with ROCK-inhibitor and ISO increased the number of neurites per cell, the total number of neurites were tracked and quantified and divided by total number of cells to see if the stimulations increased the number of neurites.

As shown in figure 9, 25 μM ROCK ($p<0,05$) increased the number of neurites per cell in the PC-12 ADH cells and in the RSC96. Stimulation with 25 μM ROCK were shown to increase ($p<0,001$) the number of neurites in the C4-2B cells.

It was demonstrated that stimulation with 50μM ROCK ($p<0,005$) induced neurite outgrowth in both PC-12 ADH cells and RSC96 cells (Figure 9A and Figure 9B). In the same way, 50μM ROCK caused an increase in number of neurites in the prostate cancer cell lines, PC-3-Luc2-GFP ($p<0,005$) and C4-2B ($p<0,01$) (Figure 9C and Figure 9D).

Interestingly, ISO (10 μM) ($p<0,05$) decreased the number of neurites in the RSC96 and this change in number of neurites was not observed in any of the other three cells after stimulation with ISO in (Figure 9).

All cell lines were ADRB2 positive as observed by immunofluorescence staining (Supplementary figure 4 and Supplementary figure 5) and the level of ADRB2 in the cell lines was determined by receptor radioligand binding assay (Supplementary figure 3). By visual inspection, it is possible to see that there is a correlation between high levels of ADRB2 and number of outgrown neurites induced by stimulation with 50 μM ROCK. As shown in figure 9, C4-2B cells grew the longest neurite upon stimulation with 50 μM ROCK, and as shown in supplementary figure 3, C4-2B cells expressed the highest level of ADRB2. These results suggest that there is a correlation between ADRB2 expression and number of outgrown neurites induced by stimulation with 50 μM ROCK.

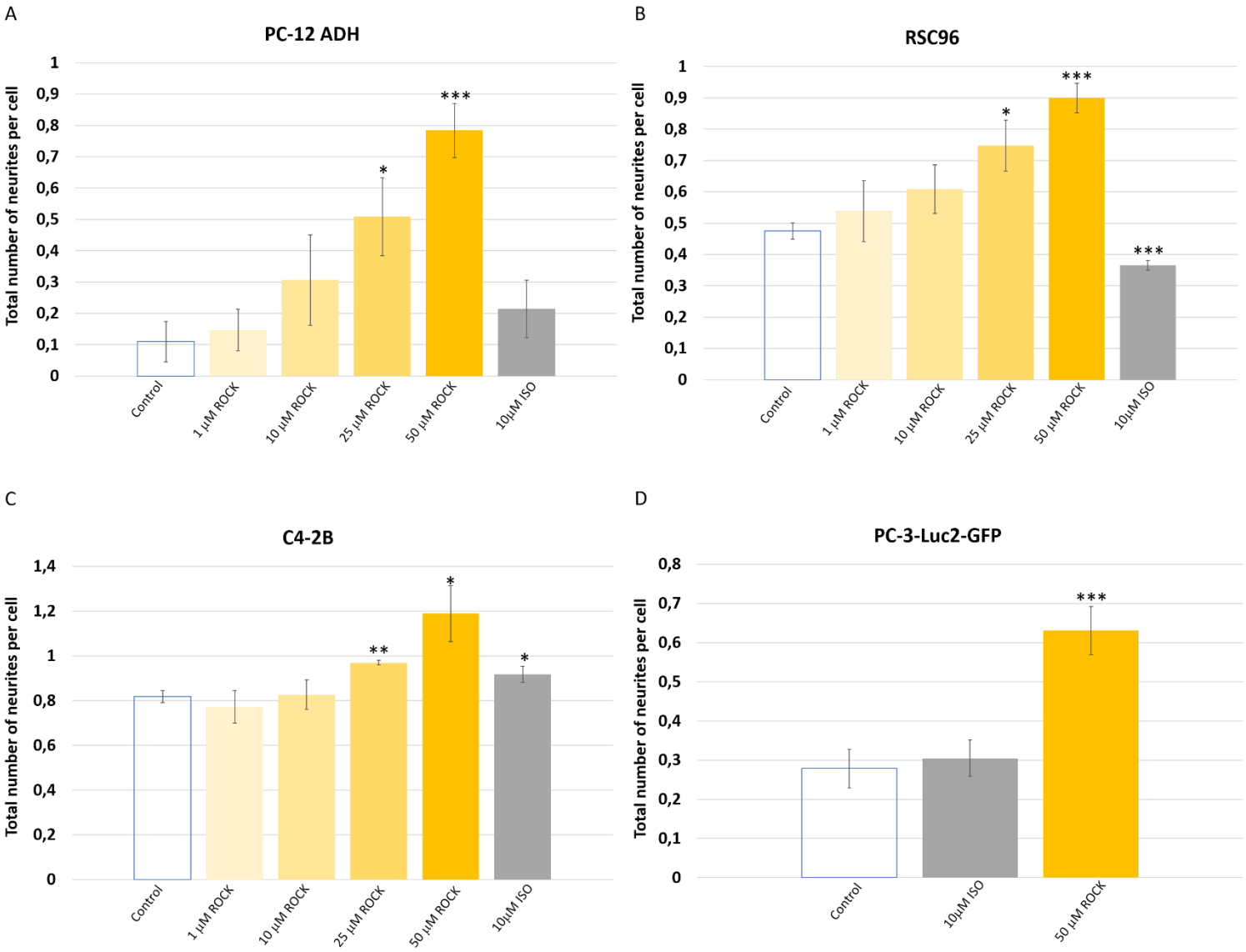

Figure 9 | Total number of neurites per cell. The number of neurites in a selected area within the image were quantified and divided by the number of cells, in order to see how the stimulations influences the number of neurites per cell compared to the control. Error bars are presented as standard deviation. *****p<0,05, ******p<0,01. (n=3)

.

4.1.4 Stimulation with ROCK-inhibitor induced a moderate increase in average neurite length

To further investigate the effect of ROCK-inhibitor and ISO on the neurite outgrowth, the average length of neurites for each concentration of ROCK-inhibitor and ISO on all cell lines were observed 48 hours upon stimulation.

Shown in Figure 10B and 10C, 10 μM ROCK influenced the average length of the neurites was increased in the RSC96 cells ($p<0,01$) and in the C4-2B cells ($p<0,05$), and is the lowest concentration of ROCK-inhibitor which increased the average neurite length.

As assed by Figure 10, stimulation with 50μM ROCK caused an increase ($p<0,01$) in the average length of the quantified and tracked neurites, while the effect was even bigger ($p<0,005$) in the PC-3-Luc2-GFP cell line (Figure 10D). It was also observed that 25 μM ROCK induced ($p<0,05$) a increase in the average length of the neurites.

It was also observed that 10 μM ISO increased ($p<0,05$) the average neurite length in the PC-3-Luc2-GFP (Figure 10D). Interestingly, it was observed that 10 μM ISO stimulation in PC-12 ADH decreased ($p<0,05$) the average length of neurites, exhibiting a inhibitory effect on the cell line (Figure 10A).

Although the stimulations statistically increased the average neurite length, by visual assessment it is possible to see that the effect is minimal in most of the cell lines (Figure 10). The highest effect of the stimulations was seen in the PC-3-Luc2-GFP cells, which was demonstrated to double the length of the neurites upon stimulation with 50 μM ROCK (Figure 10C).

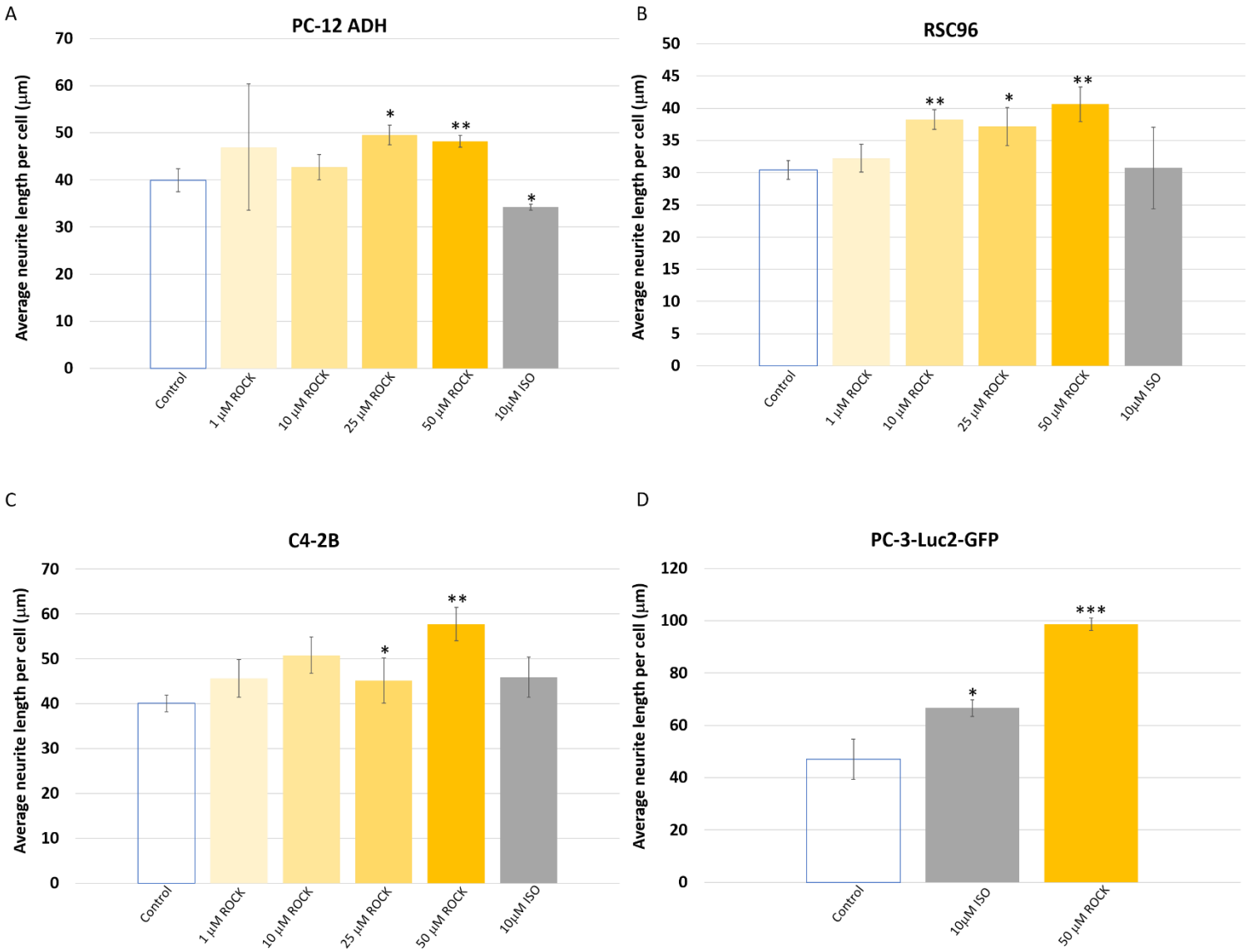

Figure 10 | The average neurite length per cell (µM). Error bars are presented as standard deviation. ***p<0,05, ****p<0,01, *****p<0,005. (n=3)

4.2 Stimulation with ROCK-inhibitor (50 μM) significantly decreased the proliferation

In order to examine the influence of the stimulations on proliferation, all cell lines were stimulated with 50 μM ROCK or 10 μM ISO and compared against the controls. The cells were harvested after 72 hours of cultivation, and then counted on NucleoCounter.

Stimulation with 50 μM ROCK were shown to decrease the proliferation in the RSC96 ($p<0,01$) (Figure 11B), as well as in the PC-12 ADH cell line and in the PC-3-Luc2-GFP cell line ($p<0,001$). The ROCK inhibitor did not affect the proliferation of C4-2B cells. Stimulation with 10 μM ISO did not have a significant influence on the cell proliferation, although a small reduction in cell number was observed in PC12 ADH and RSC96 cells (Figure 11).

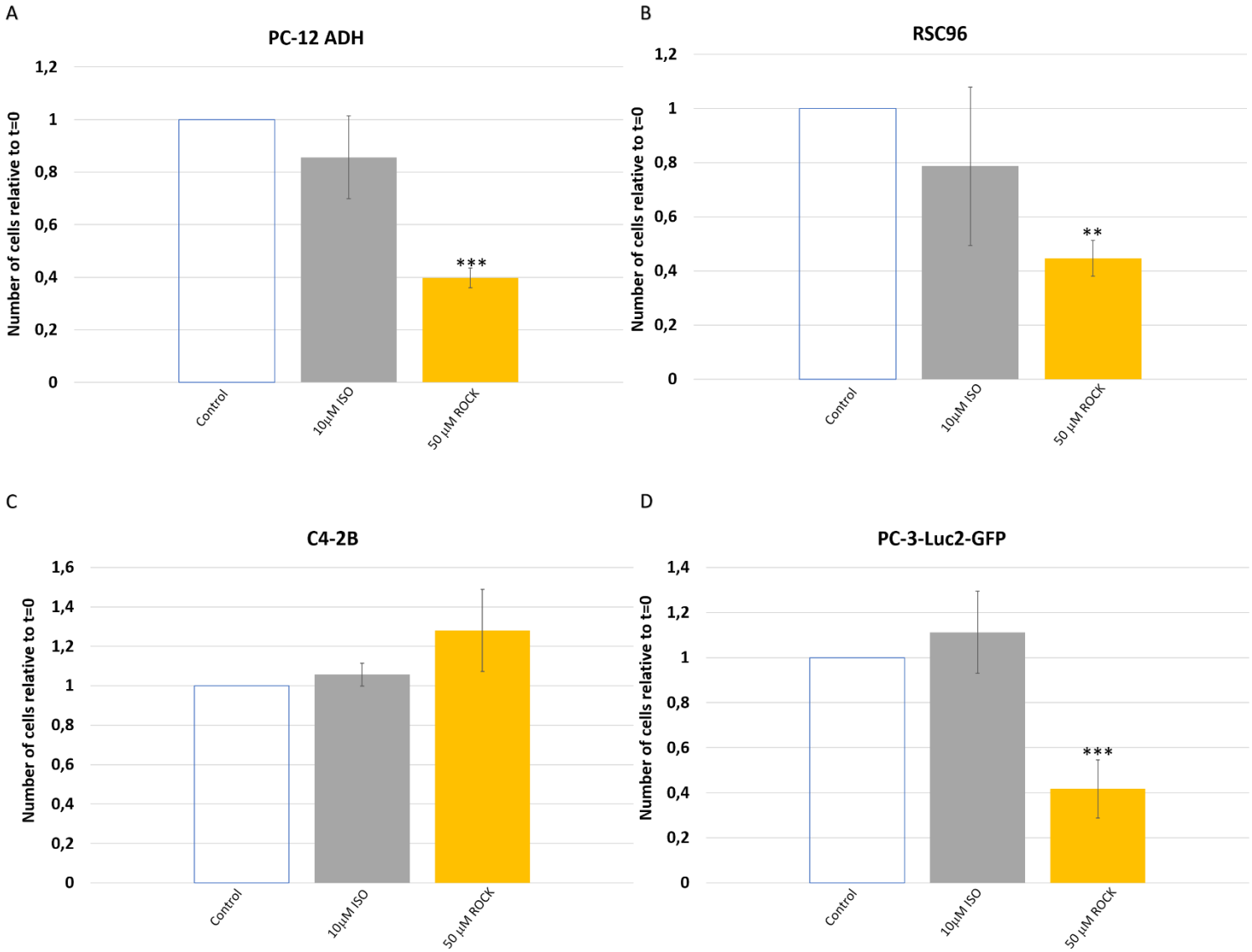

Figure 11 | The cell proliferation of stimulated cells normalized against the control (t=0) assessed by NucleoCounter. The graphs illustrate the proliferation of stimulated cells compared to the control on 72 hours upon stimulation for each cell line The cells were stimulated and counted 72 upon stimulation to illustrate the effect of each inhibitor and the stimulation medium on all cell lines. Error bars are presented as standard deviation. *****p<0,05, ******p<0,01, ***p<0,005. (n=3)

4.3 Co-culturing prostate cancer cells with nerve cells to measure the migration rate of each cell line

To investigate the migration pattern and measure the migration rate of the prostate cancer cells with the presence of neural cells, a co-culture study with PC-3-Luc2-GFP or C4-2B and PC-12 ADH/RSC96 was employed with and without stimulation with ROCK-inhibitor (50 μM), in order to observe if the ROCK-inhibitor influences the migration rate. We wanted to determine which cell line migrated the fastest based on migration rate.

As shown in figure 12 and figure 14, it was observed that the PC-3-Luc2-GFP cell line had a higher migration rate compared to the PC-12 ADH/RSC96 cells. The migration pattern for the PC-3-Luc2-GFP cells and the PC-12 ADH cells is visualized with representative images in Figure 13.

It was shown that stimulation with ROCK-inhibitor (50 μM) did not influence the migration rate of PC-3-Luc2-GFP cells (Figure 14). Based on the observations, it was proposed that ROCK-inhibitor had a moderate influence PC-12 ADH cells and RSC96 cells, decreasing the migration both combined and individually (Figure 14).

It was shown that the PC-3-Luc2-GFP cell line migrated the longest in the shortest time when co-cultured with RSC96 cell line and stimulated with ROCK-inhibitor (Figure 12). In contrast, it was found that the neural cells had the slowest migration rate in the study, further it was shown that stimulation with ROCK-inhibitor further decreases the migration rate of the cell line. Visual observations showed that the PC-12 ADH cells and RSC96 cells had approximately the same migration rate, with and without the absence of ROCK-inhibitor (Figure 14).

Interestingly, it was demonstrated that the migration rate of the neural cell line increased when both PC-12 ADH and RSC96 was cultured together (Figure 12 and Figure 14). It was revealed that PC-3-Luc2-GFP cell line had the lowest migration rate when co-cultured with the combination of PC-12 ADH and RSC96 without stimulation with ROCK-inhibitor (Figure 14).

The results indicate that PC-3-Luc2-GFP cells might have the highest migration rate, and stimulation with ROCK-inhibitor (50 μM) did not influence the migration rate. The same effect was observed with the C4-2B cells but C4-2B cells seems to have a lower migration rate than the PC-3-Luc2-GFP cells (Data not shown). These results also demonstrated that

neural cell lines had a higher migration rate when co-cultured, and that blocking ROCK activity might reduce the neural migration rate (Figure 12).

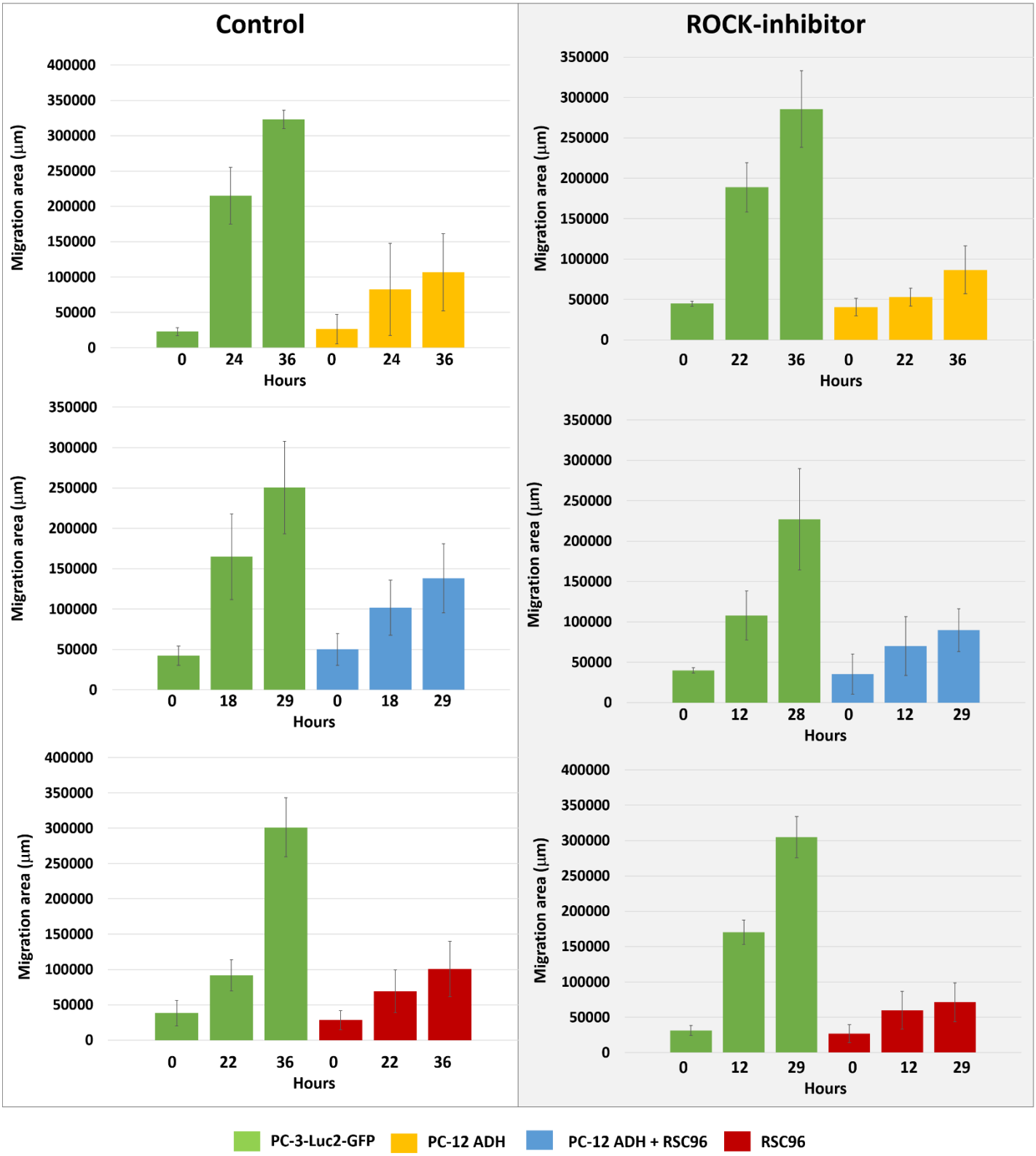

Figure 12 | Migrated area (µm) for each cell line in different combined co-cultures with and without the stimulation of ROCK-inhibitor (µM). The figure illustrates the migrated area (µm) in the time course needed for the cells to cross the middle of the insert (approximately 250000 µm) and how the different co-cultures with and without ROCK-inhibitor affects the migration speed for each cell line.

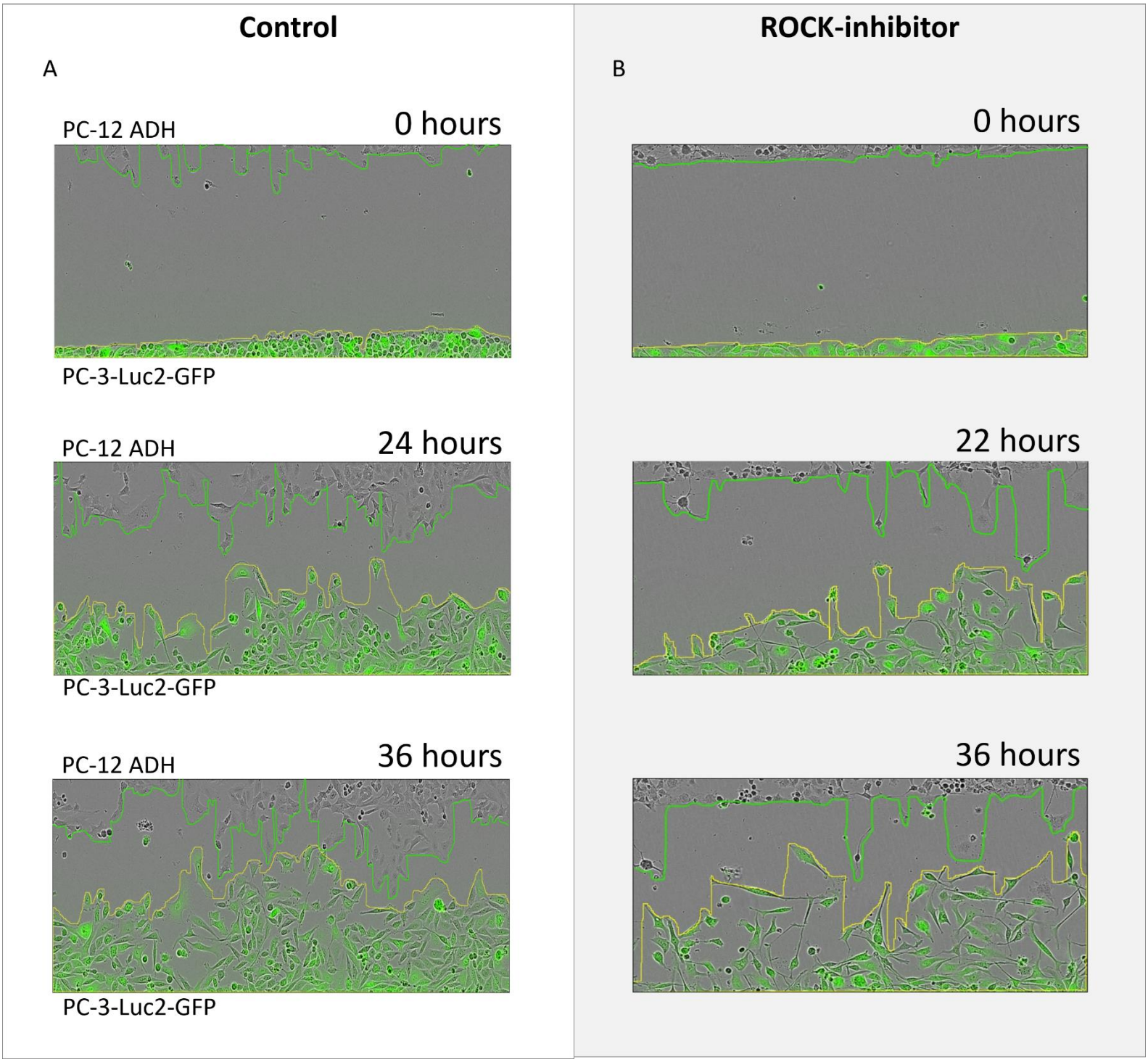

Figure 13 | The average migration rate of each co-culture, with and without stimulation of 50 µM ROCK. **(A)** Representative images of PC-3-Luc2-GFP and PC-12 ADH migration without stimulation. **(B)** The figure shows the percentage of migrated area for each cell line and the unoccupied area in the middle of the insert marked as Blank.

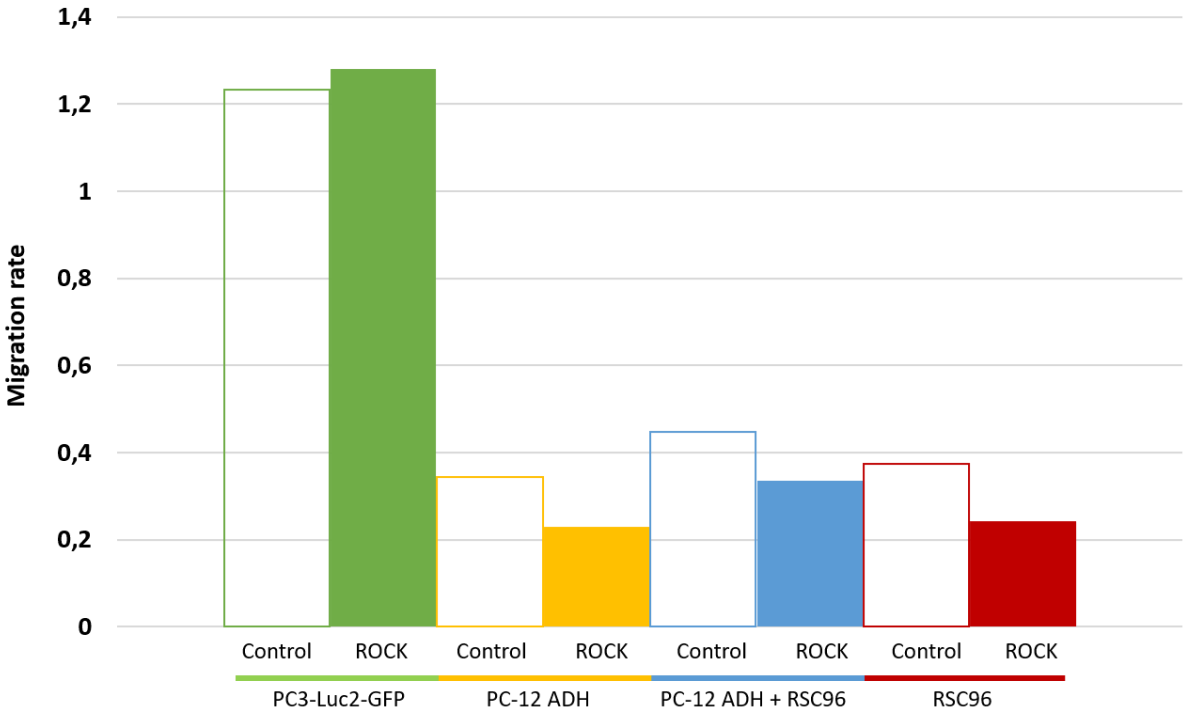

Figure 14 | The average migration rate for each cell line with and without stimulation of 50 µM ROCK. The graph illustrates the average migration rate for each cell line with and without the stimulation of 50 µM ROCK. The migration rate is obtained from the migration data based on figure 12.

4.4 Co-culturing dorsal root ganglia cells with prostate cancer cells

In order to examine the interaction of DRG derived nerve cells and prostate cancer cells (C4-2B), DRG's expressing GFP were harvested and cultivated in Ibidi 8-well glass plate on droplets of Matrigel. The C4-2B cells were added adjacent to the DRG to observe the migration of C4-2B cell through the Matrigel. Images of the ex-vivo co-culture was taken 5 days after cultivation, and C4-2B cells was tracked in order to see if the cells was capable of penetrating the Matrigel and migrate towards the DRG and DRG derived cells.

It was shown that DRG grew neurites after 2-3 days upon cultivation (Figure 15A), which was seen to grow more each day and additionally it was observed that cells expressing GFP was derived from the DRG. Further, it was noticed that the C4-2B cells was interacting with the DRG and the cells derived from the DRG (Figure 15B).

As shown in Figure 16A, it is possible to see that the C4-2B cells have formed specific patterns on and in the Matrigel. The C4-2B cells are organized along the DRG derived nerve cells, illustrating the migration of the C4-2B cells on the neurites from DRG derived nerve cells.

As assessed by visual inspection, C4-2B cells interacted with DRG derived cells in a motif suggesting that the C4-2B cells migrates on the neurites extending form the DRG derived cells (Figure 15B and Figure 160B). The same observation was seen in figure 16C, where the C4-2B cells interact with the DRG derived neural cells.

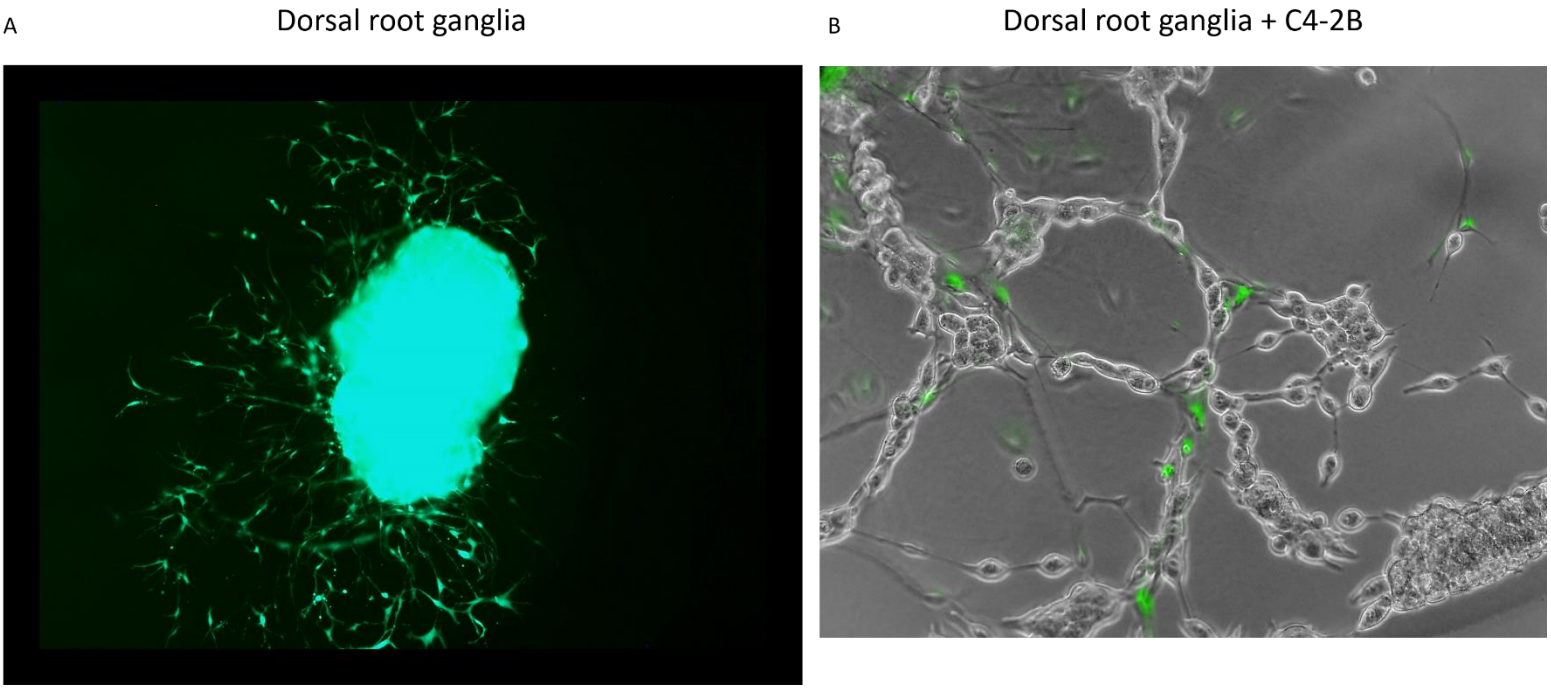

Figure 15 | Overview image of DRG expressing GFP and C4-2B cells. (A) A representative image of neurites outgrown by GFP expressing DRG with FITC-filter at 4x. **(B)** C4-2B cells forming a chain-like pattern with DRG derived GFP cells.

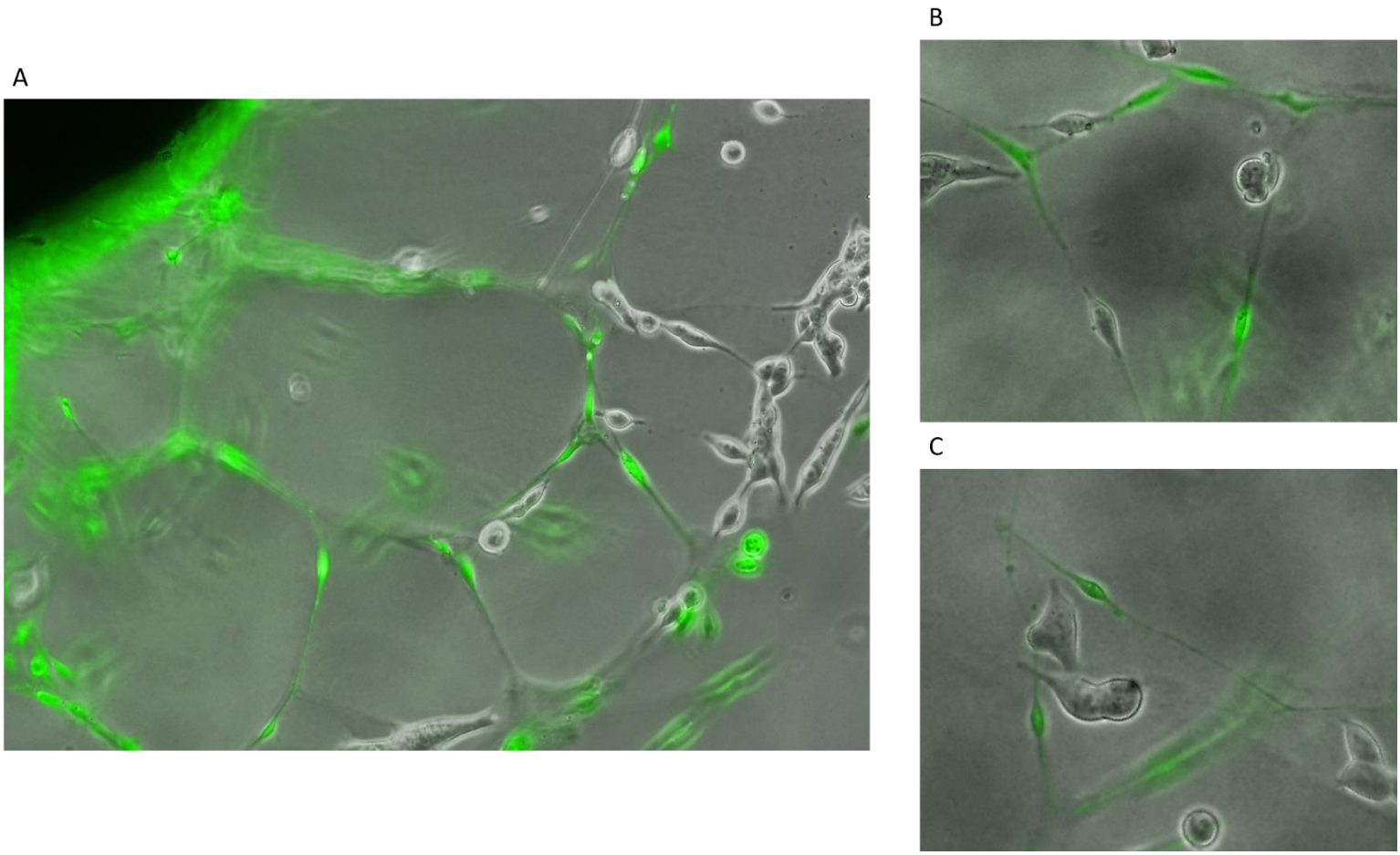

Figure 16 | Ex-vivo co-cultures study with dorsal root ganglia expressing GFP and C4-2B cells harvested adjacent to the Matrigel. GFP cells derived from the dorsal root ganglia interacting with C4-2B cells captured on fluorescence microscopy (20x), and PH images was merged with f Fluorescein isothiocyanate (FITC)-filter **(A)** A illustration of the patterns formed by DRG derived cells, interacting with C4-2B cells **(B)** A zoomed in section of a 10x image, where the interaction between the C4-2B cells and neurites extending from the DRG derived cells are illustrated. **(C)** An illustration of C4-2B cells adjacent to the neurites of the DRG derived cells.

4.5 β2-adrenegric receptor-gene (ADRB2) knockdown

To examine if reduced expression or total suppression of ADRB2 in the prostate cancer cells alters the effect of stimulations with the ROCK-inhibitor and ISO, the C4-2B cell line were transfected with clones suppressing the expression of ADRB2-gene.

4.5.1 The expression of the ADRB2-gene was not significantly altered

To examine the importance of ADRB2 expression in the prostate cancer cells and to see how low ADRB2 levels influences migration, the C4-2B cell line was transfected with a shADRB2 vector to suppress the ADRB2-gene.

C4-2B cells transfected with the shADRB2 vector did not decrease the expression of the ADRB2-gene assessed by receptor radioligand binding assay (Figure 17) and IF-staining (Supplementary Figure 6). Suggesting that the transfection was unsuccessful, and the expression of ADRB2 was not altered.

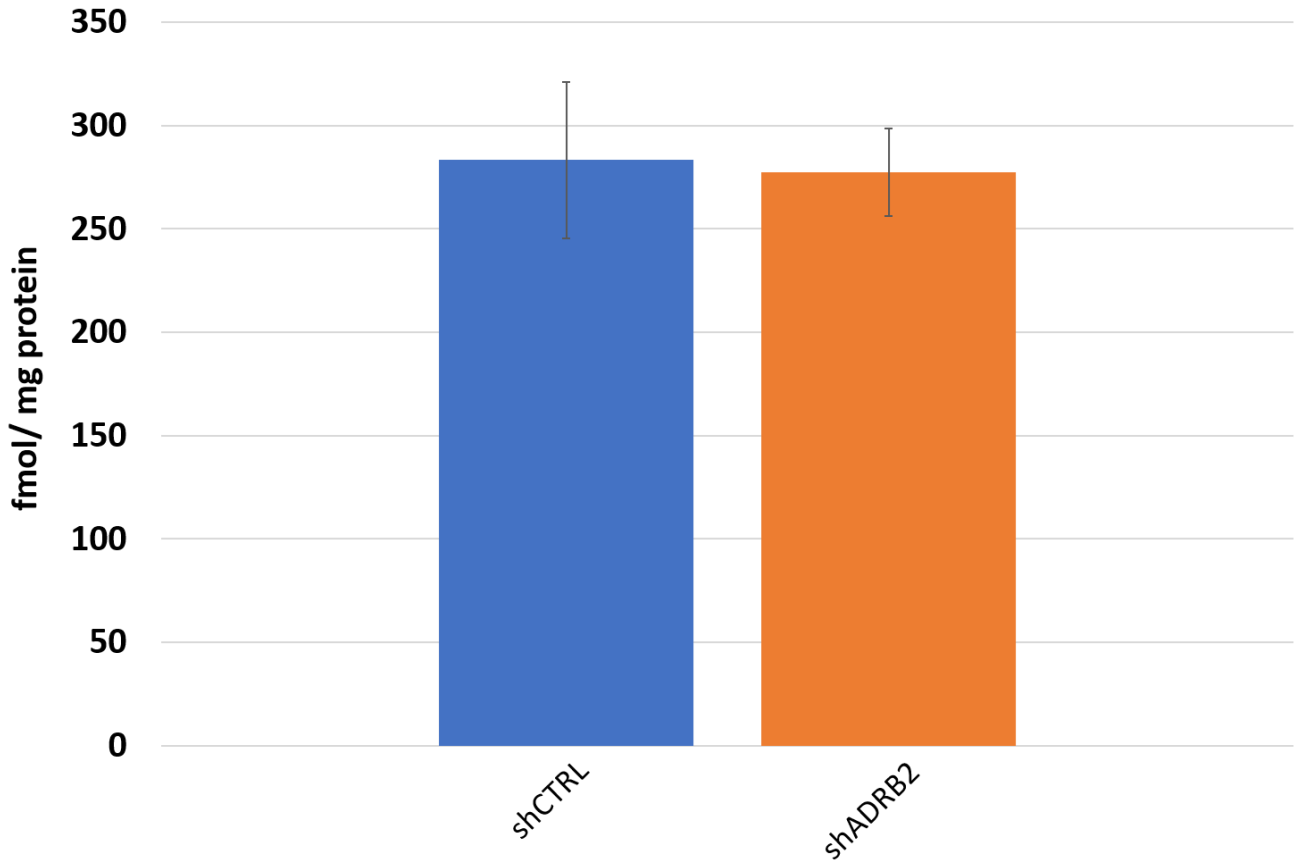

Figure 17 | Expression of ADRB2 in C4-2B transfected with shCTRL vector and with shADRB2 vector. C4-2B cells was transfected with shADRB2 in order to suppress the expression of the ADRB2 gene. A receptor radioligand binding assay was performed on all cell lines, in order to determine the expression level of ADRB2 in transfected cells. Error bars are presented as standard deviation.

5. Discussion

5.1 General discussion

5.1.1 Inducing neurite outgrowth with ROCK-inhibitor and ISO

Stimulation of cell lines with ROCK-inhibitor (Y-27623) and ISO, revealed that the 50 μM ROCK significantly induced the longest neurites and the highest number of neurites in each cell line, followed by 25 μM ROCK, whereas 10 μM ISO increased ($p<0,05$) the average neurite length in the PC-3-Luc2-GFP cell line.

In the study by Park et al. (170), a concentration-dependent induction of neurite outgrowth was observed in the PC-12 cell line treated with the ROCK inhibitor, Y-27632, in the range 0-50 μM for 3 hours. The study revealed that 50 μM ROCK induced neurite outgrowth in the highest number of cells compared to the other concentrations.

Similarly, in a study by Yin et al.(139), it was shown that both 33 μM ROCK-inhibitor and 300 ng/mL nerve growth factor (NGF) induced the outgrowth of neurites in the PC-12 ADH. Based on their findings, we stimulated all the cell lines in our study with ROCK-inhibitor. The study by Yin et al. also confirmed that PC-12 ADH developed neurite outgrowth resistance upon stimulation for 72 hours or more with several ROCK-inhibitors, significantly reducing the effect of the inhibitor. Their result was consistent with the study of Duan et al. (150).

These studies are consistent with the findings in our study, showing that increasing concentration of ROCK-inhibitor is correlated with both longer neurites and increased number of neurites. The highest concentration of ROCK-inhibitor (50 μM) induced the longest neurites (Figure 8) and the highest number of neurites (Figure 9) in each cell line in our study.

Our study as well as several other earlier studies have demonstrated that 50 μM of ROCK-inhibitor is the optimal concentration for neurite outgrowth in prostate cancer cell lines and in the neural cell lines.

In the testis cancer cell line, Nera-2, Lingor et al. revealed that 30 μM of Y-27632 elicited the maximal effect. In neural stem cells, Jia et al (171) showed that 2 μg/mL Y-27632 as the concentration which induced the greatest effect on neurite outgrowth. Further, their observations showed that stimulation for 5 days, doubled the length of the neurites. This can be due to differences in sensitivity between the cell lines, the lower concentration, or in fact that some studies have coated the cells upon culturing.

Based on earlier results and our observations, we can conclude that ROCK-inhibitor has a dose-dependent effect on neurite outgrowth, in which 50 μM ROCK induce the longest neurites and the highest number of neurites per cell compared to untreated and ISO stimulated cells.

5.1.2 ADRB2 agonist ISO was seen to influence neurite outgrowth in prostate cancer cells

Further, we also stimulated the cells with ISO, identified as a short acting ADRB2 agonist. We demonstrated that ISO increased ($p<0,05$) the average length of neurites in the PC-3-Luc2-GFP cell line, and were also shown to increase ($p<0,05$) the number of neurites in the C4-2B cell line. Furthermore, ISO did not induce any morphological change in PC-12 and RSC96 (Figure 7) assessed by visual inspection, in spite of the fact that these cell lines have high levels of ADRB2 (Supplementary figure 4).

We observed early in the study that 200 ng/mL NGF was capable of inducing neurites in a small fraction of PC12 ADH cells, but since the number of cells receiving this morphology was low compared to the effect induced by ROCK inhibitors, NGF was excluded from our study. Others have also shown that only a subpopulation of PC12 cells is able to differentiate in response to NGF. The study by Yin et al. (139) demonstrated that 300 ng/mL NGF did in fact induce neurite outgrowth in both PC-12 cells and in the PC-12 ADH cells.

The effect of NGF was also demonstrated at a lower concentration in the study by Wiatrak et al (160). In this study, it was demonstrated that 100 ng/mL NGF induced neurite outgrowth in both PC-12 ADH cells and PC-12 cells. They observed the effect of NGF for the PC-12 ADH cell was at its highest between 3-5 days of stimulation. Additionally, the study by Yin et al. and the study by Wiatrak et al. demonstrated neurite outgrowth on the PC-12 ADH cells, with the stimulation of NGF. As ROCK-inhibitor induced more and induced longer neurites than NGF, NGF was excluded from the study.

5.1.3 ADRB2 is necessary for neurite outgrowth

In this study we demonstrated that the PC-3-Luc2-GFP cells had the lowest levels of ADRB2 (Supplementary figure 3), and that PC-3-Luc2-GFP cell was the cell line most sensitive to ISO when neurite length was measured (Figure 8D and Figure 10D). Regarding regulation of number of neurites, C4-2B cells that had the highest level of ADRB2 (Supplementary figure 3), was shown to be more responsive to ISO than PC-3-Luc2-GFP cells (Figure 9). Based on this, ADRB2 is important for the development of some cell types, but that if a cell expresses ADRB2 it does not mean that neurites will be formed after activation of ADRB2, by for example ISO.

In the study by Braadland et al.(172), ADRB2 was found to vital for the induction of neurite outgrowth. They demonstrated that high levels of ADRB2 was necessary for neuroendocrine trans differentiation (NED), which was determine based on increased neurite outgrowth. It was found that overexpression of ADRB2 in both AR positive and negative cells, resulted in NE-like cells morphology. Further, by downregulating ADRB2 in the LNCaP cells, it was observed an increase in Wnt signaling, and inhibition of GSK3β was shown to suppress NED in LNCaP. Their findings demonstrate that ADRB2 is vital for NED, additionally they demonstrated that cells with higher ADRB2 expression had longer neurites and higher NED compared to cells with low ADRB2 expression. Further, to show the importance of ADRB2 in neurite outgrowth, they promoted ADRB2 overexpression in cells with low ADRB2 levels, significantly inducing neurite outgrowth, suppressing the activity of the Wnt signaling pathway. Lastly, it was shown that androgen depletion induced NED in PC cells by inducing β-adrenergic and cAMP response element-binding protein (CREB). This was shown to increase the activity of EZH2, leading to formation of β-catenin and inducing neurite outgrowth and NED by suppressing adrenergic activity through high Wnt/β-catenin activity.

Based on these findings, we can clearly see a correlation between long neurites and high ADRB2. As assessed by receptor radioligand binding assay, it was shown that C4-2B cells had the highest concentration of ADRB2 (Supplementary figure 3) and the highest number of neurites induced ($p<0,05$) by stimulation with 50 μM ROCK (Figure 9C) additionally having the longest neurites upon stimulation (Figure 8C). Our results on ROCK-inhibitor is consistent with the findings of Braadland et al. (172), proposing that ADRB2 is crucial for neurite outgrowth, and that cells with higher levels of ADRB2 is more likely to have longer and higher number of neurites.

Similarly, we observed in our study that there is a potential correlation between high levels of ADRB2 and number of outgrown neurites induced by stimulation with 50 μM ROCK. As shown in figure 8, C4-2B cells grew the longest neurite upon stimulation with 50 μM ROCK, and it was also demonstrated that 50 μM ROCK induced the highest number of neurites in the C4-2B cells (Figure 9). Interestingly, it was also shown that C4-2B cells expressed the highest level of ADRB2 (Supplementary figure 3). These results suggest that there is a correlation between ADRB2 expression and number of outgrown neurites induced by stimulation with 50 μM ROCK. As a result, it was demonstrated that C4-2B cells had the highest possibility for NED in our study.

The review by Braadland et al.(24) described the link between ADRB2 and ROCK, as it known that ROCK is a downstream protein of ADRB2 signaling in prostate cancer, there is no doubt that there is a correlation in the level of ADRB2 and sensitivity towards stimulation with ROCK-inhibitor. Further, The study by Somlyo et al. (173) demonstrated that ROCK inhibition induced neurite outgrowth in the prostate cancer cell lines PC-3 and LNCaP. Further, it is believed that PAK4 is an important actor in this signaling pathway, as it capable of directly regulating CREB, which can arbitrate the effect of the ADRB2/cAMP/PKA signaling pathway on NED in PC cells (24, 84). Based on these studies and our findings, we believe that cells with higher levels of ADRB2 has a higher probability for neurite outgrowth and NED when stimulated with ROCK-inhibitor.

5.1.4 Changes in cell proliferation/viability upon stimulation with ROCK-inhibitor and ISO

The results in our study showed that stimulation with 50 μM ROCK decreased the viability in all cell lines, except the C4-2B cell line. In contrast, the study by Jia et al.(171), demonstrated that neither 0,5-2 ug/mL Y-27632 for 4 hours or 1 ug/mL for 8 hours decreased the viability of NSCs as assessed by a MTT-assay. Compared to our experiment, we exposed the cells to a higher dose for a longer time (72 hours), which can potentially be the reason why Jia et al. did not see a decrease in viability, additionally their study was on neural stem cells, and we did in fact demonstrate the effect on both neural cell lines in the study. As shown in figure 11, we showed a decreased in proliferation in both PC-12 ADH cells ($p<0,005$) and in the RSC96 ($p<0,01$) stimulated with 50 μM ROCK. By visual inspection, it is possible to see that

stimulation with 10 μM ISO resulted in a minor decrease in proliferation of the neural cell lines (although not significantly), and increased viability in the prostate cancer cells.

In the study by Gong et al. (127), it was demonstrated the 10 μM ROCK significantly decreased the proliferation in PC-3 cells transfected with ROCK silencing vectors. In accordance with our findings, we observed a decrease ($p<0,005$) in viability for PC-3-Luc2-GFP cells stimulated with 50 μM ROCK (Figure 11D). Additionally, we demonstrated that 50 μM ROCK decreased the viability in the PC-12 ADH cells (Figure11A) and in the RSC96 (Figure 11B). Further, it was observed that Zhang et al.(174) achieved the same results in a model system of gastric cancer (GC) cells. The study demonstrated that three types of β-blockers, selective and not-selective, inhibited proliferation of the GC cells with the dose of 50 μM, as it is a high dose of β-blocker which can induce non-specific effects. Interestingly, they also demonstrated that GC cells pre-treated with agonist, attenuated the effect of the antagonists (β-blockers). Further, they verified their results by transfecting the cells with a shADRB2 vector, in order to silence the ADRB2-gene, which demonstrated that shADRB2 cells had a significantly lower proliferation compared to the control group. The ADRB2 knockdown were also shown to significantly decrease the effect of ISO on proliferation compared to the control group. Lastly, it was demonstrated that 1 μM ISO stimulation increased the viability in the GC cells, and that 50 μM propranolol and ICI118,552 significantly reduced the viability in the GC cells.

The results from the study by Gong et al.(127) and Zhang et al. (174) was in accordance with our observations, where it was shown that stimulation with ROCK-inhibitor decreased both viability and proliferation in both prostate cancer and in gastric. The study by Gong et al. (127), demonstrated that lower concentrations of ROCK-inhibitor decreased viability (10 μM). Interestingly, the difference in ADRB2 expression in between C4-2B and PC-3-Luc2-GFP (Supplementary figure 3) was observed to be the biggest, as C4-2B had the highest level and PC-3-Luc2-GFP had the lowest, this was not observed to have a big impact on ISO regulation of proliferation. Additionally, we demonstrated that 50 μM ROCK decreased viability in PC-12 ADH (Figure 11A) cells as well as in the RSC96 cells (Figure 11B). We did not observe any significant effects of ISO, but it possible for ISO to inhibit the proliferation of PC12 and RSC96 cells, while our observations indicated that it did not influence the prostate cancer cells.

5.1.5 Co-cultures of prostate cancer cells and nerve cells – Migration assay

The migration assay on the prostate cancer cell (PC-3-Luc2-GFP) co-cultured with nerve cells (PC-12 ADH) and Schwann cells (RSC96), showed that the PC-3-Luc2-GFP cell line had the highest migration rate, and similar results were observed for the C4-2B cell line (data not shown). We demonstrated that the neural cell lines (PC-12 ADH and RSC96) had a remarkable lower migration rate than the prostate cancer cell lines, further it was observed that combining both neural cell lines increased migration rate of the cells (Figure 12 and Figure 14).

The ROCK-inhibitor (50 μM) did not affect the migration rate of PC-3-Luc2-GFP or was observed to slightly enhance the migration (Figure 14). Whilst the effect was observed as minimal, our individual data from each co-culture (Figure 12), contradicted the mean data. Supporting our findings in figure 12, the effect of ROCK-inhibitor on PC-3 migration was demonstrated by Gong et al. (127). The study demonstrated that inhibition of ROCK and ROCK-knockdown had an inhibitory effect on the migration and invasion of PC-3 cells and DU145 cells, decreasing the migration rate. Combined, the study demonstrated that ROCK suppression inhibits migration, invasion and proliferation. A significant decrease in migration was observed in ROCK silenced PC-3 cells, which is in contrast with our data. The difference was minimal in our data, and we believed that stimulation with ROCK-inhibitor will have an inhibitory effect on migration and invasion. Similarly, Somlyo et al. (173) demonstrated in a in-vivo study that stimulation with 25 μM ROCK-inhibitor, decreased the migration of PC-3 as the phosphorylation of MLC was remarkably decreased.

Whilst figure 14, showing the average data for each cell line, shows no significant effect of the ROCK-inhibitor on migration, the data achieved from parallel co-culture experiments indicates that ROCK-inhibitor decreases the migration of the PC-3-Luc2-GFP cells (Figure 12). The fact that multiple studies have shown the inhibitory effect of ROCK-inhibitor on cancer cell migration, indicates that the results from figure 12 is consistent with earlier studies.

Supporting the data in Figure 12, the study by Gong et al. (127) demonstrated that PC-3 cells transfected with ROCK silencing vector, inhibited the cell migration and invasion in PC-3- and DU145 cells compared to the control group. By this, they suggested that ROCK is an active actor in metastasis in prostate cancer cells. Further, the study by Zhang et al. (174)

suggested that ADRB antagonist decreased the migration rate in GC cells, where propranolol and ICI118,1551 significantly decrease the migration rate.

As we did not examine the effect of ISO on migration, a wound scratch healing assay performed by Zhang et al. (174) demonstrated that ADRB2 agonists like stress, induced spreading of GC cells. Similarly, the study by Huang et al. (93) demonstrated that ISO did not have any influence on PC-3 and DU145 migration and invasion. Further, the study by Yu et al. (83) it was demonstrated that pre-stimulation with ISO significantly decreased the invasion of the prostate cancer cells, validating the effect of ADRB2 on invasion and metastasis (83)

Suggesting that prostate cancer cells are more likely to have higher migration rate, which could also be due to the metastatic and invasive characteristics of cancer cells, and also demonstrating the importance of ADRB2 in metastasis.

5.1.6 Co-culture model with DRG

In the DRG and C4-2B co-culture, we observed that the C4-2B cells seemed to migrate towards the DRG in the Matrigel. As the neurites on the DRG increased (Figure 16 A), it was observed that cells derived from the DRG and migrated outwards. Further, as shown in figure 15 and figure 16B, some of the C4-2B cells managed to cross the Matrigel and interact with the DRG derived cells. Our observations demonstrated that the C4-2B migrated on the neurites extending from the DRG derived cells (Figure 15). By performing this co-culture model system, we illustrated the microenvironment in perineural invasion areas, in order to illustrate how the prostate cancer cells can migrate and metastasize using the nerves as a highway to other tissues.

In the study by Deborde et al. (73), it was suggested that the Schwann cells (RSC96) attracted the pancreatic cancer cells towards the DRG. It was shown that the cancer was recruited on the neurites after 24-48 hours upon harvesting and was observed to migrate towards the DRG on the long neurites extending from the DRG. We were not able to see the migration of cancer cells towards the DRG on neurites extending, due to the high amount of C4-2B cells and the high amount of DRG derived cells. Further, they observed that the cancer cells which was not in contact with nerves, had a very low migration rate, suggesting that nerves increase the migration of cancer cells.

Early in our study, we demonstrated that RSC96 cells had the lowest migration rate when co-cultures alone with prostate cancer cells (Figure 12 and Figure 14). Interestingly, Deborde et al. (73) observed by time-lapse videos that the Schwann cells was highly dynamic, increasing the contact with the cancer cells, with is in contrast with our observations. Following, their study demonstrated that the cancer cells migrated in the direction of Schwann cells, and was recruited to the DRG. Proposing that the Schwann cells is a very important actor in this co-culture model system. Further, it was noticed that the C4-2B cells was interacting with the DRG and the cells derived from the DRG (Figure 16B), while these observation does that conclude that we observed migration of PC cells on nerves, the findings of Deborde et al. (73) propose that this is possible and is induced by Schwann cells.

5.1.7 Reverse transfection of shADRB2

The C4-2B cell line was transfected with two shADRB2 vector, shRNA-76 or shRNA-79, in which both function to suppress the expression of the ADRB2-gene but are compose of different sequences. A third vector shCTRL were also transfected, clone 81, which is composed of a non-specific sequence designed to not bind any RNA and was used as a clone. Non viable cell clones were obtained from shRNA-76.

Our results suggest that the shADRB2 vector was not successfully transfected as assessed by receptors radioligand binding assay and by immunofluorescence staining. By measuring the total amount of ADRB2 in C4-2B shCTRL and C4-2B shADRB2 (Figure 17), we did not observe any remarkable difference. As assessed by receptors radioligand binding assay, it was demonstrated that the C4-2B cell line had the highest levels of ADRB2, whilst the PC-3-Luc2-GFP cell line had the lowest (Supplementary figure 3).

By our observations and other discussed studies, we strongly believe that silencing of ADRB2 gene will result in reduced migration, proliferation, and invasiveness of the prostate cancer cells, mimicking the effect of β-blockers.

5.2 Methodological discussion

5.2.1 Selection of cell lines

The PC-12 cell line was used as the primary nerve cell line our study. Based on the study by Yin et al. (139), the PC-12 ADH subline of the PC-12 cell line was found to be more sensitive against the ROCK-inhibitor, demonstrating that ROCK-inhibitor exhibited a greater effect on the subline compare the original and was therefore preferred in our study. The PC-12 cell line is a well characterized neural cell line (sympathetic ganglion, secreting catecholamines).

It is known that PC-12 ADH cells is the adherent phenotype of the PC-12 cell line, making the subline display higher proliferation rate compared to the original PC-12 cell line and making the capable of proliferating on plastic surface. The original PC-12 cell line in the other hand, requires coated surface for enhance growth and avert aggregation (160). The fact that these cells are not human isolated cells, raises the question of whether these cells can represent NED in humans. The limitation of the PC-12 ADH cell lines is one of the arguments for performing DRG co-culture, in order to validate out findings with the PC-12 ADH cells.

The prostate cancer (PC) cell line used in our study represents castration refractory prostate cancer (CRCP) cell lines. Based on the cell lines, we cannot conclude that our results are representative for hormone-sensitive prostate cancer (HSPC). The CRPC cell lines are relevant for our study, based on the fact that most patients are treated with hormone therapy when the disease is in the metastatic phase, whereas we want target and inhibit metastasis in our study.

The Schwann cells (RSC96) are myelin producing cells, responsible for myelinating axons. Several studies have shown that these cells are responsible for recruiting prostate cancer cells to nerves, inducing PNI and resulting in metastasis. Based on this, the Schwann cells are relevant for our study in order to see if they influence the migration of the prostate cancer cells. Indicates, to be involved in the interaction between nerves and cancer cells, as demonstrated by the DRG model system by Deborde et al. (73).

The choice of these cells forms the foundation for our co-culture model systems, with prostate cancer cells and nerve cells, mimicking the TME in PNI.

5.2.2 Changes in cell proliferation/viability

The confluence of each cell line with both stimulation was obtain from the IncuCyte FLR, in order to characterize the proliferation profile of each of the cell lines and determine the effect of the stimulations on the proliferation. These data are not presented due to lack of overlap between the results and what was observed in the microscope. The growth-curves plotted based on the confluence data, was seen to have a lot outlier for each time the medium was change. Further, it was observed that medium change resulted in the loosening of some cells, C4-2B cells specifically, giving faulty confluence data and an improbable confluence.

We also corrected the confluence on later experiments by changing to the IncuCyte Zoom, using confluence mask to attain better measurement of confluence, but the results were still not acceptable.

A better method to quantify alterations in proliferation/survival is cell counting. Here we harvested each cell line in 6-well plates with the same number of cells and the same stimulative conditions as the neurite outgrowth experiment. A 6-well plate was employed in order to have two parallels for each measurement with NucleoCounter. The data was then used to support the earlier confluence data and compare the data between the two parallel experiments.

5.2.3 Optimizing the method for migration assay and developing co-culture

In the start of the study our goal was to see the interaction between the two cell types and the migration pattern of each cell line in the presence of each other. We started performing the experiments with two types of inserts, 4-well and 2-well and we determined shortly that the 4-wells were more suitable for our study and that using 4-well inserts increased the chance of capturing interaction areas when removing the insert and tracking the migration. Some of our experiments was excluded due to faulty placement of inserts, which resulted in cells growing under the insert and deforming the unoccupied area of migration.

As we optimized a migration assay with inserts, our method had its limitations. Determination of cell quantity was the biggest issue. We had already gathered data from the co-cultures with 5 000 cells, and further we determined that each insert needed to be nearly 100% occupied of cells in order to get an accurate measure of migration. This because, we observed that big gaps between the cells in each well resulted in slower migration or no migration at all, because the cells proliferated in order to fill the gaps and was seen to consume a lot of time.

Further it was determined to harvest 10 000 cells in each well, and cells was harvested in accordance to figure 6, in order to increase and optimize the area of migration between the cell lines.

Furthermore, in our migration assay we used plastic surfaces without coating, which can influence and potentially decrease the migration of the cell lines. It is believed that coating, like collagen, may influences the migration of the cell lines and enhance the migration rate of the cells, based on the fact that the cells contain transmembrane collagen receptors, which is believed to activate actomyosin (175), promoting cytokinesis and potentially increasing motility and migration (176).

Moreover, it was noticed the some of the cells had the tendance of loosening under medium shift, leading to cells appearing in different location and destroying the data. This was handled by leaving 200 μL of medium in the wells, instead of completely sucking up all the medium in the well, and as a result only 800 μL of new medium was added to the wells. Furthermore, upon optimizing our method we achieved a lot of data on all cell lines expect the C4-2B cell line, which was excluded from the migration assay because of infections in the cell culture. From our earlier experiments, we observed that the PC-3-Luc2-GFP cell line and the C4-2B cell line had a lot of similar proliferative and migrative characteristics. Importantly, it was observed that ROCK-inhibitor decreased ($p<0,005$) the proliferation of PC-3-Luc2-GFP cells, but was not able to influence the proliferation in the C4-2B cells, which was a remarkable difference between the two cell lines. Based on these observations, the PC-3-Luc2-GFP cell line was used as the primary prostate cancer cell line for the migration assay.

When the PC-12 ADH cells and RSC96 were cultured in combination, we were not able to distinguish them from one and other, left us unable to identify the fastest migration cell in combinate cultivation of PC-12 ADH and RSC96.

Further, there is several methods used for measuring and quantifying cell migration today. One of the frequent used assays is Boyden chamber migration assay, which is a transwell migration assay, were cells are loaded on into a well containing serum-free medium and a semi-permeable monolayer, separating the bottom of the well which may contain chemoattractant or nutrients. This technique forces migration of the cells through pores in the semi-permeable monolayer, using chemotaxis as the driving force. Lastly, the cells which have migrated to the membrane can be counted and stained (177). This method is highly dependent on expertise, and one of the biggest disadvantages is that the method does not

enable cell tracking over time, which is relevant for ours study. Addintioally, the method is based on manual counting of cells migrated through the membrane, and as a result we only get the needed for each cell line to migrated to the membrane (178). Further, wound scratch healing assay is performed by physically constructing a scratch on plated cells. Similar with the Boyden chamber, this method provides the time need for the cells to either migrate or proliferate to enclose the scratch. In contrast to Boyden chamber, cells can be tracked by microscopic analysis, enabling a time lapse of the ell migration.

Both of these methods focus on one cell line for each assay, whereas the migration assay we performed enables quantification of two cell groups. Additionally, the wound scratch healing assay combines the proliferative and migrative characteristics of each cell line, providing more reproducible data. Suggesting, that proliferation may be a factor for migration rate in our study. Earlier in the study, we observed that too few cells resulted in very low migration and that the cells with higher proliferation migrated further (data not shown).

5.2.4 Co-culture model with DRG

A model system with GFP expressing dorsal root ganglia and C4-2B co-culture was performed to map the migration of C4-2B cells in the presence of DRG. This model system was set up in order to mimic TME in PNI, as DRG model systems with cancer cells are frequently used for observation of cancer cells an neural cell interaction (179, 180), where DRG isolated from mouse is cultivated with human cancer cells. The importance of this model system was demonstrated in the study by Deborde et al. (73), where it was shown that Schwann cells is responsible of recruiting the cancer cells along the nerves extending from DRG, demonstrating the mechanism of PNI, an stating the importance of DRG model systems to observe interaction between cancer cells and nerve cells. An important limitation of this model system is that the cancer cells are usually human isolated whereas the DRG are isolated from mouse, which may result incompatibility in protein interactions from the different species (180). In contrast, it has been shown that metastatic cells with the ability of neural invasion does not cause incompatibility (180). Additionally, a DRG proteome analysis by Schwaid et al. (181) compared the human DRG and DRG isolated mouse, and suggested that these DRG were somewhat similar, indicating that results obtain from these model systems can be related to PNI process in human cancers, as most DRG model studies investigates the TME of PNI (51, 73, 180, 182).

By visual inspection, it was challenging to determine whether the C4-2B cells migrated in or on the Matrigel droplet containing the DRG. We observed the attraction between the C4-2B cells and the DRG derived cells, but based on our findings we cannot not conclude that one of the cells was more attracted to the other cell line, which was the biggest restriction using the fluorescence microscope for tracking. Images were taken every 24 hours. This method was not optimal for tracking the cells, due to the large quantity of the C4-2B cells and their high migrative capabilities and due to the fact that images were only taking once a day, making the method impractical, time consuming and impossible to perform time lapse of the migration.

The solution was to perform the study on the Cytation5 imaging instrument, in order to see the migration pattern of the cell. Cytation5 enables minute for minute tracking of cells, illustrating the migration patterns of C4-2B cells towards the DRG. Due to technical difficulties, we were not able to perform the experiment on the Cytation5 within the timeframe of this thesis.

5.2.5 Isolation and purification of membrane fractions

In the process of membrane isolation, it was observed that the pellets loosened from the glass tubes and was mixed with the supernatant, demolishing the protein sample. This was observed in the situations where the dissertation of the supernatant was delayed and resulted in the dissociation of the pellet. The dissociated pellets were re-centrifuged, but a much smaller pellet was observed, and majority of the protein sample was discarded along with the supernatant. Additionally, the Beckman-Coulter centrifuge crashed, leaving the sample glasses in the centrifuge. As earlier observations, it was seen that the pellet was partially dissolved in the supernatant, omitting proteins from our sample. Due to loss of protein samples, these samples were excluded from our data and results.

5.2.6 BCA-protein assay

As the BCA-protein assay is one of the most frequent used method for protein measurement, the method is compatible with both ionic and non-ionic detergents as well as other substances and materials, which are factors known to interfere with some coulometric protein assays (183). The method is capable of measuring protein concentrations between 0,5 µg/mL up to 1,5 mg/mL, which makes the method relevant for measuring a variety of protein

concentrations. The BCA-assay is known to being a extreme sensitive method, and it is proposed that it is about 100 times more sensitive compared to the Biuret method. As all methods have some limitations, it is shown that the accuracy of the results is vulnerable in the presence of amino acids like cysteine, tryptophane and tyrosine (184). Further, it is known that lipids (185) and reagents like ethylenediaminetetraacetic acid (EDTA)(186) can interfere and disturb the efficiency and sensitivity of the method (184). However, it is suggested that high protein concentration is adequate to ameliorate with these interferences (184).

The study by Reichelt et al.(187), suggested that use of BSA protein spikes in the samples can be a correction factor, as it increases the accuracy of the results. By doing this, it was shown that the efficiency and sensitivity of the method was remarkably increased, which means that the method can compete with the expensive and more advanced methods (184, 187). As most kits contains own standard curves today, enabling the user to compare the measured proteins against known sample concentrations. BSA protein standards were used in our BCA-assay as plots, in order to provide the absorbance versus the assorted concentration of known proteins.

6. Conclusions

By performing co-culture model systems, we demonstrated that PC-3-Luc2-GFP cells had the highest migration among the other cells in the study, and that stimulation with ROCK-inhibitor (50 μM) did not influence the migration rate. Based on our migration assay, we did not have enough data to determine the effect of ROCK-inhibitor on migration of prostate cancer cells, but we demonstrated that ROCK-inhibitor significantly decreased proliferation in the neural cells and in PC-3-Luc2-GFP cells. Our migrations assay also demonstrated that ROCK-inhibitor decreased neural migration. Based on earlier studies and our findings, we believe that ROCK-inhibitor decrease the migration of prostate cancer cells and among several other cancer cells, which may be a important therapeutic target as it is known that ROCK is a downstream protein of ADRB2.

By our observation and results, we can conclude that stimulation with 50 μM ROCK for 48 hours, induced neurite outgrowth and bestow the longest neurites in the neural cell lines and the prostate cancer cells. Additionally, we demonstrated that PC-3-Luc2-GFP cells had the lowest levels of ADRB2 and was most sensitive to ISO induced neurite outgrowth. Indicating an association with low ADRB2 expression and sensitivity towards ADRB2 agonist. Not resembling with these indications, the C4-2B cells was seen to having the highest level of ADRB2, and also seen to be very sensitive to stimulation with antagonist and agonist like the PC-3-Luc2-GFP cells. The PC-3-Luc2-GFP cell line was included late in the study, resulting in missing data for the concertation curve of ROCK-inhibitor and time dependent response of 50 μM ROCK. Our observations suggested that the PC-3-Luc2-GFP cells and C4-2B cells had similar migrative and proliferative characteristic, while it was demonstrated that C4-2B proliferation is not influenced by stimulation with ROCK-inhibitor (50 μM). This indicates that the migration rate of C4-2B cells stimulated with ROCK-inhibitor (50 μM) could potentially be higher compared to what's observed and known with the PC-3-Luc2-GFP cells.

Taking together, our results indicates that use of specific β-blockers can repress the growth and progression of prostate cancer along with other cancers, by decreasing proliferation, viability and migration of the prostate cancer cells, but more studies are needed in the support of β-blocker use and combinational therapies should be assessed.

7. Future aspects of the study

Our data illustrates that ROCK-inhibitor is a promising ADRB2 antagonist for inhibiting metastasis and proliferation of PC cells, as migration of PC cells is driving force in metastasis and PNI. The process of metastasis and PNI consist of many bricks, as our study demonstrates the effect of ROCK-inhibitor, indicating that ROCK is a downstream protein of ADRB2 signaling.

Further, more data are needed in order to demonstrate the influence of ROCK-inhibitor on PC migration, by using PC cell and nerve cell model systems and DRG model systems. More studies on DRG and PC model systems are necessary in order to get an understanding of the mechanism in which Schwann cells recruits PC cells on the nerves and induce PNI and metastasis. Potentially optimizing this method and enable time lapses of the interactions between PC cells and Schwann cells. Similarly, it would be of interest to identify the chemokines secreted by the Schwann cells which attracts the PC cells through chemotaxis. By identifying these chemokines, the signal pathways in which they activate can be investigated and put in a bigger perspective.

In order to determine and demonstrate the importance of ADRB2 on migration, it would be interesting to obtain data on co-culture with silenced ADRB2 or silenced ROCK PC cells, to determine their influence on migration, and give comprehension of the association between ADRB2 and ROCK. Lastly, to stimulate PC cells with β-blocker in co-culture model system with DRG, to see whether this influences PNI.

Combining these experiments and co-cultures model systems, we believed that it is possible to get an better understanding of the underlying mechanism of PC metastasis and PNI.

8. References

1. Sherwood ER, Berg LA, Mitchell NJ, McNeal JE, Kozlowski JM, Lee C. Differential cytokeratin expression in normal, hyperplastic and malignant epithelial cells from human prostate. J Urol. 1990;143(1):167-71.
2. Liu AY, Roudier MP, True LD. Heterogeneity in primary and metastatic prostate cancer as defined by cell surface CD profile. Am J Pathol. 2004;165(5):1543-56.
3. Rybak AP, Bristow RG, Kapoor A. Prostate cancer stem cells: deciphering the origins and pathways involved in prostate tumorigenesis and aggression. Oncotarget. 2015;6(4):1900-19.
4. Zahalka AH, Arnal-Estape A, Maryanovich M, Nakahara F, Cruz CD, Finley LWS, et al. Adrenergic nerves activate an angio-metabolic switch in prostate cancer. Science. 2017;358(6361):321-6.
5. Chen D, Ayala GE. Innervating Prostate Cancer. N Engl J Med. 2018;378(7):675-7.
6. Reeves F, Everaerts W, Murphy DG, Costello A. Chapter 29 - The Surgical Anatomy of the Prostate. In: Mydlo JH, Godec CJ, editors. Prostate Cancer (Second Edition). San Diego: Academic Press; 2016. p. 253-63.
7. Hu CD, Choo R, Huang J. Neuroendocrine differentiation in prostate cancer: a mechanism of radioresistance and treatment failure. Front Oncol. 2015;5:90.
8. Pernar CH, Ebot EM, Wilson KM, Mucci LA. The Epidemiology of Prostate Cancer. Cold Spring Harb Perspect Med. 2018;8(12).
9. Prostatakreft [Internet] Oslo: Kreft registeret; 2009 [updated 21.01.2021; cited 2021 10.4]. Available from: https://www.kreftregisteret.no/Temasider/kreftformer/Prostatakreft/.
10. Sejda A, Sigorski D, Gulczynski J, Wesolowski W, Kitlinska J, Izycka-Swieszewska E. Complexity of Neural Component of Tumor Microenvironment in Prostate Cancer. Pathobiology. 2020;87(2):87-99.
11. He S, He S, Chen CH, Deborde S, Bakst RL, Chernichenko N, et al. The chemokine (CCL2-CCR2) signaling axis mediates perineural invasion. Mol Cancer Res. 2015;13(2):380-90.
12. Liebig C, Ayala G, Wilks JA, Berger DH, Albo D. Perineural invasion in cancer: a review of the literature. Cancer. 2009;115(15):3379-91.
13. Ayala GE, Dai H, Ittmann M, Li R, Powell M, Frolov A, et al. Growth and survival mechanisms associated with perineural invasion in prostate cancer. Cancer Res. 2004;64(17):6082-90.

14. Croker J, Burmeister B, Foote M. Neurotropic melanoma: the management of localised disease. J Skin Cancer. 2012;2012:706452.
15. Ayala GE, Dai H, Powell M, Li R, Ding Y, Wheeler TM, et al. Cancer-related axonogenesis and neurogenesis in prostate cancer. Clin Cancer Res. 2008;14(23):7593-603.
16. Chernichenko N, Omelchenko T, Deborde S, Bakst RL, He S, Chen CH, et al. Cdc42 Mediates Cancer Cell Chemotaxis in Perineural Invasion. Mol Cancer Res. 2020;18(6):913-25.
17. Fromont G, Godet J, Pires C, Yacoub M, Dore B, Irani J. Biological significance of perineural invasion (PNI) in prostate cancer. Prostate. 2012;72(5):542-8.
18. Zareba P, Flavin R, Isikbay M, Rider JR, Gerke TA, Finn S, et al. Perineural Invasion and Risk of Lethal Prostate Cancer. Cancer Epidemiol Biomarkers Prev. 2017;26(5):719-26.
19. Shen MM, Abate-Shen C. Molecular genetics of prostate cancer: new prospects for old challenges. Genes Dev. 2010;24(18):1967-2000.
20. How does the prostate work? : Institute for Quality and Efficiency in Health Care [Internet] (IQWiG); 2011 [updated August 23, 2016; cited 2021 4.5]. Available from: https://www.ncbi.nlm.nih.gov/books/NBK279291/#!po=62.5000.
21. Ittmann M. Anatomy and Histology of the Human and Murine Prostate. Cold Spring Harb Perspect Med. 2018;8(5).
22. Henry GH, Malewska A, Joseph DB, Malladi VS, Lee J, Torrealba J, et al. A Cellular Anatomy of the Normal Adult Human Prostate and Prostatic Urethra. Cell Rep. 2018;25(12):3530-42 e5.
23. Singh O, Bolla SR. Anatomy, Abdomen and Pelvis, Prostate. StatPearls. Treasure Island (FL)2021.
24. Braadland PR, Ramberg H, Grytli HH, Tasken KA. beta-Adrenergic Receptor Signaling in Prostate Cancer. Front Oncol. 2014;4:375.
25. Ganzer R, Stolzenburg JU, Wieland WF, Brundl J. Anatomic study of periprostatic nerve distribution: immunohistochemical differentiation of parasympathetic and sympathetic nerve fibres. Eur Urol. 2012;62(6):1150-6.
26. Grozescu T, Popa F. Prostate cancer between prognosis and adequate/proper therapy. J Med Life. 2017;10(1):5-12.
27. Cuzick J, Thorat MA, Andriole G, Brawley OW, Brown PH, Culig Z, et al. Prevention and early detection of prostate cancer. Lancet Oncol. 2014;15(11):e484-92.

28. van Leenders GJ, Gage WR, Hicks JL, van Balken B, Aalders TW, Schalken JA, et al. Intermediate cells in human prostate epithelium are enriched in proliferative inflammatory atrophy. Am J Pathol. 2003;162(5):1529-37.
29. De Marzo AM, Nelson WG, Meeker AK, Coffey DS. Stem cell features of benign and malignant prostate epithelial cells. J Urol. 1998;160(6 Pt 2):2381-92.
30. Bonkhoff H, Stein U, Remberger K. Multidirectional differentiation in the normal, hyperplastic, and neoplastic human prostate: simultaneous demonstration of cell-specific epithelial markers. Hum Pathol. 1994;25(1):42-6.
31. Armbruster DA. Prostate-specific antigen: biochemistry, analytical methods, and clinical application. Clin Chem. 1993;39(2):181-95.
32. Zahalka AH, Frenette PS. Nerves in cancer. Nat Rev Cancer. 2020;20(3):143-57.
33. Karemaker JM. An introduction into autonomic nervous function. Physiol Meas. 2017;38(5):R89-R118.
34. Sternini C. Organization of the peripheral nervous system: autonomic and sensory ganglia. J Investig Dermatol Symp Proc. 1997;2(1):1-7.
35. White CW, Xie JH, Ventura S. Age-related changes in the innervation of the prostate gland: implications for prostate cancer initiation and progression. Organogenesis. 2013;9(3):206-15.
36. Doggweiler R, Zermann DH, Ishigooka M, Schmidt RA. Botox-induced prostatic involution. Prostate. 1998;37(1):44-50.
37. Lujan M, Paez A, Llanes L, Angulo J, Berenguer A. Role of autonomic innervation in rat prostatic structure maintenance: a morphometric analysis. J Urol. 1998;160(5):1919-23.
38. Kato T, Watanabe H, Shima M, Kaiho H. [Studies on the innervation of prostate. 2. Histological changes of the dog prostate after transsection of its innervating nerves]. Nihon Hinyokika Gakkai Zasshi. 1971;62(9):704-7.
39. Watanabe H, Kato H, Kato T, Morita M, Takahashi H. [Studies on the innervation of the prostate. I. Tissue respiration of the dog prostate after the cutting off of the various innervating nerves]. Nihon Hinyokika Gakkai Zasshi. 1967;58(4):381-5.
40. Powell MS, Li R, Dai H, Sayeeduddin M, Wheeler TM, Ayala GE. Neuroanatomy of the normal prostate. Prostate. 2005;65(1):52-7.
41. Farnsworth WE. Prostate stroma: physiology. Prostate. 1999;38(1):60-72.
42. Koopman FA, Stoof SP, Straub RH, Van Maanen MA, Vervoordeldonk MJ, Tak PP. Restoring the balance of the autonomic nervous system as an innovative approach to the treatment of rheumatoid arthritis. Mol Med. 2011;17(9-10):937-48.

43. March B, Faulkner S, Jobling P, Steigler A, Blatt A, Denham J, et al. Tumour innervation and neurosignalling in prostate cancer. Nat Rev Urol. 2020;17(2):119-30.
44. Ventura S, Pennefather J, Mitchelson F. Cholinergic innervation and function in the prostate gland. Pharmacol Ther. 2002;94(1-2):93-112.
45. Carlson AB, Kraus GP. Physiology, Cholinergic Receptors. StatPearls. Treasure Island (FL)2021.
46. Heilbronn E, Bartfai T. Muscarinic acetylcholine receptor. Prog Neurobiol. 1978;11(3-4):171-88.
47. Goepel M, Wittmann A, Rubben H, Michel MC. Comparison of adrenoceptor subtype expression in porcine and human bladder and prostate. Urol Res. 1997;25(3):199-206.
48. Magnon C, Hall SJ, Lin J, Xue X, Gerber L, Freedland SJ, et al. Autonomic nerve development contributes to prostate cancer progression. Science. 2013;341(6142):1236361.
49. Olar A, He D, Florentin D, Ding Y, Ayala G. Biologic correlates and significance of axonogenesis in prostate cancer. Hum Pathol. 2014;45(7):1358-64.
50. Pundavela J, Demont Y, Jobling P, Lincz LF, Roselli S, Thorne RF, et al. ProNGF correlates with Gleason score and is a potential driver of nerve infiltration in prostate cancer. Am J Pathol. 2014;184(12):3156-62.
51. Ayala GE, Wheeler TM, Shine HD, Schmelz M, Frolov A, Chakraborty S, et al. In vitro dorsal root ganglia and human prostate cell line interaction: redefining perineural invasion in prostate cancer. Prostate. 2001;49(3):213-23.
52. Chung LW, Baseman A, Assikis V, Zhau HE. Molecular insights into prostate cancer progression: the missing link of tumor microenvironment. J Urol. 2005;173(1):10-20.
53. Zhao CM, Hayakawa Y, Kodama Y, Muthupalani S, Westphalen CB, Andersen GT, et al. Denervation suppresses gastric tumorigenesis. Sci Transl Med. 2014;6(250):250ra115.
54. Kobayashi N, Asamoto S, Doi H, Ikeda Y, Matusmoto K. Spontaneous regression of herniated cervical disc. Spine J. 2003;3(2):171-3.
55. Francis F, Koulakoff A, Boucher D, Chafey P, Schaar B, Vinet MC, et al. Doublecortin is a developmentally regulated, microtubule-associated protein expressed in migrating and differentiating neurons. Neuron. 1999;23(2):247-56.
56. Couillard-Despres S, Winner B, Schaubeck S, Aigner R, Vroemen M, Weidner N, et al. Doublecortin expression levels in adult brain reflect neurogenesis. Eur J Neurosci. 2005;21(1):1-14.

57. Brown JP, Couillard-Despres S, Cooper-Kuhn CM, Winkler J, Aigner L, Kuhn HG. Transient expression of doublecortin during adult neurogenesis. J Comp Neurol. 2003;467(1):1-10.
58. Dobrenis K, Gauthier LR, Barroca V, Magnon C. Granulocyte colony-stimulating factor off-target effect on nerve outgrowth promotes prostate cancer development. Int J Cancer. 2015;136(4):982-8.
59. Mauffrey P, Tchitchek N, Barroca V, Bemelmans AP, Firlej V, Allory Y, et al. Progenitors from the central nervous system drive neurogenesis in cancer. Nature. 2019;569(7758):672-8.
60. Arese M, Bussolino F, Pergolizzi M, Bizzozero L, Pascal D. Tumor progression: the neuronal input. Ann Transl Med. 2018;6(5):89.
61. Huang T, Fan Q, Wang Y, Cui Y, Wang Z, Yang L, et al. Schwann Cell-Derived CCL2 Promotes the Perineural Invasion of Cervical Cancer. Front Oncol. 2020;10:19.
62. Bapat AA, Hostetter G, Von Hoff DD, Han H. Perineural invasion and associated pain in pancreatic cancer. Nat Rev Cancer. 2011;11(10):695-707.
63. Binmadi NO, Basile JR. Perineural invasion in oral squamous cell carcinoma: a discussion of significance and review of the literature. Oral Oncol. 2011;47(11):1005-10.
64. Marchesi F, Piemonti L, Mantovani A, Allavena P. Molecular mechanisms of perineural invasion, a forgotten pathway of dissemination and metastasis. Cytokine Growth Factor Rev. 2010;21(1):77-82.
65. Fernandez EJ, Lolis E. Structure, function, and inhibition of chemokines. Annu Rev Pharmacol Toxicol. 2002;42:469-99.
66. Murphy PM. Chemokines and the molecular basis of cancer metastasis. N Engl J Med. 2001;345(11):833-5.
67. Kulbe H, Levinson NR, Balkwill F, Wilson JL. The chemokine network in cancer--much more than directing cell movement. Int J Dev Biol. 2004;48(5-6):489-96.
68. Roussos ET, Condeelis JS, Patsialou A. Chemotaxis in cancer. Nat Rev Cancer. 2011;11(8):573-87.
69. Muller A, Homey B, Soto H, Ge N, Catron D, Buchanan ME, et al. Involvement of chemokine receptors in breast cancer metastasis. Nature. 2001;410(6824):50-6.
70. Ben-Baruch A. Organ selectivity in metastasis: regulation by chemokines and their receptors. Clin Exp Metastasis. 2008;25(4):345-56.

71. Guo K, Ma Q, Li J, Wang Z, Shan T, Li W, et al. Interaction of the sympathetic nerve with pancreatic cancer cells promotes perineural invasion through the activation of STAT3 signaling. Mol Cancer Ther. 2013;12(3):264-73.
72. Jessen KR, Mirsky R, Lloyd AC. Schwann Cells: Development and Role in Nerve Repair. Cold Spring Harb Perspect Biol. 2015;7(7):a020487.
73. Deborde S, Omelchenko T, Lyubchik A, Zhou Y, He S, McNamara WF, et al. Schwann cells induce cancer cell dispersion and invasion. J Clin Invest. 2016;126(4):1538-54.
74. Demir IE, Boldis A, Pfitzinger PL, Teller S, Brunner E, Klose N, et al. Investigation of Schwann cells at neoplastic cell sites before the onset of cancer invasion. J Natl Cancer Inst. 2014;106(8).
75. Xue CB, Wang A, Meloni D, Zhang K, Kong L, Feng H, et al. Discovery of INCB3344, a potent, selective and orally bioavailable antagonist of human and murine CCR2. Bioorg Med Chem Lett. 2010;20(24):7473-8.
76. Dagouassat M, Suffee N, Hlawaty H, Haddad O, Charni F, Laguillier C, et al. Monocyte chemoattractant protein-1 (MCP-1)/CCL2 secreted by hepatic myofibroblasts promotes migration and invasion of human hepatoma cells. Int J Cancer. 2010;126(5):1095-108.
77. McCorry LK. Physiology of the autonomic nervous system. Am J Pharm Educ. 2007;71(4):78.
78. Kasbohm EA, Guo R, Yowell CW, Bagchi G, Kelly P, Arora P, et al. Androgen receptor activation by G(s) signaling in prostate cancer cells. J Biol Chem. 2005;280(12):11583-9.
79. Cox ME, Deeble PD, Bissonette EA, Parsons SJ. Activated 3',5'-cyclic AMP-dependent protein kinase is sufficient to induce neuroendocrine-like differentiation of the LNCaP prostate tumor cell line. J Biol Chem. 2000;275(18):13812-8.
80. Wells CM, Whale AD, Parsons M, Masters JR, Jones GE. PAK4: a pluripotent kinase that regulates prostate cancer cell adhesion. J Cell Sci. 2010;123(Pt 10):1663-73.
81. Ramberg H, Eide T, Krobert KA, Levy FO, Dizeyi N, Bjartell AS, et al. Hormonal regulation of beta2-adrenergic receptor level in prostate cancer. Prostate. 2008;68(10):1133-42.
82. Cerami E, Gao J, Dogrusoz U, Gross BE, Sumer SO, Aksoy BA, et al. The cBio cancer genomics portal: an open platform for exploring multidimensional cancer genomics data. Cancer Discov. 2012;2(5):401-4.

83. Yu J, Cao Q, Mehra R, Laxman B, Yu J, Tomlins SA, et al. Integrative genomics analysis reveals silencing of beta-adrenergic signaling by polycomb in prostate cancer. Cancer Cell. 2007;12(5):419-31.
84. Park MH, Lee HS, Lee CS, You ST, Kim DJ, Park BH, et al. p21-Activated kinase 4 promotes prostate cancer progression through CREB. Oncogene. 2013;32(19):2475-82.
85. Park SY, Kang JH, Jeong KJ, Lee J, Han JW, Choi WS, et al. Norepinephrine induces VEGF expression and angiogenesis by a hypoxia-inducible factor-1alpha protein-dependent mechanism. Int J Cancer. 2011;128(10):2306-16.
86. Plecas B, Glavaski A, Solarovic T. Propranolol treatment affects ventral prostate blood vessels and serum testosterone concentrations in adult rats. Andrologia. 1997;29(2):109-14.
87. Lang K, Drell TLt, Lindecke A, Niggemann B, Kaltschmidt C, Zaenker KS, et al. Induction of a metastatogenic tumor cell type by neurotransmitters and its pharmacological inhibition by established drugs. Int J Cancer. 2004;112(2):231-8.
88. Chen W, Mao K, Liu Z, Dinh-Xuan AT. The role of the RhoA/Rho kinase pathway in angiogenesis and its potential value in prostate cancer (Review). Oncol Lett. 2014;8(5):1907-11.
89. Chen W, Mao K, Hua-Huy T, Bei Y, Liu Z, Dinh-Xuan AT. Fasudil inhibits prostate cancer-induced angiogenesis in vitro. Oncol Rep. 2014;32(6):2795-802.
90. Rasiah KK, Kench JG, Gardiner-Garden M, Biankin AV, Golovsky D, Brenner PC, et al. Aberrant neuropeptide Y and macrophage inhibitory cytokine-1 expression are early events in prostate cancer development and are associated with poor prognosis. Cancer Epidemiol Biomarkers Prev. 2006;15(4):711-6.
91. Mulcrone PL, Campbell JP, Clement-Demange L, Anbinder AL, Merkel AR, Brekken RA, et al. Skeletal Colonization by Breast Cancer Cells Is Stimulated by an Osteoblast and beta2AR-Dependent Neo-Angiogenic Switch. J Bone Miner Res. 2017;32(7):1442-54.
92. Campbell JP, Karolak MR, Ma Y, Perrien DS, Masood-Campbell SK, Penner NL, et al. Stimulation of host bone marrow stromal cells by sympathetic nerves promotes breast cancer bone metastasis in mice. PLoS Biol. 2012;10(7):e1001363.
93. Huang Z, Li G, Zhang Z, Gu R, Wang W, Lai X, et al. beta2AR-HIF-1alpha-CXCL12 signaling of osteoblasts activated by isoproterenol promotes migration and invasion of prostate cancer cells. BMC Cancer. 2019;19(1):1142.
94. Partecke LI, Speerforck S, Kading A, Seubert F, Kuhn S, Lorenz E, et al. Chronic stress increases experimental pancreatic cancer growth, reduces survival and can be antagonised by beta-adrenergic receptor blockade. Pancreatology. 2016;16(3):423-33.

95. Hassan S, Karpova Y, Baiz D, Yancey D, Pullikuth A, Flores A, et al. Behavioral stress accelerates prostate cancer development in mice. J Clin Invest. 2013;123(2):874-86.
96. Lillberg K, Verkasalo PK, Kaprio J, Teppo L, Helenius H, Koskenvuo M. Stressful life events and risk of breast cancer in 10,808 women: a cohort study. Am J Epidemiol. 2003;157(5):415-23.
97. Antoni MH, Lutgendorf SK, Cole SW, Dhabhar FS, Sephton SE, McDonald PG, et al. The influence of bio-behavioural factors on tumour biology: pathways and mechanisms. Nat Rev Cancer. 2006;6(3):240-8.
98. Borre M, Nerstrom B, Overgaard J. Association between immunohistochemical expression of vascular endothelial growth factor (VEGF), VEGF-expressing neuroendocrine-differentiated tumor cells, and outcome in prostate cancer patients subjected to watchful waiting. Clin Cancer Res. 2000;6(5):1882-90.
99. Sun Y, Niu J, Huang J. Neuroendocrine differentiation in prostate cancer. Am J Transl Res. 2009;1(2):148-62.
100. Vashchenko N, Abrahamsson PA. Neuroendocrine differentiation in prostate cancer: implications for new treatment modalities. Eur Urol. 2005;47(2):147-55.
101. Nelson EC, Cambio AJ, Yang JC, Ok JH, Lara PN, Jr., Evans CP. Clinical implications of neuroendocrine differentiation in prostate cancer. Prostate Cancer Prostatic Dis. 2007;10(1):6-14.
102. Kakies C, Hakenberg OW, Gunia S, Erbersdobler A. Prostate cancer with Paneth cell-like neuroendocrine differentiation and extensive perineural invasion: coincidence or causal relationship? Pathol Res Pract. 2011;207(11):715-7.
103. Yuan TC, Veeramani S, Lin MF. Neuroendocrine-like prostate cancer cells: neuroendocrine transdifferentiation of prostate adenocarcinoma cells. Endocr Relat Cancer. 2007;14(3):531-47.
104. Cox ME, Deeble PD, Lakhani S, Parsons SJ. Acquisition of neuroendocrine characteristics by prostate tumor cells is reversible: implications for prostate cancer progression. Cancer Res. 1999;59(15):3821-30.
105. Cindolo L, Cantile M, Vacherot F, Terry S, de la Taille A. Neuroendocrine differentiation in prostate cancer: from lab to bedside. Urol Int. 2007;79(4):287-96.
106. Conteduca V, Aieta M, Amadori D, De Giorgi U. Neuroendocrine differentiation in prostate cancer: current and emerging therapy strategies. Crit Rev Oncol Hematol. 2014;92(1):11-24.

107. Kvissel AK, Ramberg H, Eide T, Svindland A, Skalhegg BS, Tasken KA. Androgen dependent regulation of protein kinase A subunits in prostate cancer cells. Cell Signal. 2007;19(2):401-9.
108. Theodorescu D, Broder SR, Boyd JC, Mills SE, Frierson HF, Jr. p53, bcl-2 and retinoblastoma proteins as long-term prognostic markers in localized carcinoma of the prostate. J Urol. 1997;158(1):131-7.
109. Deeble PD, Murphy DJ, Parsons SJ, Cox ME. Interleukin-6- and cyclic AMP-mediated signaling potentiates neuroendocrine differentiation of LNCaP prostate tumor cells. Mol Cell Biol. 2001;21(24):8471-82.
110. Merkle D, Hoffmann R. Roles of cAMP and cAMP-dependent protein kinase in the progression of prostate cancer: cross-talk with the androgen receptor. Cell Signal. 2011;23(3):507-15.
111. Zelivianski S, Verni M, Moore C, Kondrikov D, Taylor R, Lin MF. Multipathways for transdifferentiation of human prostate cancer cells into neuroendocrine-like phenotype. Biochim Biophys Acta. 2001;1539(1-2):28-43.
112. Spiotto MT, Chung TD. STAT3 mediates IL-6-induced neuroendocrine differentiation in prostate cancer cells. Prostate. 2000;42(3):186-95.
113. Lee SO, Chun JY, Nadiminty N, Lou W, Gao AC. Interleukin-6 undergoes transition from growth inhibitor associated with neuroendocrine differentiation to stimulator accompanied by androgen receptor activation during LNCaP prostate cancer cell progression. Prostate. 2007;67(7):764-73.
114. Huang J, Wu C, di Sant'Agnese PA, Yao JL, Cheng L, Na Y. Function and molecular mechanisms of neuroendocrine cells in prostate cancer. Anal Quant Cytol Histol. 2007;29(3):128-38.
115. Burgio SL, Conteduca V, Menna C, Carretta E, Rossi L, Bianchi E, et al. Chromogranin A predicts outcome in prostate cancer patients treated with abiraterone. Endocr Relat Cancer. 2014;21(3):487-93.
116. Lin D, Wyatt AW, Xue H, Wang Y, Dong X, Haegert A, et al. High fidelity patient-derived xenografts for accelerating prostate cancer discovery and drug development. Cancer Res. 2014;74(4):1272-83.
117. Bang YJ, Pirnia F, Fang WG, Kang WK, Sartor O, Whitesell L, et al. Terminal neuroendocrine differentiation of human prostate carcinoma cells in response to increased intracellular cyclic AMP. Proc Natl Acad Sci U S A. 1994;91(12):5330-4.

118. Hassan S, Karpova Y, Flores A, D'Agostino R, Jr., Kulik G. Surgical stress delays prostate involution in mice. PLoS One. 2013;8(11):e78175.
119. Farini D, Puglianiello A, Mammi C, Siracusa G, Moretti C. Dual effect of pituitary adenylate cyclase activating polypeptide on prostate tumor LNCaP cells: short- and long-term exposure affect proliferation and neuroendocrine differentiation. Endocrinology. 2003;144(4):1631-43.
120. Goodin JL, Rutherford CL. Identification of differentially expressed genes during cyclic adenosine monophosphate-induced neuroendocrine differentiation in the human prostatic adenocarcinoma cell line LNCaP. Mol Carcinog. 2002;33(2):88-98.
121. Abrahamsson PA. Neuroendocrine cells in tumour growth of the prostate. Endocr Relat Cancer. 1999;6(4):503-19.
122. Iwamura M, Abrahamsson PA, Foss KA, Wu G, Cockett AT, Deftos LJ. Parathyroid hormone-related protein: a potential autocrine growth regulator in human prostate cancer cell lines. Urology. 1994;43(5):675-9.
123. Segal NH, Cohen RJ, Haffejee Z, Savage N. BCL-2 proto-oncogene expression in prostate cancer and its relationship to the prostatic neuroendocrine cell. Arch Pathol Lab Med. 1994;118(6):616-8.
124. Xing N, Qian J, Bostwick D, Bergstralh E, Young CY. Neuroendocrine cells in human prostate over-express the anti-apoptosis protein survivin. Prostate. 2001;48(1):7-15.
125. Decker AM, Jung Y, Cackowski FC, Yumoto K, Wang J, Taichman RS. Sympathetic Signaling Reactivates Quiescent Disseminated Prostate Cancer Cells in the Bone Marrow. Mol Cancer Res. 2017;15(12):1644-55.
126. Amin E, Dubey BN, Zhang SC, Gremer L, Dvorsky R, Moll JM, et al. Rho-kinase: regulation, (dys)function, and inhibition. Biol Chem. 2013;394(11):1399-410.
127. Gong H, Zhou L, Khelfat L, Qiu G, Wang Y, Mao K, et al. Rho-Associated Protein Kinase (ROCK) Promotes Proliferation and Migration of PC-3 and DU145 Prostate Cancer Cells by Targeting LIM Kinase 1 (LIMK1) and Matrix Metalloproteinase-2 (MMP-2). Med Sci Monit. 2019;25:3090-9.
128. Zhang C, Zhang S, Zhang Z, He J, Xu Y, Liu S. ROCK has a crucial role in regulating prostate tumor growth through interaction with c-Myc. Oncogene. 2014;33(49):5582-91.
129. Riento K, Totty N, Villalonga P, Garg R, Guasch R, Ridley AJ. RhoE function is regulated by ROCK I-mediated phosphorylation. EMBO J. 2005;24(6):1170-80.

130. Zhang Y, Li X, Qi J, Wang J, Liu X, Zhang H, et al. Rock2 controls TGFbeta signaling and inhibits mesoderm induction in zebrafish embryos. J Cell Sci. 2009;122(Pt 13):2197-207.
131. Hahmann C, Schroeter T. Rho-kinase inhibitors as therapeutics: from pan inhibition to isoform selectivity. Cell Mol Life Sci. 2010;67(2):171-7.
132. Liu S. The ROCK signaling and breast cancer metastasis. Mol Biol Rep. 2011;38(2):1363-6.
133. Lochhead PA, Wickman G, Mezna M, Olson MF. Activating ROCK1 somatic mutations in human cancer. Oncogene. 2010;29(17):2591-8.
134. Liu S, Goldstein RH, Scepansky EM, Rosenblatt M. Inhibition of rho-associated kinase signaling prevents breast cancer metastasis to human bone. Cancer Res. 2009;69(22):8742-51.
135. Lane J, Martin TA, Mansel RE, Jiang WG. The expression and prognostic value of the guanine nucleotide exchange factors (GEFs) Trio, Vav1 and TIAM-1 in human breast cancer. Int Semin Surg Oncol. 2008;5:23.
136. Lin SL, Chang D, Ying SY. Hyaluronan stimulates transformation of androgen-independent prostate cancer. Carcinogenesis. 2007;28(2):310-20.
137. Routhier A, Astuccio M, Lahey D, Monfredo N, Johnson A, Callahan W, et al. Pharmacological inhibition of Rho-kinase signaling with Y-27632 blocks melanoma tumor growth. Oncol Rep. 2010;23(3):861-7.
138. Boku S, Nakagawa S, Toda H, Kato A, Takamura N, Omiya Y, et al. ROCK2 regulates bFGF-induced proliferation of SH-SY5Y cells through GSK-3beta and beta-catenin pathway. Brain Res. 2013;1492:7-17.
139. Yin H, Hou X, Tao T, Lv X, Zhang L, Duan W. Neurite outgrowth resistance to rho kinase inhibitors in PC12 Adh cell. Cell Biol Int. 2015;39(5):563-76.
140. Mueller BK, Mack H, Teusch N. Rho kinase, a promising drug target for neurological disorders. Nat Rev Drug Discov. 2005;4(5):387-98.
141. Kubo T, Yamashita T. Rho-ROCK inhibitors for the treatment of CNS injury. Recent Pat CNS Drug Discov. 2007;2(3):173-9.
142. Fournier AE, GrandPre T, Strittmatter SM. Identification of a receptor mediating Nogo-66 inhibition of axonal regeneration. Nature. 2001;409(6818):341-6.
143. Hiraga T. [Molecular targets for the treatment of bone metastases]. Clin Calcium. 2006;16(1):159-65.

144. Impellizzeri D, Mazzon E, Paterniti I, Esposito E, Cuzzocrea S. Effect of fasudil, a selective inhibitor of Rho kinase activity, in the secondary injury associated with the experimental model of spinal cord trauma. J Pharmacol Exp Ther. 2012;343(1):21-33.
145. Fujita A, Hattori Y, Takeuchi T, Kamata Y, Hata F. NGF induces neurite outgrowth via a decrease in phosphorylation of myosin light chain in PC12 cells. Neuroreport. 2001;12(16):3599-602.
146. Nusser N, Gosmanova E, Zheng Y, Tigyi G. Nerve growth factor signals through TrkA, phosphatidylinositol 3-kinase, and Rac1 to inactivate RhoA during the initiation of neuronal differentiation of PC12 cells. J Biol Chem. 2002;277(39):35840-6.
147. Minase T, Ishima T, Itoh K, Hashimoto K. Potentiation of nerve growth factor-induced neurite outgrowth by the ROCK inhibitor Y-27632: a possible role of IP(3) receptors. Eur J Pharmacol. 2010;648(1-3):67-73.
148. Duan WG, Shang J, Jiang ZZ, Yao JC, Yun Y, Yan M, et al. Rho kinase inhibitor Y-27632 down-regulates norepinephrine synthesis and release in PC12 cells. Basic Clin Pharmacol Toxicol. 2009;104(6):434-40.
149. Fukuda T, Takekoshi K, Nanmoku T, Ishii K, Isobe K, Kawakami Y. Inhibition of the RhoA/Rho kinase system attenuates catecholamine biosynthesis in PC 12 rat pheochromocytoma cells. Biochim Biophys Acta. 2005;1726(1):28-33.
150. Duan W, Que L, Lv X, Li Q, Yin H, Zhang L. Tolerance of neurite outgrowth to Rho kinase inhibitors decreased by cyclooxygenase-2 inhibitor. Neural Regen Res. 2012;7(34):2705-12.
151. Que L, Duan W, Zhang L, Jiang Z Differences of neurite outgrowth induced by rho kinase inhibitors between in PC12 cell line and PC12 Adh cell line

J Yunnan University 33: 370–2. 2011.
152. Cardwell CR, Coleman HG, Murray LJ, O'Sullivan JM, Powe DG. Beta-blocker usage and prostate cancer survival: a nested case-control study in the UK Clinical Practice Research Datalink cohort. Cancer Epidemiol. 2014;38(3):279-85.
153. Assayag J, Pollak MN, Azoulay L. Post-diagnostic use of beta-blockers and the risk of death in patients with prostate cancer. Eur J Cancer. 2014;50(16):2838-45.
154. Lu H, Liu X, Guo F, Tan S, Wang G, Liu H, et al. Impact of beta-blockers on prostate cancer mortality: a meta-analysis of 16,825 patients. Onco Targets Ther. 2015;8:985-90.

155. Grytli HH, Fagerland MW, Fossa SD, Tasken KA, Haheim LL. Use of beta-blockers is associated with prostate cancer-specific survival in prostate cancer patients on androgen deprivation therapy. Prostate. 2013;73(3):250-60.
156. Grytli HH, Fagerland MW, Fossa SD, Tasken KA. Association between use of beta-blockers and prostate cancer-specific survival: a cohort study of 3561 prostate cancer patients with high-risk or metastatic disease. Eur Urol. 2014;65(3):635-41.
157. Choi CH, Song T, Kim TH, Choi JK, Park JY, Yoon A, et al. Meta-analysis of the effects of beta blocker on survival time in cancer patients. J Cancer Res Clin Oncol. 2014;140(7):1179-88.
158. Powe DG, Voss MJ, Zanker KS, Habashy HO, Green AR, Ellis IO, et al. Beta-blocker drug therapy reduces secondary cancer formation in breast cancer and improves cancer specific survival. Oncotarget. 2010;1(7):628-38.
159. Melhem-Bertrandt A, Chavez-Macgregor M, Lei X, Brown EN, Lee RT, Meric-Bernstam F, et al. Beta-blocker use is associated with improved relapse-free survival in patients with triple-negative breast cancer. J Clin Oncol. 2011;29(19):2645-52.
160. Wiatrak B, Kubis-Kubiak A, Piwowar A, Barg E. PC12 Cell Line: Cell Types, Coating of Culture Vessels, Differentiation and Other Culture Conditions. Cells. 2020;9(4).
161. Zhou M, Hu M, He S, Li B, Liu C, Min J, et al. Effects of RSC96 Schwann Cell-Derived Exosomes on Proliferation, Senescence, and Apoptosis of Dorsal Root Ganglion Cells In Vitro. Med Sci Monit. 2018;24:7841-9.
162. Fawcett JW, Keynes RJ. Peripheral nerve regeneration. Annu Rev Neurosci. 1990;13:43-60.
163. Bunge RP. The role of the Schwann cell in trophic support and regeneration. J Neurol. 1994;242(1 Suppl 1):S19-21.
164. Thalmann GN, Anezinis PE, Chang SM, Zhau HE, Kim EE, Hopwood VL, et al. Androgen-independent cancer progression and bone metastasis in the LNCaP model of human prostate cancer. Cancer Res. 1994;54(10):2577-81.
165. Wu HC, Hsieh JT, Gleave ME, Brown NM, Pathak S, Chung LW. Derivation of androgen-independent human LNCaP prostatic cancer cell sublines: role of bone stromal cells. Int J Cancer. 1994;57(3):406-12.
166. Eliminate human bias in cell counting Using the Via1-Cassette™ and Via2-Cassette™ [Internet] Denmark: ChemoMetec; 2020 [updated 2020; cited 2020 19.12]. Available from: https://chemometec.com/via-cassette-page/.

167. Moore CB, Guthrie EH, Huang MT, Taxman DJ. Short hairpin RNA (shRNA): design, delivery, and assessment of gene knockdown. Methods Mol Biol. 2010;629:141-58.
168. Lambeth LS, Smith CA. Short hairpin RNA-mediated gene silencing. Methods Mol Biol. 2013;942:205-32.
169. Erfle H, Neumann B, Liebel U, Rogers P, Held M, Walter T, et al. Reverse transfection on cell arrays for high content screening microscopy. Nat Protoc. 2007;2(2):392-9.
170. Park SY, An JM, Seo JT, Seo SR. Y-27632 Induces Neurite Outgrowth by Activating the NOX1-Mediated AKT and PAK1 Phosphorylation Cascades in PC12 Cells. Int J Mol Sci. 2020;21(20).
171. Jia XF, Ye F, Wang YB, Feng DX. ROCK inhibition enhances neurite outgrowth in neural stem cells by upregulating YAP expression in vitro. Neural Regen Res. 2016;11(6):983-7.
172. Braadland PR, Ramberg H, Grytli HH, Urbanucci A, Nielsen HK, Guldvik IJ, et al. The beta2-Adrenergic Receptor Is a Molecular Switch for Neuroendocrine Transdifferentiation of Prostate Cancer Cells. Mol Cancer Res. 2019;17(11):2154-68.
173. Somlyo AV, Bradshaw D, Ramos S, Murphy C, Myers CE, Somlyo AP. Rho-kinase inhibitor retards migration and in vivo dissemination of human prostate cancer cells. Biochem Biophys Res Commun. 2000;269(3):652-9.
174. Zhang X, Zhang Y, He Z, Yin K, Li B, Zhang L, et al. Chronic stress promotes gastric cancer progression and metastasis: an essential role for ADRB2. Cell Death Dis. 2019;10(11):788.
175. Pandya P, Orgaz JL, Sanz-Moreno V. Actomyosin contractility and collective migration: may the force be with you. Curr Opin Cell Biol. 2017;48:87-96.
176. Hashimoto K, Yamashita K, Enoyoshi K, Dahan X, Takeuchi T, Kori H, et al. The effects of coating culture dishes with collagen on fibroblast cell shape and swirling pattern formation. J Biol Phys. 2020;46(4):351-69.
177. Liang CC, Park AY, Guan JL. In vitro scratch assay: a convenient and inexpensive method for analysis of cell migration in vitro. Nat Protoc. 2007;2(2):329-33.
178. Guy JB, Espenel S, Vallard A, Battiston-Montagne P, Wozny AS, Ardail D, et al. Evaluation of the Cell Invasion and Migration Process: A Comparison of the Video Microscope-based Scratch Wound Assay and the Boyden Chamber Assay. J Vis Exp. 2017(129).

179. Dai D, Lin P, Wang Y, Zhou X, Tao J, Jiang D, et al. Association of NQO1 and TNF polymorphisms with Parkinson's disease: A meta-analysis of 15 genetic association studies. Biomed Rep. 2014;2(5):713-8.
180. Na'ara S, Gil Z, Amit M. In Vitro Modeling of Cancerous Neural Invasion: The Dorsal Root Ganglion Model. J Vis Exp. 2016(110):e52990.
181. Schwaid AG, Krasowka-Zoladek A, Chi A, Cornella-Taracido I. Comparison of the Rat and Human Dorsal Root Ganglion Proteome. Sci Rep. 2018;8(1):13469.
182. Huyett P, Gilbert M, Liu L, Ferris RL, Kim S. A Model for Perineural Invasion in Head and Neck Squamous Cell Carcinoma. J Vis Exp. 2017(119).
183. Walker JM. The bicinchoninic acid (BCA) assay for protein quantitation. Methods Mol Biol. 1994;32:5-8.
184. Noble JE, Bailey MJ. Quantitation of protein. Methods Enzymol. 2009;463:73-95.
185. Kessler RJ, Fanestil DD. Interference by lipids in the determination of protein using bicinchoninic acid. Anal Biochem. 1986;159(1):138-42.
186. Wiechelman KJ, Braun RD, Fitzpatrick JD. Investigation of the bicinchoninic acid protein assay: identification of the groups responsible for color formation. Anal Biochem. 1988;175(1):231-7.
187. Reichelt WN, Waldschitz D, Herwig C, Neutsch L. Bioprocess monitoring: minimizing sample matrix effects for total protein quantification with bicinchoninic acid assay. J Ind Microbiol Biotechnol. 2016;43(9):1271-80.

Supplementary/Appendix

Laboratory Hygiene

All work with cells were done in the cell lab at the LAF (Laminar Flow) cabinet.

To avoid contamination of cell cultures in the cell lab, many steps were taken to ensure a sterile environment. Gloves were constantly used in the lab which were sprayed with ethanol (70%). All bottles and equipment that were put in the incubator and into the LAF cabinet were sprayed well with ethanol. Contaminated equipment were not used and were discarded. Between users, the LAF cabinet was sprayed well with ethanol and washed well to avoid bacterial growth and for the next person to come to a clean workplace. Mycoplasma tests were employed on each cell line in order to avoid bacterial infection. The waste container was labeled and treated according to Radiumhospitalets regulations for handling biological waste.

The LAF benches were cleaned regularly every week.

STE-buffer

	Stock Concentration	Final Concentration	Volume of stock for(mL):		
			50 mL	100 mL	500 mL
Sucrose	70% w/v	27% w/w	21,6	43,1	215,5
Tris-HCL-pH 7,5 (20°C)	1 mM	50 mM	2,5	5	25
EDTA	500 mM	5 mM	0,5	1	5
dH_2O to (m):			50	100	500

Table 5 | Preparation of STE-buffer used for isolation and purification of membrane proteins.

Supplementary figures

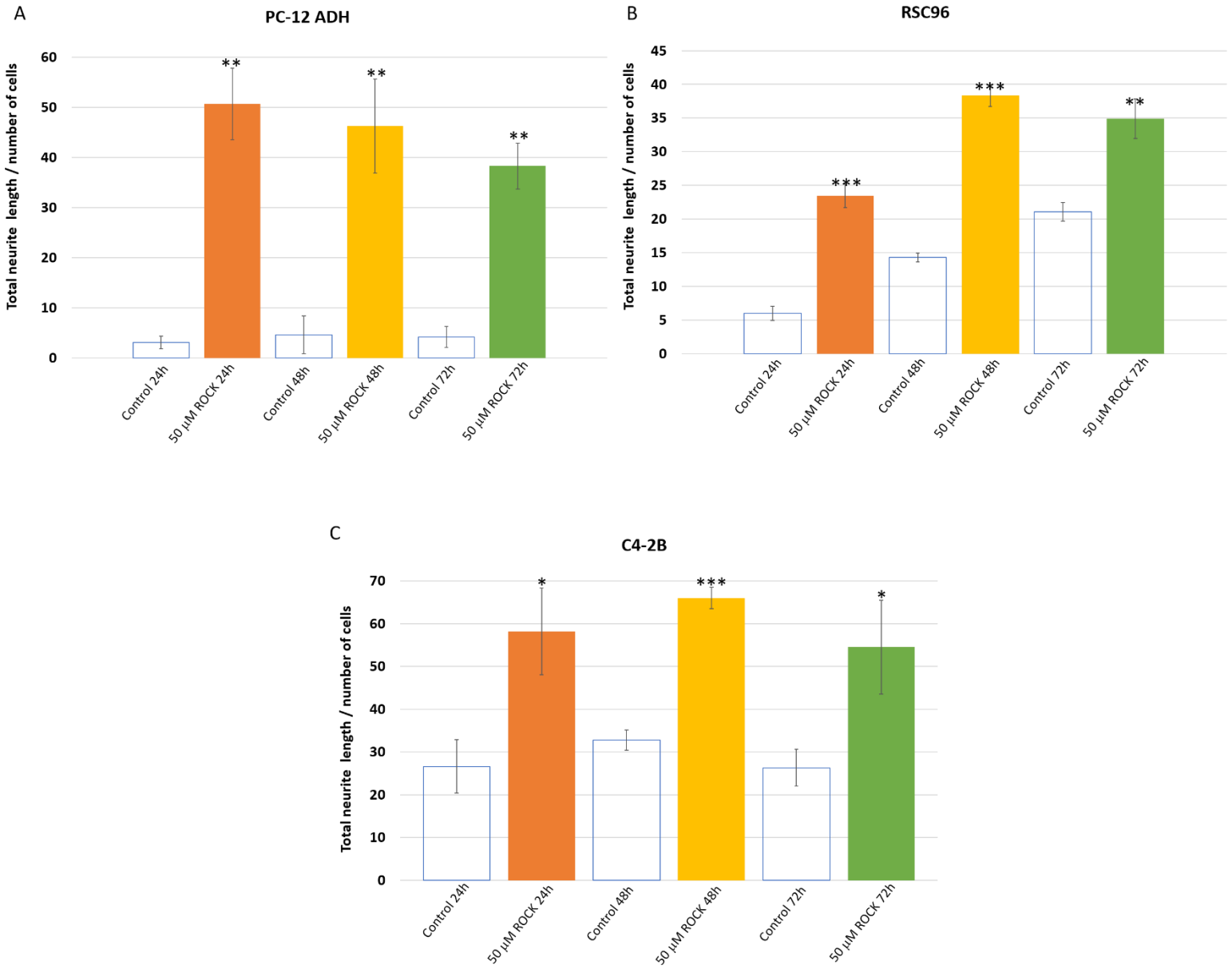

Supplementary figure 1 | A time interval to illustrate and determine the effect of 50 µM ROCK during 72 hours of stimulation. To determine the total of hours in which the 50 µM ROCK induces the longest neurites, each cell line were stimulated with the ROCK-inhibitor for a total of 72 hours. The data was used to determine the total of hours in which the inhibitor induces the longest neurites. Error bars are presented as standard deviation. *****p<0,05, ******p<0,01, ***p<0,005. (n=3)

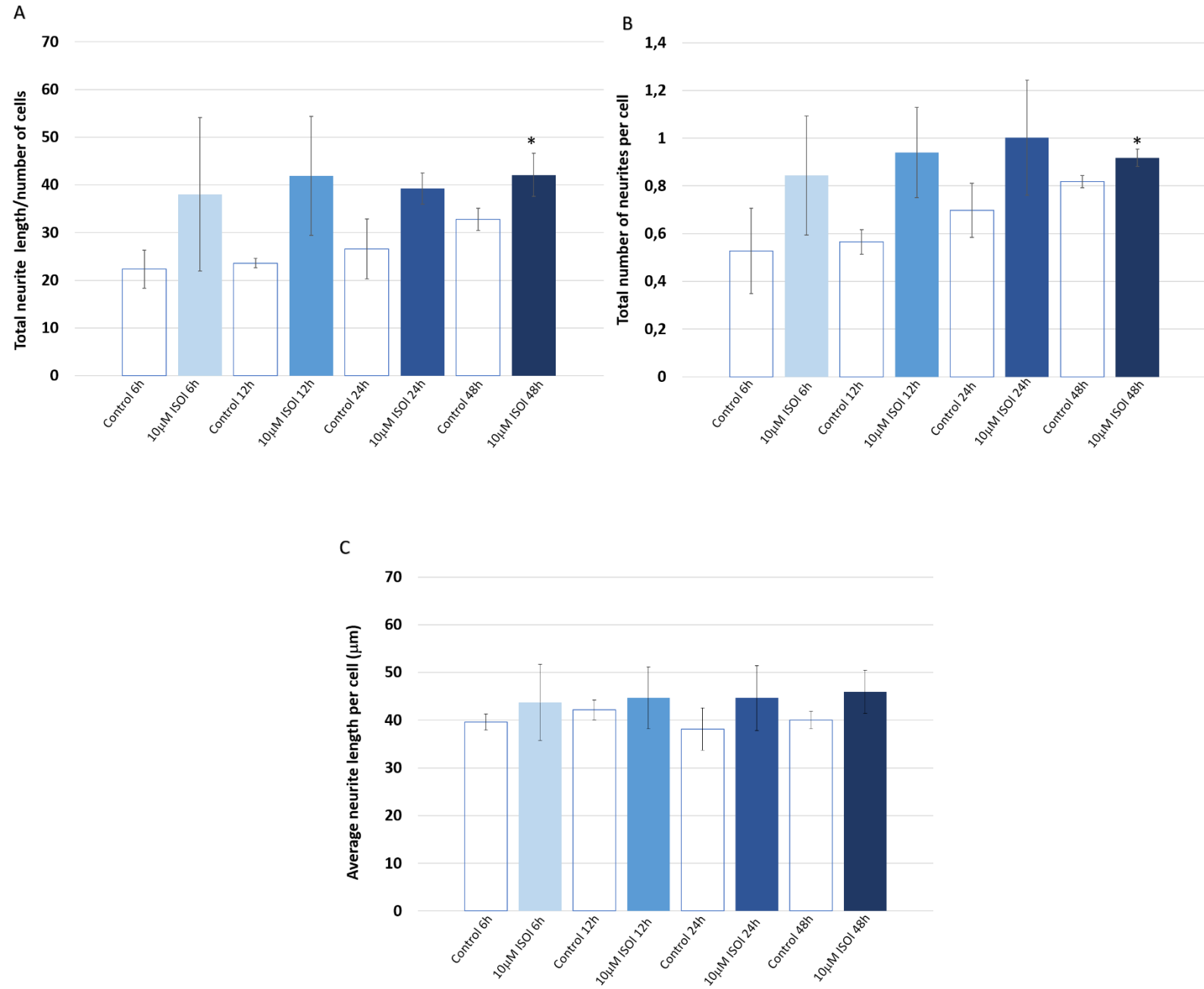

Supplementary Figure 2 | **A time interval to illustrate and determine the effect of 10 µM ISO during 48 hours of stimulation in C4-2B cells**. To determine the total of ours in which the 10 µM ISO induces the longest neurites, the C4-2B cell line were stimulated with ISO for a total of 48 hours. **(A)** The total length of neurites divided by the number of cells. The figure illustrates the average for the total length of neurites divided by the total amount of cells for each stimulation. Error bars are presented as standard deviation. **(B)** The number of neurites in a selected area within the image were quantified and divided by the number of cells, in order to see how the stimulations influences the number of neurites per cell compared to the control **(C)** The average neurite length of cells stimulated with ISO for 48 hours compared to the controls. The data was used to determine the total of hours in which the inhibitor induces the longest neurites. Error bars are presented as standard deviation. *****$p<0,05$. (n=3)

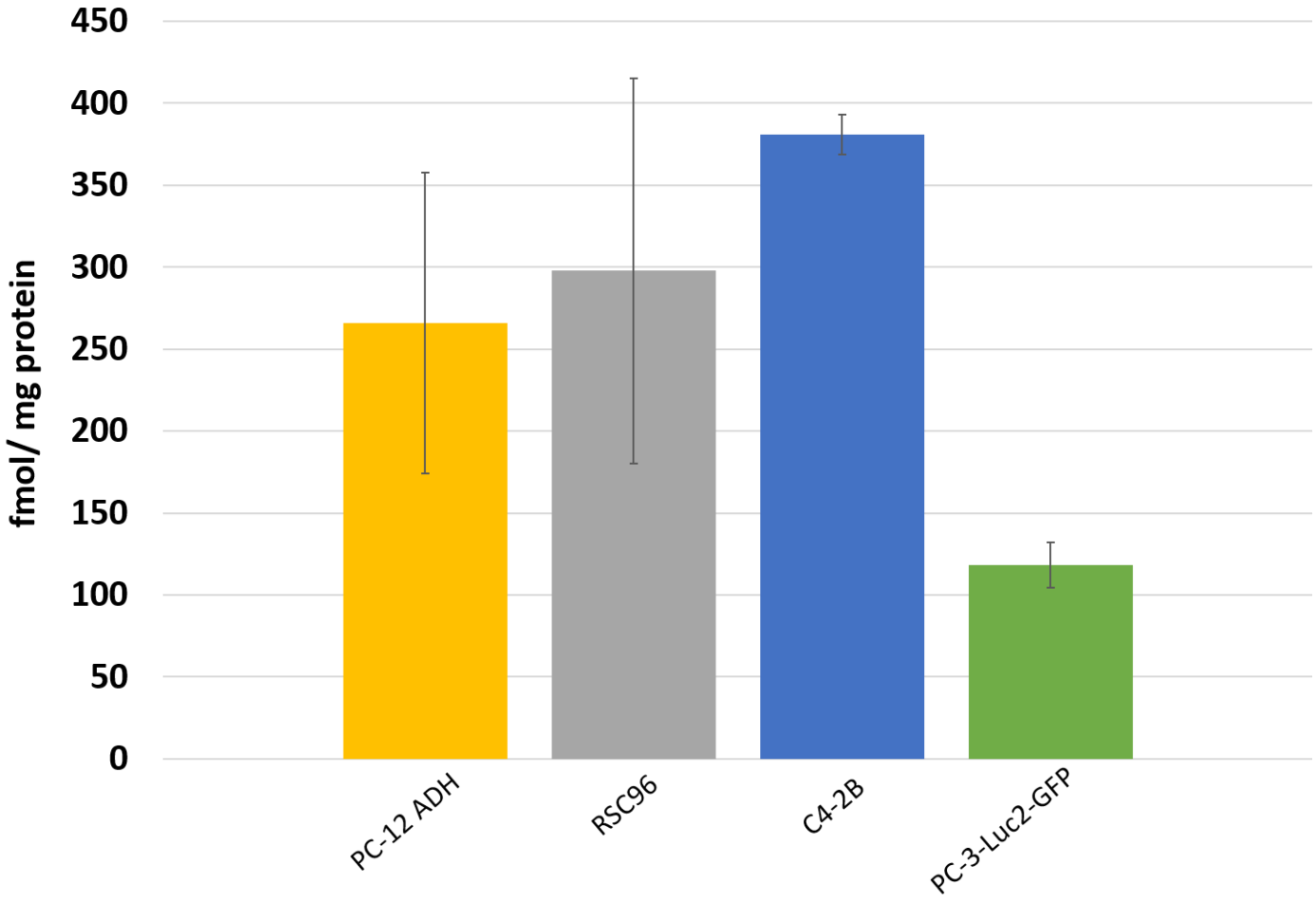

Supplementary Figure 3 | The level of ADRB2 in all cell lines determined by receptor radioligand binding assay. A receptor radioligand binding assay was performed on all cell lines, in order to determine the expression level of ADRB2 in each cell line Error bars are presented

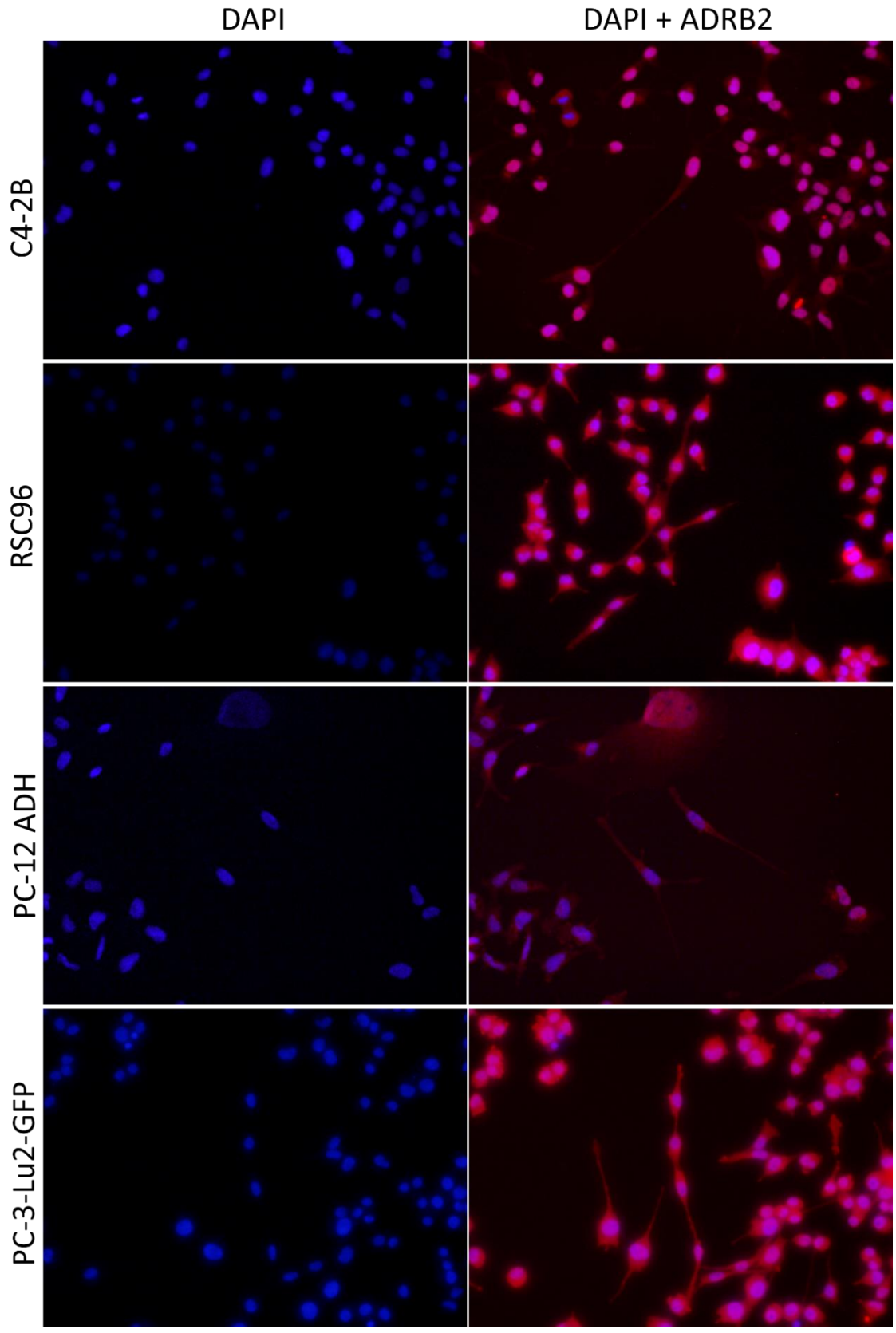

Supplementary Figure 4 | Representative fluorescence microscopy images of immunofluorescent stained cells for ADRB2 detection. All cell lines was stained immunofluorescence antibodies in order to detect the presence of ADRB2 with the TRITC filter on the fluorescence microscope

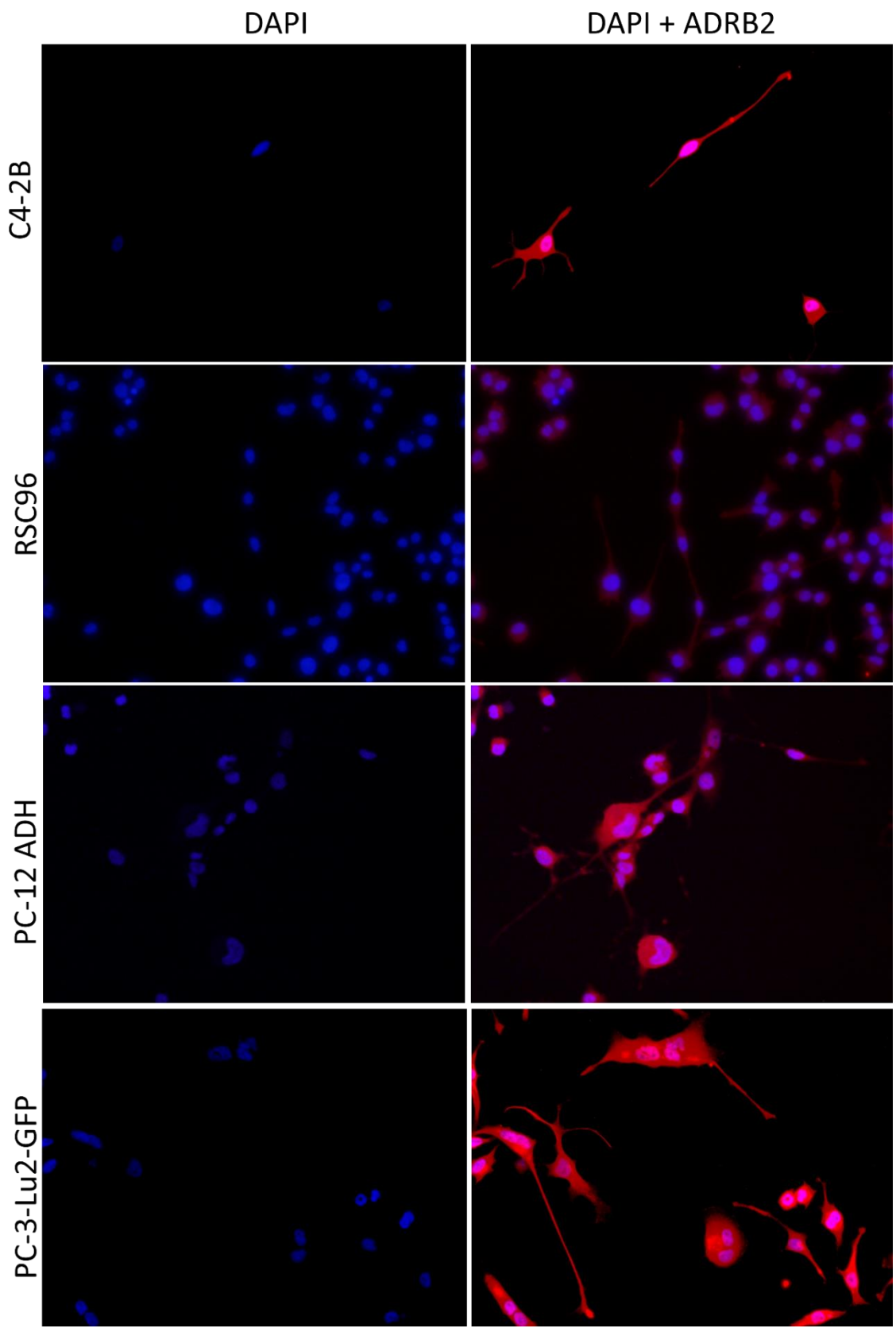

Supplementary figure 5 | Representative fluorescence microscopy images of immunofluorescent stained cells for ADRB2 detection treated with 50 μM ROCK. All cell lines was stimulated with 50 μM ROCK 48 hours prior to immunofluorescence staining with antibodies in order to det

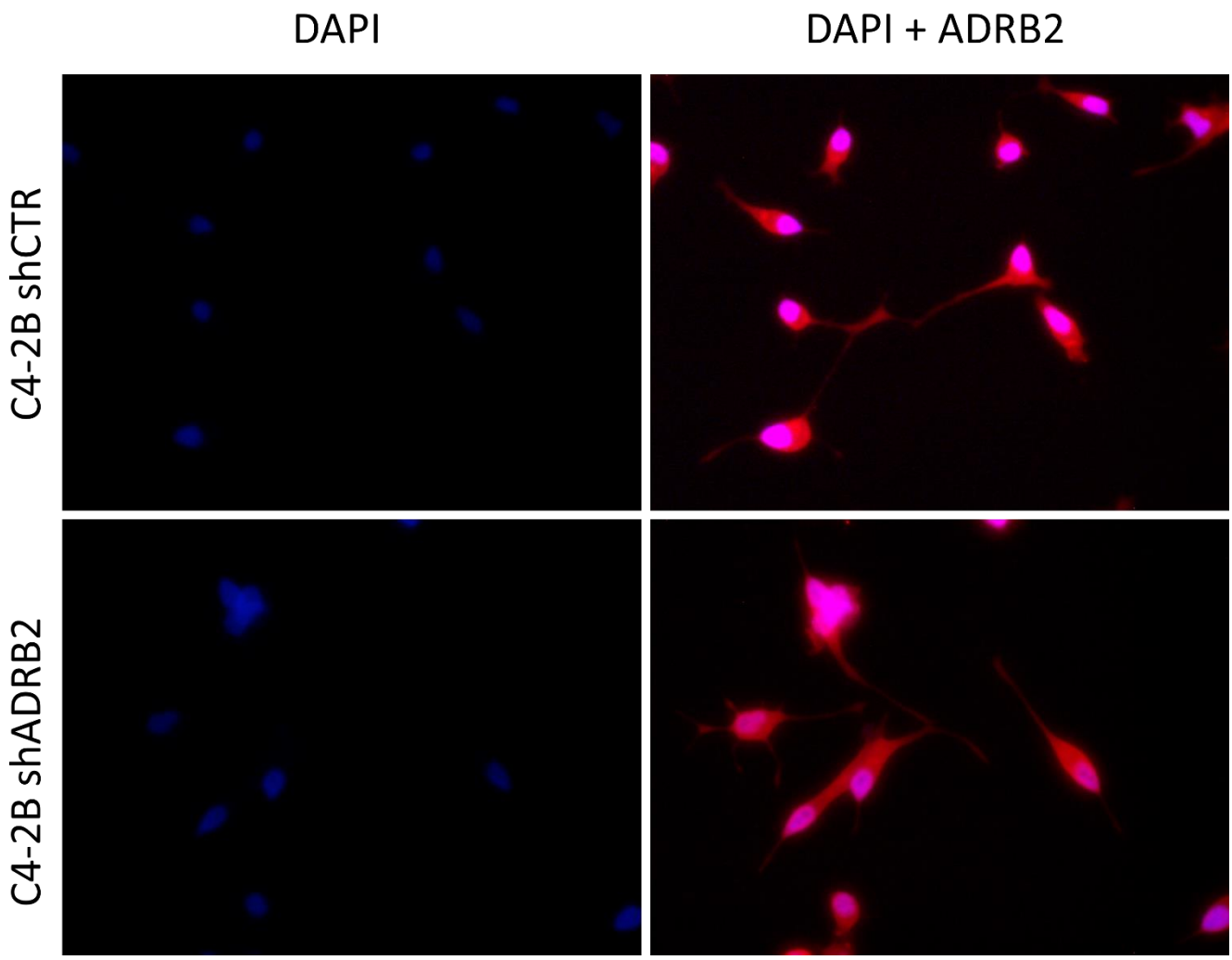

Supplementary figure 6 | Immunofluorescence staining of ADRB2 knockout cell line and the control knockout cell line. The KO-cell lines were stained with immunofluorescence antibodies in order to detect ADRB2 and compare the level of expression by visual assessment. As shown, every cell line was ADRB2+ and images was taken on 20x.